Brigham Young University
BYU ScholarsArchive

All Theses and Dissertations

2017-12-01

A Comparison Between Self-Cleaning Properties via Rolling Droplets and Condensation on Superhyrophobic Surfaces

David Leland Miller
Brigham Young University

Follow this and additional works at: https://scholarsarchive.byu.edu/etd

 Part of the Mechanical Engineering Commons

BYU ScholarsArchive Citation

Miller, David Leland, "A Comparison Between Self-Cleaning Properties via Rolling Droplets and Condensation on Superhyrophobic Surfaces" (2017). *All Theses and Dissertations*. 6594.
https://scholarsarchive.byu.edu/etd/6594

This Thesis is brought to you for free and open access by BYU ScholarsArchive. It has been accepted for inclusion in All Theses and Dissertations by an authorized administrator of BYU ScholarsArchive. For more information, please contact scholarsarchive@byu.edu, ellen_amatangelo@byu.edu.

A Comparison Between Self-Cleaning Properites via Rolling Droplets and Condensation on Superhydrophobic Surfaces

David Leland Miller

A thesis submitted to the faculty of
Brigham Young University
in partial fulfillment of the requirements for the degree of

Master of Science

Julie Crockett, Chair
Daniel Maynes
Brian Iverson

Department of Mechanical Engineering

Brigham Young University

Copyright © 2017 David Leland Miller

All Rights Reserved

ABSTRACT

A Comparison Between Self-Cleaning Properites via Rolling Droplets and Condensation on Superhydrophobic Surfaces

David Leland Miller
Department of Mechanical Engineering, BYU
Master of Science

Superhydrophobic (SH) surfaces are super water repellent surfaces on which a droplet of water will bead up like a marble and roll off the surface with minimal tilting of the surface. This is caused by the combination of a hydrophobic coating and a rough surface structure. To achieve thermodynamic stability, surface tension of the water pulls the droplet into this shape to minimize the contact area between the droplet and the surface. This creates a high contact angle (CA) between the droplet and the surface and a low sliding angle (SA) of which the droplet begins to roll off the surface. SH surfaces have a variety of potential applications such as drag reduction, anti-icing, improved heat transfer through condensation, and self-cleaning. Numerous reports have been dedicated to exploring the fluid dynamic behavior of water droplets on SH surfaces. This thesis focuses on exploring the self-cleaning properties of SH surfaces. Surfaces contaminated with salt, tobacco, and pollen are cleaned by rolling water droplets over the surface or condensing water on the surface such that when large enough, these droplets roll away due to gravity. SH surfaces explored here are composed of micro-scale or nano-scale rib and cavity structures and and are compared with smooth, hydrophobic surfaces with a similar hydrophobic coating.

To determine the self-cleaning efficiency of each surface, the CA and SA were measured before and after each surface was cleaned. In this study, it was observed that the presence of each of the three contaminates considered greatly affects the overall hydrophobicity of the surface, as indicated by the CA and SA. Ideally, as the contaminates are removed from the surface, the hydrophobicity of the surface improves to match the hydrophobicity of a clean surface. This is best seen on surfaces contaminated with salt as the CA and SA match that of a clean surface after only two to three water droplets roll over the surface or after the first condensed water droplets roll off the surface. This implies that all the salt particles are removed from the SH surface. Surfaces contaminated with tobacco showed that the hydrophobicity improves to a limited extent when cleaned with rolling water droplets or condensation but never is capable of matching the hydrophobicity of a clean surface. This suggests that only a portion of the tobacco residue is capable of being removed from the surface by either of the two cleaning methods considered in this thesis. Finally, when water came in contact with pollen on the surfaces, it experienced hydrodynamic osmosis leading to cellular bursting. After cellular bursting, the surface behaves as a hydrophilic surface and self-cleaning properties were never observed on any surface contaminated with pollen. Thus, overall this study shows that rolling water droplets over a contaminated surface and condensing water droplets on a contaminated surface are both viable means of utilizing the self-cleaning properties on SH surfaces. For the contaminates considered in this study, the efficiency of the self-cleaning surfaces is shown to be the same for both micro-structured and nano-structured surfaces.

Keywords: Superhydorphobic, Self-Cleaning, Lotus Effect, Condensation

ACKNOWLEDGMENTS

I would like to express my sincerest appreciation to Dr. Julie Crockett for all the support she has offered me over the past two and a half years. She has spent countless hours "Crockett-izing" (thoroughly reviewing) my papers, including this thesis, and teaching me to become a better researcher, student, and writer. I would also like to thank Dr. Maynes and Dr. Iverson, who along with Dr. Crockett, asked the difficult questions every week in our lab meetings which made me think through every little detail of my work.

I would also like to thank Moxtex, Inc who provided the finacial support for the first year of my graduate studies and Fred Lane (aka Santa Clause) for serving as the project liaison. Fred offered numerous insights into the industrial applications of this work and frequently answered the difficult question "why does any of this matter."

Several good friends and lab-mates, including Chad Stucki, Kimberly Stevens, Adam Cowley, Matthew Searle, Preston Emerson, and Cristian Clavijo, have made the journey fun and enjoyable. They have willingly answered so many of my questions over the past few years and have given me feedback on how I could improve my own research. I would especially like to thank Kimberly Stevens who shared with me her goniometer code which became a critical part of this project. Also, Taylor Schroedter, Kristy Palombo, and Preston Elmer all participated in this research as undergraduate research assistants and spent countless hours rolling droplets over the surfaces and watching water condense to collect the data for this thesis.

Finally, I must thank my parents for always believing in me and encouraging me to keep going, even at times when I less than enjoyed my research. And above everyone else, I must thank my wife Haley who has brought more happiness into my life over the past two years than I could ever imagine. She has become my primary support and has demonstrated so much love and patience towards me. She and our sons, Carter, Lincoln, and Elliott, make life exciting.

TABLE OF CONTENTS

LIST OF TABLES

LIST OF FIGURES

NOMENCLATURE

SH	Abbreviation for Superhydrophobic
CA	Abbreviation for Contact Angle
SA	Abbreviation for Sliding Angle
CA^*	Non-Dimensional Contact Angle
SA^*	Non-Dimensional Sliding Angle
CA_i	CA after i number of rolling droplets or i number condensation cycles
CA_{clean}	CA on a clean surface
$CA_{initial}$	CA on a contamiante surface prior to cleaning
SA_i	SA after i number of rolling droplets or i number condensation cycles
SA_{clean}	SA on a clean surface
$SA_{initial}$	SA on a contamiante surface prior to cleaning
SEM	Abbreviatin of Scanning Electron Microscopy
θ	Calculated Contact Angle
α	Calculated Sliding Angle
θ_A	Advancing Contact Angle
θ_R	Receding Contact Angle
m	Mass of Droplet
g	Graviational Constant
r_{drop}	Droplet Radius
r	Roughness Factor
F_c	Cavity Fraction
θ^0	Young's Contact Angle
γ_{LV}	Liquid-Vapor Surface Tension
γ_{SG}	Solid-Gas Surface Tension
γ_{SL}	Solid-Liquid Surface Tension
ΔP	LaPlace Pressure
R_i	Curvature radii of Meniscus
τ_w	Shear stress at wall
μ	Fluid Shear Stress
u	Fluid Velocity
y	Direction Perpendicular to Surface
λ	Slip Length
u_s	Slip Velocity
W_c	Surface Pitch
W	Width of Cavities
h	Height of Surface Features
T_d	Dew Point Temperature
T	Ambient Temperature
RH	Relative Humidity
B_o	Biot Number
$\Delta\rho$	Difference in density between water droplet and surrounding air

CHAPTER 1. INTRODUCTION

1.1 Motivation

One of the most notable aspects of the Lotus leaf is its ability to maintain a clean surface, free of both water droplets and contaminates deposited on the surface. When water droplets roll over the leaf, particles on the leaf's surface preferentially adhere to the water droplet rather than the leaf's surface. This water can come in the form of both rain and condensation. Because a unique chemical coating, micro-structures, and nano-structures make up the surface of the lotus leaf, water droplets on the Lotus leaf bead up like a marble and quickly roll off the leaf, removing any contaminates in its path. The ability of the Lotus leaf to maintain its cleanliness is known as the Lotus Effect and is caused by a unique characteristic of the leaf called superhydrophobicity [1,3,4].

Superhydrophobic (SH) surfaces, such as the lotus leaf, are extremely water repellent surfaces. When water droplets are placed on these surfaces, they bead up like a marble and exhibit a high contact angle ($>120°$) between the droplet and the surface. This high contact angle reduces the total contact area between the droplet and the surface, thus minimizing the adhesive force between the droplet and the surface. Then, like a marble on a surface, minimal tilting of the surface causes the droplet to easily roll off the surface. SH surfaces are made up of two components: a rough surface structure and a hydrophobic chemical coating. The rough surface structure can be any type of surface structure on the nano-scale, micro-scale, or a combination of the two. The chemical coating can be any natively hydrophobic coating such as Teflon®, silanes, or waxes. Because of these two factors, the water droplets exhibit this marble like behavior in order to achieve thermodynamic stability.

Mimicking the Lotus Effect has many potential industrial applications in which surface contaminates can inhibit the efficiency of many products. One such application needing self-cleaning surfaces is improved optical visibility through window. This could be applied to personal glasses, building windows, or vehicle windshields. In the case of vehicle windshields, utilizing

Figure 1.1: Water droplets on SH surfaces bead up like a marble exhibiting a high CA and SA.

self-cleaning properties can lead to an improved driver visibility. A second application of self-cleaning surfaces can be found in the solar panel industry. Removing contaminates from solar panels can result in more efficient solar cells, thus generating more electricity. And finally, a third potential application of self-cleaning surfaces could be minimizing bacterial growth on a surface. This study looks at the fundamental cleaning dynamics of artificial, self-cleaning surfaces which will be beneficial in developing SH surfaces for each of the above listed applications.

1.2 Background

1.2.1 Introduction to Superhydrophobic Surfaces

SH surfaces are unique surfaces in which water droplets are repelled from the surface. Because of chemical and structural make up of SH surfaces, water droplets on these surfaces bead up like a marble creating a very high contact angle (CA) between the droplet and the surface at the solid-liquid interface, as shown in Figure 1.1. The CA is indicated as θ in Figure 1.1. With the smallest degree of tilt of the surface, the water droplet will roll off the surface like a marble. This phenomena is due to the surface tension of the water droplet in which a marble-like shape achieves thermodynamic stability and minimizes the surface energy of the water droplet [5].

Two distinct characteristics define SH surfaces: a high solid-liquid CA between a static sessile water droplet and the SH surface ($>120°$) and a low droplet hysteresis ($<10°$) [6–8]. To define a hysteresis, a surface is tilted with a water droplet on it such that the CA of the leading edge

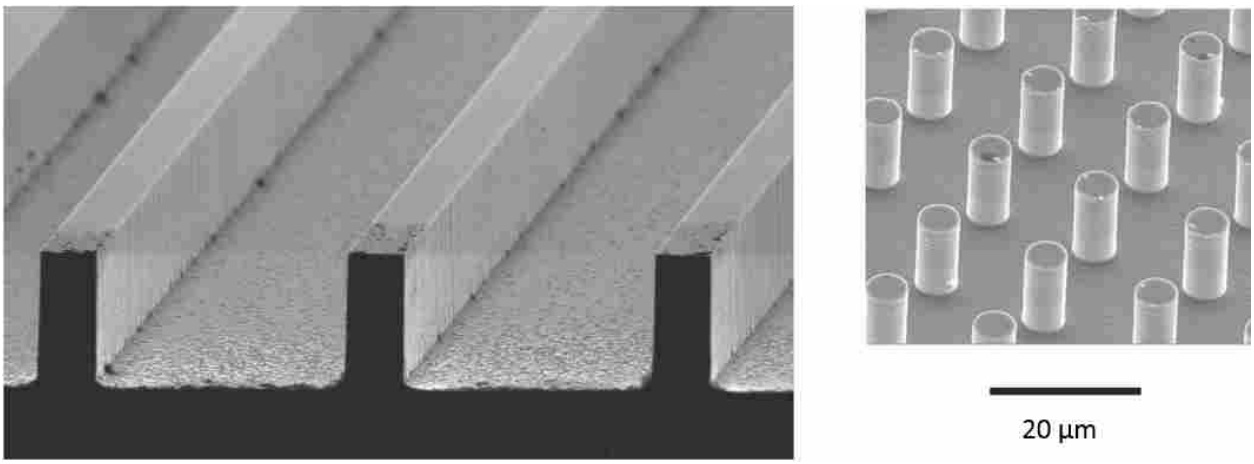

Figure 1.2: SEM images of the rib structures (left) and post structures (right) used for the surface structure of SH surfaces. The scale shown is the same for both images.

of the droplet increases while the CA of the trailing edge of the droplet decreases. These angles are respectively known as the advancing and receding angles and the hysteresis is the difference between these two angles [9]. On SH surfaces, both the advancing and receding angle are high ($>120°$) and nearly equal, resulting in a very low hysteresis. A third property related to the hysteresis is the sliding angle (SA) of the droplet, or the minimum angle required for the droplet to begin rolling off the surface. The SA, α can be calculated from the advancing (θ_A) and receding (θ_R) angles in equation 1.1

$$mg\sin(\alpha) = r_{drop}\pi\gamma_{LV}(\cos\theta_R - \cos\theta_A) \tag{1.1}$$

where m is the mass of the droplet, g is the gravitational constant, r_{drop} is the radius of the droplet, and γ_{LV} is the liquid-vapor surface tension [10–12]. The SA on SH surfaces is typically less than 15°and can be as low as 0-1°depending on the SH surface [3, 8, 12, 13].

SH surfaces are created by the combination of a rough surface structure and a natively hydrophobic chemical coating. The rough surface structure can be composed of any type of surface structure on the micrometer scale, nanometer scale, or a combination of the two known as a two-tier surface structure. To allow for a systematic study of various geometries to identify key parameters influencing the super-hydrophobicity of the surface, some surface structures take the shape of rib or post patterns as shown Scanning Electron Microscopy (SEM) images in Figure

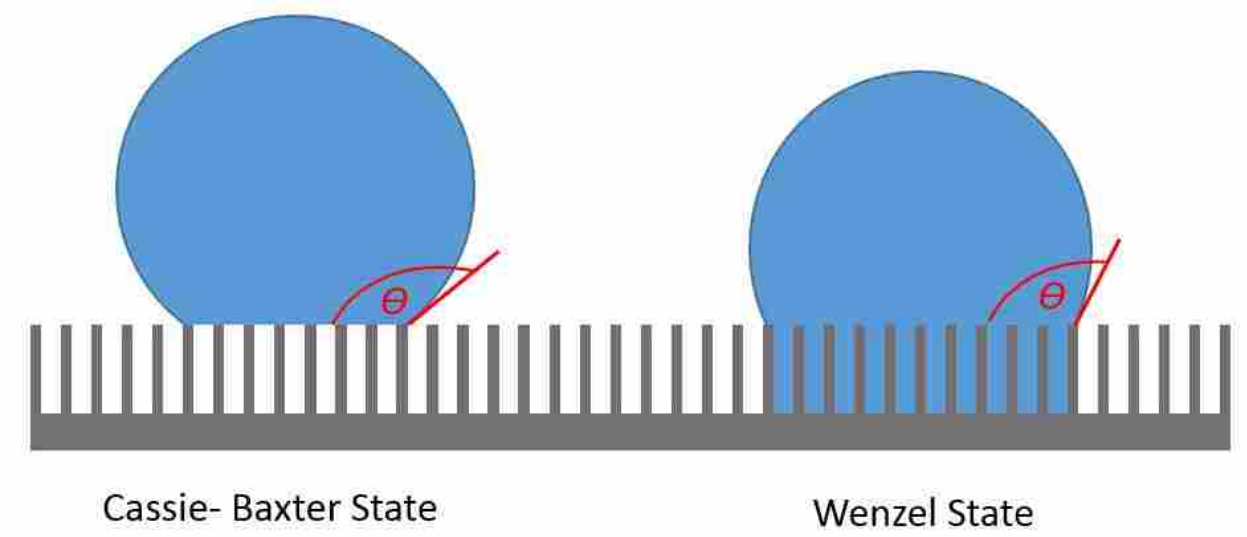

Figure 1.3: Schematic of water droplet in the Cassie-Baxter state (left) and the Wenzel state (right) on a SH surface. Note that the water droplet sits on top of the rib structures in the Cassie-Baxter state and floods the rib structures in the Wenzel state. Note that this schematic is not to scale.

1.2 [14]. However, random surface structuring is also commonly used for ease of manufacturing. Hydrophobic coatings can be any natively hydrophobic material such as Teflon®, silanes, or waxes. The combination of the surface roughness and hydrophobic coating causes a droplet of water to bead up like a marble due to the surface tension between the water droplet, the surrounding air, the SH surface and the air in the cavities of the surface..

On SH surfaces, the water droplet can exist in one of two states shown in Figure 1.3. In the first state, known as the Cassie-Baxter state, the water droplet sits on top of the surface structures with air filling the cavities below the droplet as shown in Figure 1.3 (left). These air cavities minimize the area in which the droplet is in contact with the surface, thus minimizing the attractive forces between the droplet and the surface. A meniscus (not shown) between the surface structures supports the water droplet on top of the surface structure, preventing the droplet from flooding the cavities. This meniscus is maintained by the surface tension between the water droplet and the air inside the cavities. Consequently, the water droplet exhibits the highest possible CA. This creates a very mobile droplet, rolling at the lowest possible SA. Cassie and Baxter showed that the CA, θ, of a droplet in this state can be calculated using the Cassie-Baxter equation given in Equation 1.2 [15]

$$\cos(\theta) = rF_c \cos\theta^0 + F_c - 1 \tag{1.2}$$

where r is the roughness factor, or the ratio between the total surface area and projected area, and F_c is the cavity fraction, or ratio between the area on top of the surface structures and the projected area. The cavity fraction will be further defined in Section 1.2.3. The Young's contact angle, θ^0 is the CA of a droplet on smooth hydrophobic surfaces with the same hydrophobic coating and can be calculated by Equation 1.3

$$\gamma_{LV}\cos\theta^0 = \gamma_{SG} - \gamma_{SL} \tag{1.3}$$

where γ_{LV}, γ_{SG}, γ_{SL} is the surface tension between the liquid-vapor, solid-gas, and solid-liquid interfaces respectively. Generally speaking, γ_{LG} is the dominate term which influences the overall behavior of any liquid, including water, on a SH surface.

If the hydrostatic pressure of the droplet exceeds the LaPlace pressure, the droplet will flood the cavities transitioning to the Wenzel state as shown in Figure 1.3 (right). This is the second state in which a droplet can exist on a SH surface. The LaPlace pressure is given as

$$\Delta P = \gamma_{LG}(1/R_1 + 1/R_2) \tag{1.4}$$

where R_1 and R_2 are the two primary radii of curvature of the meniscus between the cavities. In the Wenzel state, the droplet is pinned to the surface because of the increased liquid-solid surface contact area. Consequently, the CA decreases and the SA increases. Note the difference in CA, θ, between the Cassie-Baxter droplet and the Wenzel droplet in Figure 1.3. This is important because the droplet is not as mobile on the surface and therefore can not roll off the surface as easily [16]. The CA, θ, of a droplet in the Wenzel state on a SH surface can be calculated using Equation 1.5.

$$\cos(\theta) = r\cos\theta^0 \tag{1.5}$$

again where r is the roughness factor and θ^0 is Young's contact angle. In some cases, such as condensation, the droplets can exist in a mixture of the Cassie-Baxter and Wenzel state. This occurs when some sections of the droplet are suspended over the rib cavities in the Cassie-Baxter state and other areas of the droplet penetrate into the cavities. Consequently, the CA and SA of these droplets typically measure in between a droplet fully in the Cassie-Baxter state and the Wenzel state.

I now give a background on how SH are manufactured followed by an overview of some of the applications related SH surfaces including drag reduction, anti-icing and de-icing, condensation, and self-cleaning.

1.2.2 Manufacturing Methods of Superhydrophobic Surfaces

Multiple methods have been developed to manufacture SH surfaces. These methods vary widely from subtractive methods to additive methods. Regardless of the method, the primary goal is to create a rough surface structure that is hydrophobic, either natively or by the use of a hydrophobic coating. Surface structures also greatly vary from random roughening of the surface to very organized and uniform surface structures. Researchers may opt to focus on surfaces structures arranged in repeating patterns, such as ribs and posts, to better predict the fluid dynamic behavior of the surface. However, manufacturing these surfaces can be more complex, expensive, and time consuming than random roughening manufacturing processes. Each process results in a different scale, type, and robustness of the surface. Consequently, a great deal of research articles have been written towards this topic of manufacturing SH surfaces.

Subtractive methods for manufacturing are those which remove material. In the case of SH surfaces, this generally means carving, etching, or machining the surface structures out of the existing surface. One such method for this is referred to as templation. Templation is useful for mimicking the surface structure of a pre-exisiting surface, such as the Lotus leaf and other SH surfaces found in nature. Essentially, a master textured surface is used for molding a new surface and then lifted off, dissolved, or removed some other way from the newly formed SH surface [17–19]. Another method used to create SH surfaces is via photolithography. This method involves using using irradiation through a mask to create a desired feature pattern on the photoresists on the surface. Then, using various etching techniques such as plasma and chemical etching, the surface features of the surface are carved out of the parent material. Typically, a hydrophobic coating must be applied to the structured surface to render the surface super hydrophobic. [4, 14, 20, 21]. Finally, plasma treatment is a third method which can be utilized for subtractive manufacturing of SH surfaces. In this process, plasma etching accelerates reactive atoms and ions in the boundary layer between the substrate to create deep cavities with steep walls [22–24]. A hydrophobic coating may

need to be then applied to the surface depending if the original substrate was natively hydrophobic or not.

Additive methods, bottom-up methods involve building up surface structures like building blocks. These methods can used in nano-structure fabrication on SH surfaces and may combined with subtractive methods to create a two-tier surface exhibiting both micro-structured and nano-structured features. One common additive method is referred to as chemical deposition. In this process, products of chemical reactions deposit on suitable substrates creating a variety of surface structures and morphologies. Various depositions methods can be used including chemical bath deposition, chemical vapor deposition, and electrochemical deposition [25–27]. Another additive method called colloidal assemblies utilizes van der Waals forces of various closely packed particles on the surface to create a textured surface. These particles can either be spin-coated or dip coated to the surface [28, 29]. A third additive manufacturing process to create SH surfaces is called layer- by- layer deposition. As the name of this method implies, polyanions and polycations are alternatively applied to a surface using their electrostatic charge to build up the surface structure necessary for the SH surface [30–32] . Often times, for any additive method, the material applied to the surface is natively hydrophobic and so application of a hydrophobic coating is not always necessary.

One of the biggest challenges of SH surfaces is creating a surface which will maintain its superhydrophobicity. Natural SH surfaces found in nature have a unique advantage as the living organism can continually replace and self-heal its surface structure and SH coating. This is primarily due to cellular reproduction. Artificial SH surfaces do not have this advantage and so wear down with time, frequently due to abrasion to the micro-structures and nano-structures or coating. At this time and to this author's knowledge, few studies have demonstrated surface roughness-regenerating surfaces [33]. Degradation of the hydrophobic coating also limits the current use of SH surfaces. Some researchers are investigating surfaces in which additional hydrophobic chemicals can be stored in a porous media and can replace the exterior, hydrophobic coating as it degrades [34–36]. However, unlike natural hydrophobic coatings, these surfaces still only have a finite life span until all the hydrophobic chemical has been degraded. Because of this, much work is still needed to develop commercially available, durable, hydrophobic surfaces. Li et al. and Xue

et. al give a more detailed and extensive summary of the manufacturing processes fro SH surfaces discussed in this section [33, 37].

1.2.3 Drag Reduction on Superhydrophobic Surfaces

One unique aspect of SH surfaces is the reduction of solid-liquid contact area between a droplet in the Cassie-Baxter state and the surface as was shown in the left panel of Figure 1.3. Due to the air filled cavities, water can flow over a SH surface in the Cassie-Baxter state with a shear free condition exist above the gas. However, if the hydrostatic pressure of the fluid increases above the LaPlace pressure (Equation 1.4), the water will flood the cavities and transition to the Wenzel state.

Typically, on a non-SH surface, a no-slip condition exists in which the fluid directly in contact with the surface flows at the same velocity as the surface. This means, that if the surface is stationary, the fluid directly in contact with the surface must also be stationary regardless of the velocity of the fluid through the rest of the system. This creates a velocity profile in which the velocity of the fluid changes spatially. This velocity profile results in a shear stress at the surface, τ_w, which can be calculated using Equation 1.6

$$\tau_w = \mu \left. \frac{\partial u}{\partial y} \right|_{wall} \tag{1.6}$$

where μ is the viscosity of the fluid, u is the velocity of the fluid parallel to the wall, and y is the direction perpendicular to the surface.

However, at the air-water interface of the cavities, the low viscosity of the air exerts very little shear stress on the water [38]. Where an air-water interface exists, as indicated by the blue regions of Figure 1.4a, the no slip condition is replaced by a shear free boundary condition. The water-solid interface regions on top of the surface structures, where the no slip condition still holds, are indicated by the red region of Figure 1.4a. An aggregate shear stress of the two regions results in an apparent slip at the plane of the water-surface interface. Figure 1.4b shows a representative aggregate velocity profile of a fluid flowing over a SH surface as indicated by the red arrows and the solid red line. As is evident by this velocity profile, a velocity at the surface exists and is termed a slip velocity, u_s.

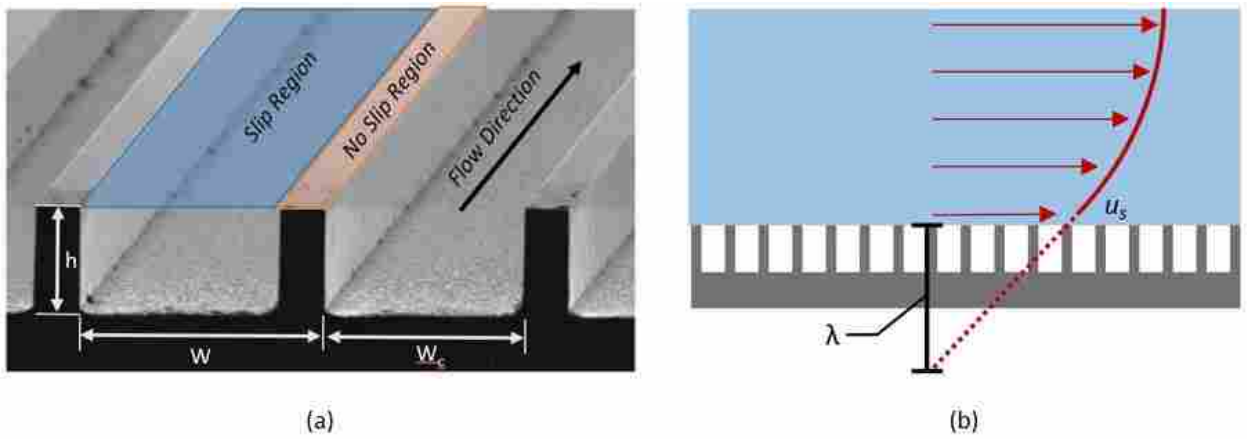

Figure 1.4: (a) SEM image with air-water interfaces indicated in blue and solid-water interfaces indicated in red. (b) The aggregate velocity profile over a SH surface indicated by red arrows. Note that in Figure (a), the flow direction is longitudinal to the rib structures and in Figure (b) the flow direction is transverse to the rib structures.

The slip length, λ, shown in Figure 1.4b, represents the distance into the surface the velocity profile would extend to reach a no slip condition. This slip length is based on a local extrapolation of the velocity profile, as indicated by the red dotted line. This can be used to calculate the slip velocity, u_s, of the surface given Equation 1.7 [39],

$$u_s = \lambda \left. \frac{\partial u}{\partial y} \right|_{wall} \tag{1.7}$$

which is the aggregate velocity of the fluid at the plane of the wall. The slip length is a function of the cavity fraction and naturally increases as the cavity fraction increases. Intuitively, this is expected as increasing the air- water interface region would increase the shear-free region of the surface, presuming the fluid remains in the Cassie-Baxter state.

Utilizing SH surfaces for the purpose of drag reduction can be advantageous in many industrial scenarios including shipping, piping, and micro-fluidics. In some cases, SH surface have shown a drag reduction of up to 40% [10, 38]. The geometric configuration of the micro-structures of SH surfaces has proven to be a significant factor in achieving the greatest drag reduction. Several researchers have shown that flow longitudinally along rib structures is preferred so as to create long uninterrupted paths of shear-free flow. Additionally, rib-structures consistently out perform post

structures. Also, researchers have shown that post structures perform better in a regular, repeating pattern as opposed to a staggered patten [10].

There are two significant challenges towards the application of SH surfaces in industries for the purpose of drag reduction. The first is the durability of the SH surface. As discussed in Section 1.2.2, abrasion to the surface quickly wears down the surface structures and hydrophobic coating. Explicitly, even though the overall shear stress is reduced due to the water-air interface, the reduced water-solid interface means that the shear stress is more centralized on the surface features causing increased wear on the surface. The second challenge is if the hydrostatic pressure exceeds the LaPlace pressure, than water will flood the surface and transition to the Wenzel state [40, 41]. When this happens, the advantageous shear-free region and is replaced by greater contact area of the water-solid interface, resulting in a drag increase. While some researchers have investigated restoring the Cassie-Baxter state by keeping the cavities pressurized, injecting air bubbles, gas generation, and electrolytic recovery, most proposed solutions have proven challenging and problematic [42]. Developing a durable and feasible surface structure is the primary focus of many researchers to achieve drag reducing surfaces.

1.2.4 Anti-Icing and De-Icing using Superhydrophobic Surfaces

Ice build up is a critical issue in many industries and results in the failure of systems including airplanes, wind turbines, and power lines. Each winter, ice results in billions of dollars in damages [43]. SH surfaces have also shown potential to assist in preventing ice build up and de-icing [44, 45].

Icing on surfaces can occur in two different ways. First, small micro-droplets in the air can impact a sub-cooled surface and subsequently freeze to that surface creating a layer of ice across the surface. Second, water droplets can nucleate on a supercooled surface and subsequently freeze over into frost. This is referred to as condensation frosting. Using SH surfaces, two different methods, known as the anti-icing approach and de-icing approach, have been developed to prevent and remove ice from a surface.

Anti-icing is a passive method which prevents water droplets from building up on a SH surface. Because of the low hysteresis of SH surfaces, micro-droplets in the air that impact the surface are easily able to bounce or slide off the surface due to external forces such as gravity

and aerodynamic drag. Additionally, because of the reduced water-solid interface between the droplet and surface (presuming the droplets are in the Cassie-Baxter state), heat transfer between the droplet and surface is minimized. Consequently, the onset of heterogeneous ice nucleation is delayed long enough for the droplet to roll off the surface. Many researchers have shown that in a laboratory setting this is an effective way to prevent water droplets from freezing on the surface [46–50].

In addition to micro-droplets impinging on a surface, ice frequently forms via condensation frosting. This occurs in humid environments where water molecules in the air condense on a subcooled surface and immediately freeze to the surface. Unfortunately, due to condensation beginning everywhere on the surface, including within the cavities of the surface structure, condensation frosting can still occur on these surfaces, although total ice buildup is still diminished [47, 51–54]. Consequently, more active approaches are needed to prevent ice from forming on SH surfaces, such as applying heat to the surface. This is referred to as a de-icing approach.

De-icing can occur at one of two phases of the ice build up. First, the surface can be heated after the frost has already formed on the surface. Murphy et. al recently showed that frost on supercooled surfaces can be easily removed during melting on nano-structured surfaces. During condensation frosting the frost essentially freezes around the entire nano-structured surfaces, including in the cavities of the surface structures. However, as the frost melts, the water droplets in the cavities spontaneously transition to the Cassie-Baxter state, exhibiting all the desirable properties of a droplet in such a state including a low hysteresis and SH. This make the droplet very mobile and able to slide off the surface with minimal external forces [55].

Antonini et. al investigated an scenario in which they combined anti-icing and de-icing methods. In their study, they examine how ice builds up on a NACA0021 airfoil where the leading edge is heated in a climate controlled closed loop wind tunnel. Without heating, ice would build up on the airfoil. However, heating the airfoil along the leading edge of the wing delayed ice formation on the surface, but did not prevent it. Water droplets would form along the leading edge and be pushed towards the back of the wing due to aerodynamic drag. Because only the leading edge was heated, the water droplets would freeze along the trailing edge of the wing. The same droplets formed on an airfoil coated with a SH surface. However, because of the low hysteresis and SA, the droplets were quickly swept away due to aerodynamic drag so that no ice build up could

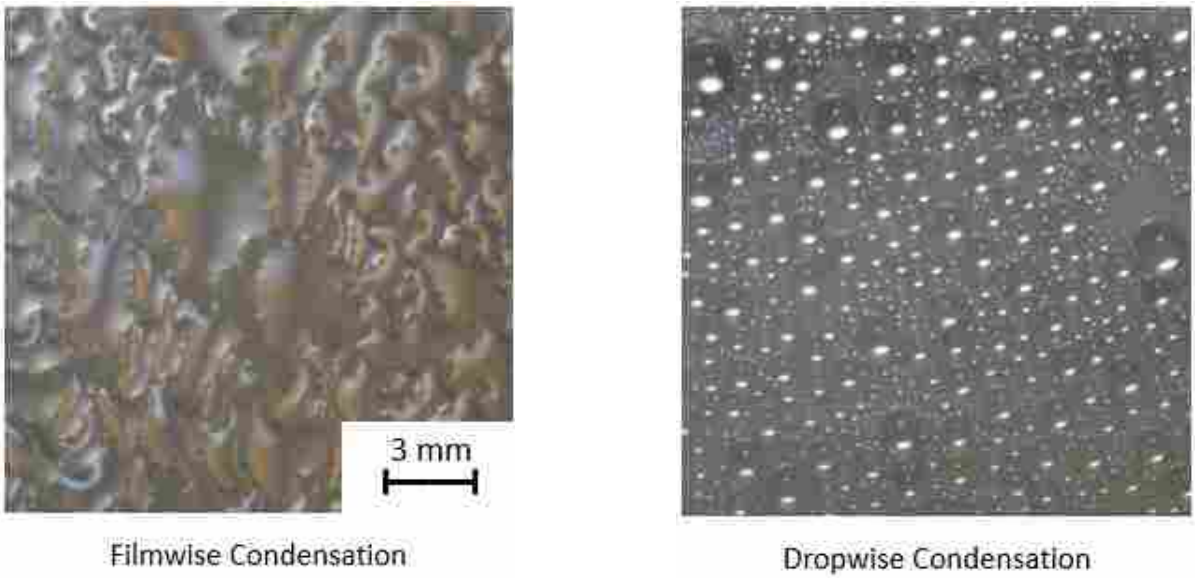

(a) (b)

Figure 1.5: (a) Filmwise condensation occurs on smooth, hydrophilic surfaces where the condensed water forms a thin film across the entire surface. (b) Dropwise condensation occurs on SH surfaces where the water droplets bead up like a marble and are easily mobile on the surface.

occur on the surface. From their study, they conclude that the combination of heating the leading edge and coating the surface with a SH surface can be very beneficial in preventing ice build up on the surface [56].

1.2.5 Condensation on Superhydrophobic Surfaces

SH surfaces also show improved heat transfer potential through condensation. Condensation is frequently observed in nature and an extremely important aspect in many industrial applications such as energy production, water harvesting, water desalination, thermal management, and environmental control [57]. All these systems can benefit greatly from improved heat transfer through the application of SH surfaces.

When water vapor cools on a smooth, hydrophilic surface, it transitions from a gaseous to a liquid state. Because water droplets are attracted to hydrophilic surfaces, the droplets will spread out across the surface, maximizing the contact area with the surface. As these droplets coalesce together, they create a film of water across the surface. As the film layer of water thickens due to continued condensation, the heat transfer resistance also increases which reduces the overall

efficiency of the condensing system. This type of condensation is referred to as filmwise condensation and and is shown in Figure 1.5a in which the film of condensed droplets has spread across the entirety of the surface.

On SH surfaces, condensation is drastically different and has been the topic of a number of research articles [58–63]. Because of the hydrophobic nature of the surface, the condensed droplets bead up as shown in Figure 1.5b. Due to the concentrated heat transfer, the majority of the condensed droplet initially nucleate in the cavities of the surface structures and grow to fill these cavities [64]. Consequently, often times these condensed droplets are in the Wenzel state, especially on micro-structured surfaces. Wier and McCarthy confirmed that these water droplets are in the Wenzel state by comparing the hysteresis of the surface before and after water droplets condensed on the surface. In the case where condensed droplets were present, the hysteresis was significantly higher than the hysteresis on dry surfaces implying that the condensed droplets were in the Wenzel state [11].

Several articles, however, have reported that these condensed droplets can jump from the Wenzel state to the Cassie-Baxter state upon coalescence with other droplets. Boreyko and Chen showed that when two droplets coalesce and minimize their surface energy, the excess energy is released and the new combined droplet spontaneously jumps off the surface. This is caused by the liquid bridge between the two coalescing droplets impinging upon the SH surface and pushing the droplet away from the surface. When the surface is orientated horizontally, the newly formed droplet is found sitting in the Cassie-Baxter state after it has spontaneously jumped off the surface and fallen back down [58]. Qu et al. observed that droplets that initially nucleated around two-tiered posts can jump laterally across the surface. When they do so, these droplets run into other condensing droplets initiating a second droplet coalescence event and spontaneous jumping [65]. Dorrer et al. observed that droplets can exist in both the Cassie-Baxter state and Wenzel state. They showed that dewetting of the surface, or transition from the Wenzel to the Cassie-State, can occur when a condensed droplet in the Wenzel state coalesces with a droplet in the Cassie-Baxter state [66]. This spontaneous jumping motion has primarily been observed on nano-structured surfaces and two-tiered structured surfaces. In the case of many pure micro-structured surfaces, the energy released is not sufficient enough to overcome the adhesive forces between the droplet

and the surface structures and the droplets do not jump, but may transition from the Wenzel to the Cassie-Baxter state.

The advantage that SH surfaces offer during condensation in terms of heat transfer is the mobility of the condensed droplet on the SH surface. Again, because of the low hysteresis and SA of the surface, newly condensed droplets can be removed from the surface with minimal external force. Additionally, condensed droplets that jump off the SH surfaces orientated vertically to not fall back onto the surface. There are three significant factors related to the improved heat transfer as condensed droplets are removed from the surface. First, energy the water vapor absorbed during the condensation process is also physically removed from the surface when the droplet jumps or rolls off the surface. Second, as the condensed droplets are swept away or jump off the surface, nucleation sites where they were sitting on the surface are continually freed. Nucleation sites of condensation represent high heat fluxes as droplets form and are typically found at defects on the surface. Because these nucleation sites are continually made available, higher heat transfer rates occur. Finally, as noted during filmwise condensation, the condensed film of water acts as an additional thermal resistance layer and partially insulates the surface. Because no film of water develops on the surface, this additional thermal resistance does not exist during dropwise condensation. All these factors lead to increased heat transfer coefficients on SH surfaces during condensation [57].

1.2.6 Self-Cleaning Properties of Superhydrophobic Surfaces

Finally, SH surfaces have shown potential for serving as passive, self-cleaning surfaces [1, 3, 12]. As discussed in Section 1.1, there are a number of applications in which SH surfaces can be utilized as self-cleaning surfaces. These include but are not limited to improved visibility through windows, improved irradiation absorption on solar panels, and minimized bacteria growth on a SH surface [67]. While the concept of self-cleaning surfaces is generally accepted, few studies have investigated how effective SH surfaces are at removing different contaminants from the surface. This study aims to add to the overall understanding of the self-cleaning dynamics and to compare the cleaning efficiency on SH surfaces when each contaminated surfaces is cleaned by rolling water droplets over the surface and by exposing the surface to condensation such that the condensed droplets clean the surface.

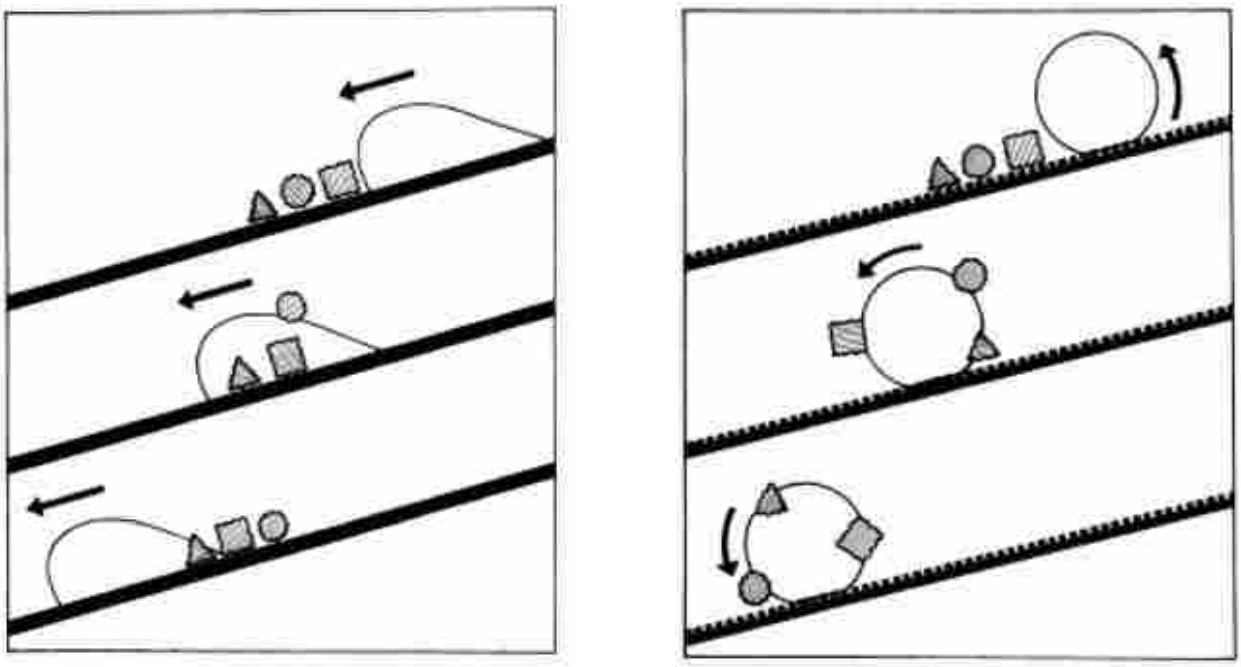

(a) (b)

Figure 1.6: Schematic showing a water droplet sliding over a smooth surface (a) and rolling over a SH surface (b). In case (a), the contaminates, represented by the triangle, circle, and square, are left behind on the surface while in case (b) the same contaminates adhere to the rolling droplet and are removed from the surface. (Figure adapted from Barthlott and Neinhuis's work [1]).

When an arbitrary object is placed on an inclined surface, it can roll down the surface, slide down the surface, or stay stationary on the surface. Typically, circular objects, like cylinders and spheres, prefer to roll down the surface while other objects, like cubes, will slide down the surface or remain stationary on the surface. Rolling occurs when the center of gravity and frictional force of an object creates a coupled moment sufficiently large enough to form a pivot point on the leaded edge of the object. This is generally caused by the minimized contact area between a cylinder or sphere and the surface. This same phenomena is seen when water droplets are placed on an inclined SH surface. Essentially, because of the high contact angle and low hysteresis, the water droplet behaves like a sphere and rolls, not slides, off any inclined SH surface [13].

This behavior of water droplets rolling over SH surfaces is key for self-cleaning. Barthlott and Neinhuis illustrate how a water droplet removes contaminants from a surface as shown in Figure 1.6a. In the left panel, a water droplet with a large hysteresis is shown sliding on a smooth surface. As this water droplet slides across the surface, it encounters some particulates, represented

by a triangle, circle, and square, which it picks up. Because of the small receding angle on the tail end of the droplet, these particulates are left behind on the surface as the droplet continues down the slope. Conversely, in Figure 1.6b, a water droplet is shown rolling over a SH surface. Because of surface tension, the water droplet maintains its spherical shape as it rolls over the SH surface. When this droplet encounters the same contaminants, the particles adhere to the droplet and the rolling motion of the droplet prevents the particles from being deposited on the surface again. This is primarily caused by the high receding angle, or trailing angle, of the droplet which gives both the droplet and the attached contaminants rolling momentum. Consequently, these particles roll with the droplet as it rolls off the surface, thus creating a self-cleaning effect [1]. This self cleaning phenomena causing by rolling droplets on a SH surface was first seen on the lotus leaf and thus coined the "Lotus Effect" in 1977 [68].

Quan et. al confirmed these observation in their study on self-cleaning surfaces via droplet impingement. Using high speed imaging, they studied droplets impinging on SH surfaces, hydrophobic surfaces, and hydrophilic surfaces contaminated with dust particles and observed that the receding angle is the deciding factor in the droplet's ability to remove the dust particle. They conclude that self-cleaning is realized in two steps, first that the particle adheres to the droplet and second that the droplet recoils and releases after impinging on the SH surface [67]. Performing a force balance analysis, they conclude that interface force between the dust particles and the droplet and the Van der Waals forces between the dust particle and the surface are dominating forces which determines if a impinging droplet will remove a dust particle from the surface [67, 69, 70].

Yu et. al claim that there are four primary criteria for self cleaning surfaces: 1) high CA, 2) low SA, 3) low adhesion force between the surface and the particles, and 4) proper particle size [71]. Several articles have been published discussing various techniques to make SH surfaces to satisfy these requirements [72–83]. However, only three studies have been performed to systematically analyze the dynamics and efficiency of self-cleaning surfaces [1, 3, 12]. Between these studies, the general consensus is that nearly all particles loosely deposited can be removed from SH surfaces. Surprisingly, beyond these three studies, very little work has focus on the efficiency of SH surfaces.

First, Barthlott and Neinhuis investigated water droplets rolling over various contaminated leaves and estimated how effective these leaves were at removing the natural contaminates from the

leaf's surface. In their study, they examined the self-cleaning properties of eight different species of plants, half of which had leaves that exhibited SH properties and the other half which exhibited hydrophilic properties. Each leaf was contaminated with several different particulates including dried soil, barium sulphate, silicon carbide (SC) dust, quartz dust, and more. The contaminated leaves were then cleaned for 2 mins using a sprinkler which produced water droplets between 0.5-3 mm in diameter to simulate a rain shower. Using SEM imaging to count the number of particles on the surface both before and after the simulated rain, it was determined that the hydrophilic leaves retained 40-80% of the contaminates on their surface while all the contaminates were removed from the SH leaves [1]. In a separate report, Barthlott and Neinhuis give an overview of the various plants that exist which can exhibit self-cleaning properties and discuss the molecular characteristics of these plants [84].

Furstner et. al considered the self-cleaning properties on three types of artificial SH surfaces including silicon wafer with various post arrays, replicates of water-repellent leaves, and commercial metal foils hydrophobized with a fluoridating agent. Each surface was then contaminated with a luminescent and hydrophobic powder and then cleaned using a fog treatment which produced micro-droplets on the surface ranging from 8-20μm and by simulated rain showers similar to the cleaning process used by Barthlott and Neinhuis. Using SEM imaging, the number of particles on the surface were counted before and after the surfaces were cleaned. Their results showed that the fog treatment was very effective at removing contaminates from the surface for surfaces with pronounced structures less than 5μm. Without these cavities, a film of water would form on their surfaces. Additionally, by varying the Weber number of the rain droplets in the simulated rain shower, Furstner et. al were able to vary the impact pressure of droplets on the contaminated surface. This experiment showed that less contaminates remained on the surface with greater the impact pressure. From their study, Furstner et. al determine that kinetic energy is one of the major factors that influence the overall cleaning efficiency of the surface [12].

Bhushan et. al. performed similar studies on artificial SH surfaces in which they considered the difference cleaning efficiencies of various surface structures. In their study, they consider surfaces composed of nano-structures, micro-structures, and two-tier structures composed of both micro-structures and nano-structures. Two chemical hydrophobic coatings were utilized including plant wax extracted from the Lotus leaf and alkane n-hexatriacontane ($C_{36}H_{74}$). Their surfaces

were contaminated with Silicon Carbide (SiC) and subjected to the same simulated rain storm as Barthlott and Neinhuis. Silicon Carbide (SiC) was chosen for of its similar hydrophilicity, shape, and size to that of natural dirt. During cleaning, the surfaces were situated at their respective SA (3-10°) and 45°. Using SEM images, the number of particles on the surface were counted both before and after the surface was cleaned. The results of their study show two factors related to self-cleaning properties. First, the tilt angle of the surface played a significant role in the self-cleaning efficiency as the surfaces tilted at 45° consistently had less particles on the surface than the respective surfaces situated at their SA. Second, they determined that surfaces with two-tiered structures consistently exhibit higher cleaning efficiencies than micro-structured and nano structured surfaces, which were about equal. This is because the two-tiered structure minimized the contact area of both the water droplets and the contaminating particles [3].

One unique aspect that this thesis considers is utilizing the self-cleaning properties of SH surfaces during condensation. To this author's knowledge, only two studies have considered this possibility to date [2, 85]. The first study was performed by Wisdom et. al. in which they considered the condensation on cicada wings, a natural SH surface. As discussed previously, condensed droplets on certain surfaces may experience a spontaneous jumping motion upon coalescence with other condensed droplets. During their study, Wisdom et. al. observed that the condensed droplets would engulf and lift the particulates off the surface when it coalesced with other condensed droplets and experienced this spontaneous jumping motion. This is advantageous as the Van der Waals forces, which promotes adhesion of the particulate to the surface, primarily acts perpendicular to the surface. Consequently, the out-of-plane jumping motion dislodges the adhered particulate from the surface. Other cleaning methods such as air or water streams remove the contaminate by the use of shear stress which acts parallel to the surface. Wisdom et. al dubbed this self propelled cleaning method as the "Cicada Effect" because it was first observed on cicada wings [85].

Watson et. al. observed that the lotus leaf lives in an environment which experiences long season without rain, but still experiences condensation on a regular basis. They show that similar to a cicada wing, particulates are removed from the lotus leaf via jumping condensed droplets. During these dry seasons, condensation is the primary way in which contaminates are removed from the lotus leaf. The implication of this is that surfaces placed in an environment that experiences frequent condensation can passively clean themselves without any outside interference [2].

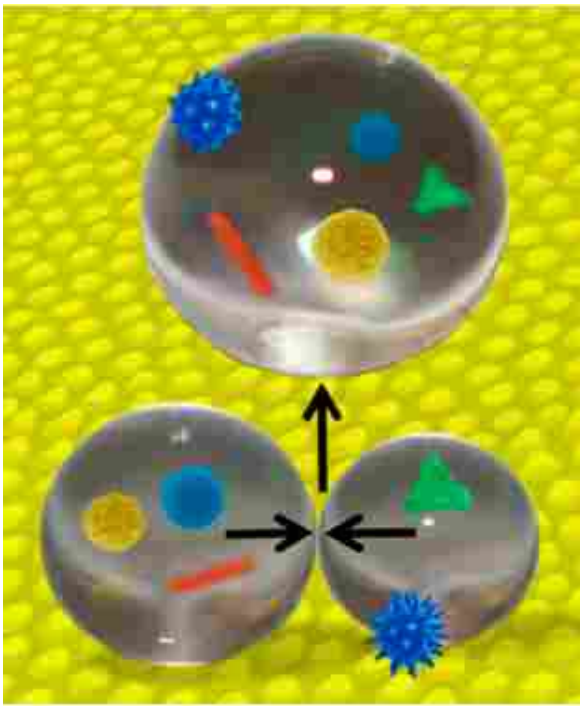

Figure 1.7: Schematic demonstrating the cicada effect in which two small condensed droplets coalesce and spontaneously jump off the surface, removing any contaminate adhered to or engulfed by the droplet. This figure is adapted from Watson et al. [2]

Furthermore, Watson et. al. illustrates the "Cicada Effect" as shown in Figure 1.7 in which a schematic of two small, condensed droplets are shown coalescing together and jumping off the surface. Various particles, represented by red, yellow, green, and blue particulates, are shown entrapped by the two initial droplets and still engulfed in the coalesced droplet after coalescence and jumping off the surface. If the surface is vertical, the aggregate droplet will not fall back onto the surface due to gravity. Thus, the contaminates engulfed by the condensed droplets are successfully removed from the surface.

1.3 Contributions

While Wisdom et. al and Watson et al. have established the practicality of self-cleaning surfaces via condensation, studies have not yet quantitatively measured the efficiency of utilizing condensation as a method of self-cleaning SH surfaces. Additionally, to date no study compares the efficiency of cleaning via condensation to the more traditional approach of cleaning via simulated rain showers and rolling droplets over the surface as performed by Barthlott, Furstner and Bhushan.

This study seeks to bridge the gap between these two cleaning methods to better understand the dynamics of self-cleaning surfaces and concludes that condensation and rolling droplets can have the same cleaning efficiency on SH surfaces.

Additionally, this thesis considers the effects of surface structure size on the cleaning efficiency of the SH surfaces. To do this, the cleaning efficiency on various SH surface structures, including micro-structured surfaces, nano-structured surfaces, and smooth hydrophobic surfaces, are examined in this study. The results of this thesis show that the cleaning efficiency is unaffected by surface structure size. However, this thesis concludes that SH surfaces are preferable to smooth, hydrophobic surfaces for self-cleaning applications because of the mobility of the droplet, as indicated by the SA of the surface. To date, only Bhushan et al. report the effects of surface structure size on the the cleaning efficiency of SH surfaces [3].

Finally, the contaminates used in this study, including salt, tobacco, and pollen, vary significantly from the contaminates used in previous studies. These three contaminates are common contaminates found in nature that typically have negative effects on industrial applications. This thesis shows that the cleaning efficiency of the SH surface is primarily driven by the contaminate and not the cleaning method or surface structure. To date, most contaminates used in self cleaning studies have all been loosely bound and scattered across the surface. Consequently, these contaminates are easily removed as water droplets roll over the surface. Because of the stronger adhesion between tobacco and the surface and pollen and the surface, this study shows that not all contaminates can be removed from SH surface.

1.4 Thesis Organization

The overview presented of several different applications of SH surfaces has noted that not much work has been dedicated to understanding the intricacies of the self-cleaning properties of SH surfaces. For this reason, I aim to further explore the efficiency of the self-cleaning properties of SH surfaces as they are cleaned by water droplets rolling over the surface and by condensation. In the subsequent chapters of this thesis, experiments will be described for evaluating how effectively various contaminates are removed from two types of SH surfaces. One will be composed of micro-structures and the other with nano-structures. They will be cleaned via rolling water droplets and via condensation. Contaminates considered include salt deposits, tobacco residue, and pollen.

Chapter 2 of this thesis will discuss the methodology used in the experiments including the contamination procedures, cleaning procedures, and a discussion of how the surface cleanliness is evaluated. Chapter 3 of this thesis will present and discuss the results of the experiments performed. This will include a discussion of how effectively each contaminate was removed from the surface, a comparison between the two cleaning methods used in this study, and an analysis of the effect of surface structure scale. Lastly, Chapter 4 will present the important conclusions drawn from this study as well as ideas for future work. The raw data collected for this study will be presented in Appendix A.

CHAPTER 2. METHODOLOGY

This chapter describes the methodology used throughout this study. It is broken up into five sections. The first section discusses the processes used to contaminate the surfaces. Then, the two cleaning processes used in this study are described. The third section gives a description of the equipment used to measure the CA and SA on each SH surface. Fourth, a discussion with regard to determing the cleaning efficiency of each cleaning method is presented. The final section summarizes the overall process used in this study.

This study primarily focuses on comparing the cleaning efficiency of micro-structured SH surfaces to the cleaning efficiency of a nano-structured SH surfaces. Two methods to clean the surfaces are examined including first rolling water droplets over the surface and second condensing droplets on the surface until the droplets grow large enough to roll off the surface. The CA and SA are used to estimate the surface cleanliness. Surfaces contaminates considered in this study include salt, tobacco, and pollen.

The micro-structured surfaces were fabricated in the Brigham Young University clean room. This is accomplished using photolithography and surface etching techniques to create a rib pattern structures on silicon wafers. Teflon® coating, a natively hydrophobic coating, was then applied to the structured surfaces rendering the surface superhydrophobic [14, 86]. The micro-structures used for this study are 25μm tall and an approximate pitch of 15μm with a 70% cavity fraction.

Nano-structured surfaces used in this study were provided by Moxtek, Inc. Details of the fabrication processes and the applied hydrophobic coating for these nano-structured surfaces are proprietary and will not be disclosed in this thesis. The nano-structured ribs are nominally two orders of magnitude smaller than the micro-structured surfaces at a few hundred nanometers tall with a pitch approximately 100 nm wide. The cavity fraction agin is 70% to provide a more direct comparson between the micro-structured and nano-structured surfaces.

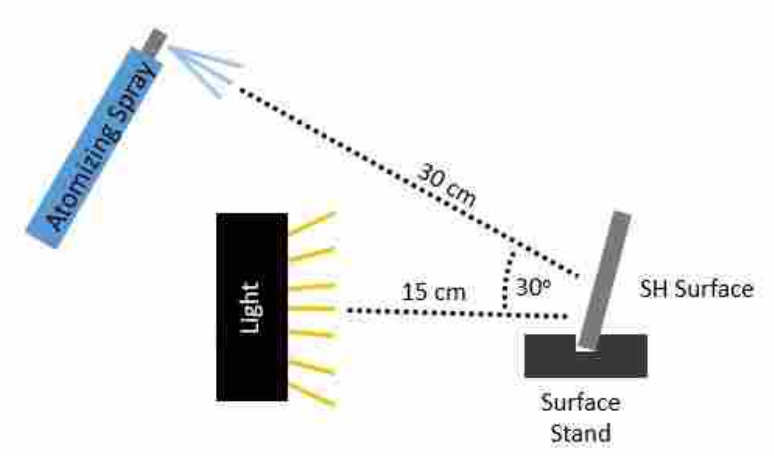

Figure 2.1: Schematic of setup to contaminate SH surface with salt. Note, measurments are not to scale.

The self cleaning properties on smooth surfaces with Teflon® coating or the proprietary coating used on the nano-structured surfaces are also considered in this study. These surfaces do not consist of any micro or nano structures, allowing for a controlled surface where only the surface chemistry is varied. Smooth surfaces composed of the Teflon® used on micro-structured surfaces and smooth surfaces composed of the proprietary hydrophobic coating used on the nano-structured surfaces are both considered in this study.

2.1 Contamination Processes

This study focuses on removing 3 common contaminates that may accumulate on exposed surfaces in industrial applications: salt, tobacco, and pollen. This section is dedicated to discussing how each of these surfaces are contaminated. Each contaminate greatly effects the hydrophobicity and self-cleaning properties of the SH surface. As such, these effects of each contaminate will be individually discussed later in this study.

2.1.1 Salt Deposits

An atomizing spray bottle containing saturated salt water was utilized to contaminate the SH surfaces with salt. The setup to contaminate a SH surface with salt is shown in Figure 2.1. The surface was placed under a halogen light, 15 cm away from the light base, and allowed to heat

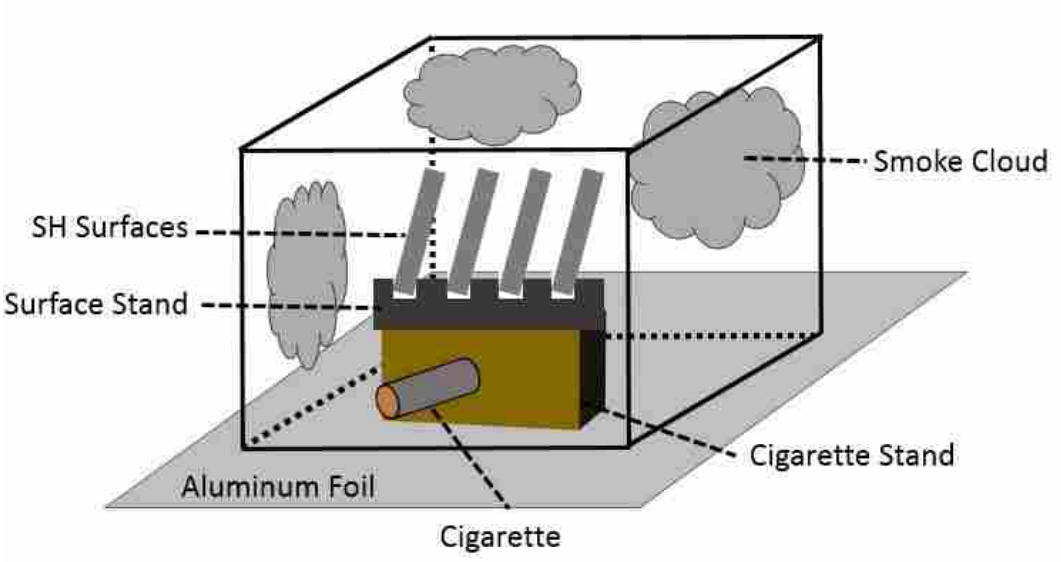

Figure 2.2: Schematic of setup to contaminate SH surface with tobacco.

due to the intensity of the light to approximately 80°C . The saturated salt water was then sprayed on the surface from approximately 30 cm away from the surface at a 30° angle. This covered the surface with salt saturated micro-droplets. The atomizing spray bottle discharged 0.158±0.02g of saturated salt water per spray. The water was then evaporated from the surface, leaving behind small salt crystals. Evaporation occurred quickly because of the high heat from the halogen light and low local relative humidity (about 20%).

The amount of saturated salt water discharged from the atomizing spray bottle was determined by discharging a single spray of the saturated salt solution into a dry paper towel from 30 cm away and at an angle of 30° (similar to the salt contamination process). The mass of the paper towel was measured both when dry and wet and the differnece indicated the mass of the salt water deposited on the paper towel . This process was repeated 20 times, resulting in an average discharged mass of 0.158±0.02g. Only the mass ofthe salt water solution and not the total mass of the salt discharged from the spray bottel was determined using this approach. To ensure the salt solution was saturated, enough salt was mixed into the solution such that salt crystals were always present in the solution and could not be further dissolved into the water.

Figure 2.3: Pollen from Morning Glories (left), Petunias (middle), and Daylily (right) flowers were used to test the self-cleaning properties on SH surfaces.

2.1.2 Tobacco Residue

Tobacco residue was deposited on a SH surface by completely burning a single 0.85g cigarette 80 mm long. Marlboro® cigarettes were used because of their popularity throughout the United States [87, 88] . This was done under a fume hood in a 12cm x 12cm x 12cm enclosed box referred to as a burn box and is shown in Figure 2.2. Four surfaces were contaminated at a time, each situated nearly vertically approximately 5cm above the cigarette. The enclosed burn box was used to confine the smoke from the cigarette to the air immediately surrounding the surfaces, accelerating the tobacco deposition rate. The contained smoke could then adhere to the SH surfaces. The surfaces were only removed from the burn box once the cigarette was completely burned and the smoke had dissipated. Tin foil was placed under the cigarette to collect the ashes from the cigarette.

2.1.3 Pollen Particles

Ipomoea purpurea (Morning Glories), Petunia integrifolia (Petunias), and Hererocallis (Daylily), all shown in Figure 2.3, were used to deposit pollen particles on the surface. This was accomplished by folding back the flower petals and gently shaking the stamen and pistil portions of the flower until pollen particles fell onto the surface. The stamen and pistil portion of the flower is the stem inside of the flower where the pollen rests.

While this deposition method does not produce an even distribution, it was sufficient for the needs of this study. Due to the nature of the pollen sticking to the surface when water droplets come in contact with it, the cleaning methods used in this study were unable to remove any pollen from the surface and thus a process that produces a more even distribution was not pursued. Consequently, only observations with regards to a water droplet's interaction with the pollen particles were able to be made and reported.

2.2 Cleaning Processes

In this study, two methods were utilized to clean the SH surfaces. The first was rolling water droplets over a contaminated surface. The second was condensing water droplets on the surface and allowing them to grow large enough to roll off the surface. The following sections will describe each of these cleaning methods in detail.

2.2.1 Cleaning Via Rolling Droplets

On SH surfaces, droplets generally roll instead of slide across the surface. As they do so, they may pick up contaminates in their path. The first step of this study was to analyze the cleaning efficiency of these rolling water droplets over a contaminated SH surface. For contaminates that can be removed from the surface, a distinct droplet path forms a droplet rolls over a contaminated surface. In this droplet path, all particulates visible to the naked eye are removed by the rolling droplet. For example, Figure 2.4a shows a nano-structured SH surface contaminated with salt particles, as indicated by the white particles on the surface. Figure 2.4b shows the same surface after three individual water droplets rolled over the surface, creating three distinct droplet paths on the surface as indicated by the thick, straight, dark lines on the surface. Using image processing techniques, 99-100% of the visible particles were successfully removed from the surface. To enhance the visual contrast between the salt and the droplet path in Figure 2.4, more salt was deposited on the surface than is typically used to test the surfaces. These droplet paths were seen on all surfaces contaminated with both salt and tobacco after a water droplet rolled over the surface.

To attempt to clean a SH surface with rolling water droplets, each contaminated surface was placed on a tilting stage at a 45° angle and a single droplet 2-2.5 mm in diameter was placed on the

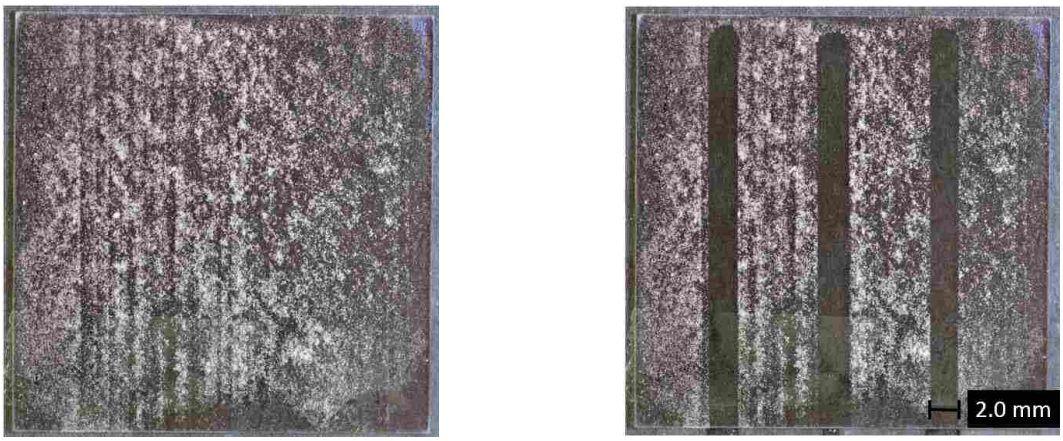

(a) (b)

Figure 2.4: One a distinct feature of self-cleaning is the droplet path, which is where particulates have been removed from the surface after water droplets roll over the surface. (a) Shows a surface with salt particles loosely placed on the surface. (b) Shows the same surface as (a) after 2 mm water droplets rolled over the surface.

surface. Because the SH surface was situated at an angle greater than the largest SA, the droplet would immediately roll off the surface as soon as it was placed on the surface. Additionally, the surface was situated so that the droplet would only roll along the ribs. As the droplet rolled off the surface, it would remove contaminates in its path. The CA and SA were then measured in the droplet path to determine the "surface cleanliness." Details of the definition of "surface cleanliness" related to the CA and SA are discussed in Section 2.4. Two to four subsequent droplets were then placed on the surface when tilted to 45° and allowed to roll off further removing any contaminates on the surface. Each subsequent water droplet was placed in the exact same spot as the previous droplet to ensure each water droplet followed the same droplet path. Smooth surfaces contaminated with tobacco required larger droplets (about 3 mm in diameter) and higher angles (between 65-90°) before to the droplet would roll off and clean the surface. Without this, the smaller droplets would remain pinned to the surface, even when the surface was raised to a vertical position.

2.2.2 Cleaning Via Condensation

The second method used in this study to clean SH surfaces was condensing water droplets on contaminated SH surfaces. When a condensed droplet on a vertically oriented surface reached a critical diameter of 0.75±0.2mm on micro-structured surfaces and 1.1±0.2mm on nano-structured

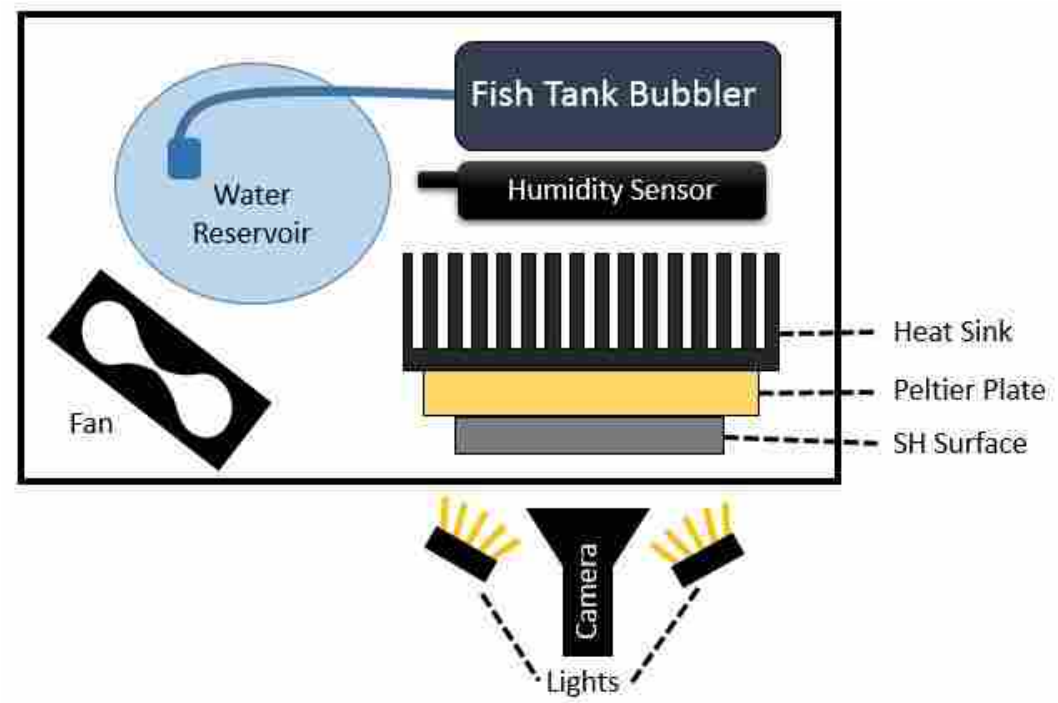

Figure 2.5: Schematic of the humidity box from a top down view used to condense water droplets on SH surfaces. A peliter plate was used to cool each surface below the dew point temperature of the environment.

surfaces, the force of gravity exceeded the force of surface tension holding the droplet to the SH surface and the droplets would roll off the surface. Ideally when this happened, the droplet would remove all the contaminates in its path. For purposes of this study, the surface was situated so that the rib structures of each surface were vertical. As discussed in Section 1.2.5, several researchers have observed condensed droplets spontaneously jumping off SH surfaces. In this study, the condensed droplets did not jump but rolled off the surface. The distinction between droplets rolling off the surface and jumping off the surface is related to the surface energy associated with the nano-structured and micro-structured surfaces. Typically, jumping droplets occur on two-tiered surfaces which have a high surface energy.

To condense water droplets on the SH surfaces, a 10 cm x 18 cm x 28 cm humidity box capable of creating an environment between 80-90% humidity was constructed. A schematic of this humidity box is shown in Figure 2.5. A humidity sensor was initially placed in the humidty box and continually reported the humidity to be between 80-90%. The temperature and pressure of the enclosed environment were held at ambient conditions of 23°and 86 KPa. The SH surface

was placed vertically inside the humidity box on a Peltier cold plate such that the rib structures on each surface were also vertical. The surface temperature of the SH surface was then lowered approximately 3-5° below the dew point temperature. This temperature, which is based on the environment's humidity, temperature, and pressure is calculated using the Magnus Formula shown in equation 2.1

$$T_d = \frac{B_1[\ln \frac{RH}{100} + \frac{A_1 T}{B_1+T}]}{A_1 - \ln \frac{RH}{100} - \frac{A_1 T}{B_1+T}} \tag{2.1}$$

where T_d is the dew point temperature, T is the ambient temperature [89], RH is the relative humidity of the environment and is a function of temperature, pressure, and total water vapor present in the gas. Alduchov and Eskridge calculated $A_1 = 17.625$ and $B_1 = 243.04°\ C$ based on vapor pressure measurements [90]. As long as the surface was cooler than the dew point temperature, water droplets condensed on the surface. These condensed micro-droplets were allowed to coalesce with neighboring droplets and continue to grow until they reached a critical diameter of 0.75±0.2mm on micro-structured surfaces and 1.1±0.2mm on nano-structured surfaces. After this, the droplets would roll off the surface.

To create a humid environment, a small open dish of water was placed inside the humidity box. Using a fish tank bubbler, small micro-air bubbles were pumped through the water which would quickly absorb water vapor via mass diffusion, reaching nearly 100% humidity in the air bubbles. When these bubbles reached the top of the water, the humid air would be released into the surrounding environment, thus increasing the overall humidity of the environment. The fish tank bubbler pump was placed inside the humid environment to maintain a closed system and not pump additional dry air into the humid environment. A small computer fan was used to mix the water vapor with the surrounding air inside the humidity box to establish a constant humidity throughout the environment. The fan was positioned in the environment as to not blow directly across the SH surfaces. This prevented any shear stress from acting on the condensed droplets causing the droplets to roll off the surface prematurely. A DSLR camera was placed in front of the humid box to video droplets condensing on the surface.

One observation made during this study was the cyclic pattern in which the condensed droplets would roll off the surface. As each condensed droplet reached the critical diameter, the condensed droplet would first roll off the surface removing all droplets, and ideally contaminates,

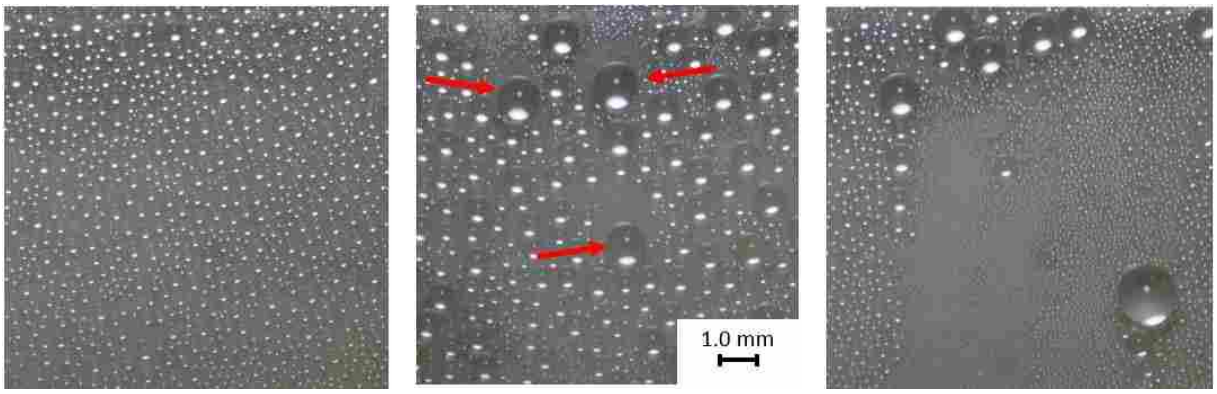

(a) (b) (c)

Figure 2.6: (a) Droplets growing during the initial stages of a condensation cycle on nano-structured surface, 15 mins into the condensation cycle . (b) Condensed droplets 60 mins into a condensation cycle. Droplets (about 1.1 mm in diameter) just prior to rolling off the surface are indicated by red arrows. (c) Droplets growing in the previous rolling droplet paths' indicating the beginning of a second condensation cycle, approximately 90 mins into the condensation cycle. Each image shows the same area on the surface with a consistent scale between images.

in its path. This would then open up nucleation sites, allowing new droplets to form in the droplet path. With time, approximately 90 mins on the nano-structured surfaces and 45 mins on the micro-structured surfaces, all the initially formed droplets on the surface had rolled off the surface and were replaced by newly condensed droplets. The droplets that reached the critical diameter tended to originate on the top third of the surface and so no more than one droplet rolled over any single location. A series of droplets forming and rolling off the surface is termed a "condensation cycle" for the purposes of this work.

A condensation cycle is best seen in Figure 2.6. This figure shows a clean, nano-structured surface undergoing condensation. The surrounding environment has 80-90% humidity, with ambient temperature and pressure. The surface was cooled to 15° C. Initially, in Figure 2.6a, the condensed droplets grow and coalesce at approximately the same rate, all appearing to be similar in size. As the droplets grow large enough to reach the critical diameter, the gravitational force exceeds that of the surface tension holding the droplet to the surface and the droplet rolls off the surface, removing all other droplets in its path. Droplets near the critical diameter are indicated be the red arrows in Figure 2.6b. Once a droplet has completely rolled off the surface, new droplets begin to grow in the initial droplet's path, as seen in Figure 2.6c. A new condensation cycle begins when all the initial condensed droplets have rolled off the surface. These condensation cycles are

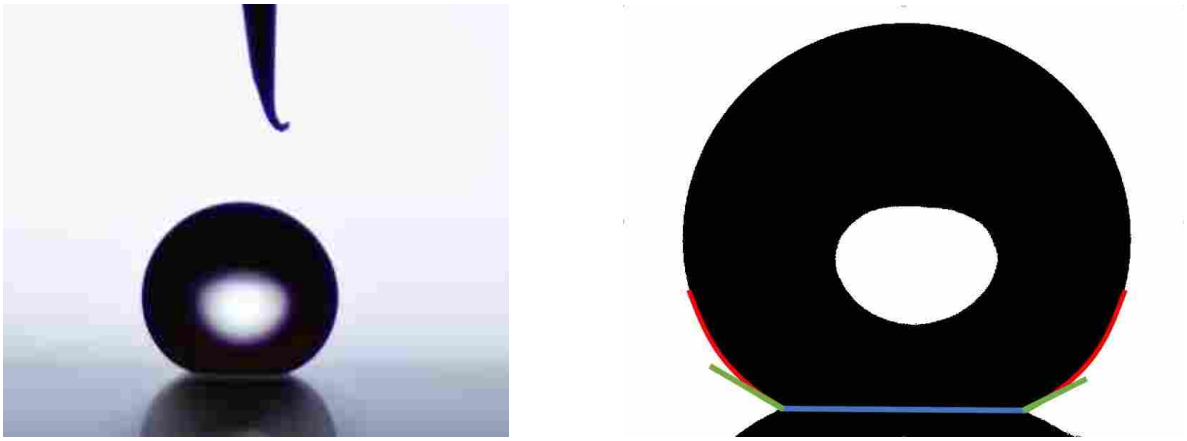

(a) (b)

Figure 2.7: (a) Image of a Sessile Droplet used to measure CA. (b) Post processed image use to measure CA. The blue line shows the triple contact line of the droplet, the red line shows the 5th order polynomial fit to both edges of the droplet, and the green line shows the tangent line to the polynomial fit at the triple contact line.

used in defining distinct intervals over which cleaning occurs via condensation on a contaminated surface.

2.3 Contact Angle and Sliding Angle Measurements

This study uses the CA and SA measurements as two indicators of the surface's hydrophobicity. This section is dedicated to describing how each of these data points are measured. One effect of the rib patterns on the SH surfaces is a difference in CA and SA when looking transversely vs longitudinally across the ribs. In general, the CA and SA in the longitudinal direction are higher and lower respectively than in the transverse direction. Here, only the CA and SA in the longitudinal direction are measured and reported. However, the results of the measured CA and SA presented in Chapter 3 are expected to be the same, with a shift, for the transverse direction.

2.3.1 Contact Angle

Contact angles are measured using a goniometer created by Kimberly Stevens of Brigham Young University (awaiting publication). This goniometer images a 2 mm diameter, sessile droplet on a SH surface using a Nikon D5200 SLR camera. Back lighting creates a silhouette of the sessile

droplet in the image as shown in Figure 2.7a. Image processing techniques using an automated polynomial fitting (APF) scheme were utilized to find the base line, or triple contact line, of the droplet. This line is the circumferential path where liquid, solid, and gas phase intersect and is indicated by the blue line in Figure 2.7b. Additionally, using APF techniques, both the left and right edges are found and a 5th order polynomial is fitted to each edge as indicated by the curved red lines [91, 92]. Using this data, the tangent line to the polynomial fit at the triple contact line is calculated and is indicated by the green line in Figure 2.7b. Subsequently the angle between the tangent line and base line can both be calculated. This angle is the resulting contact angle. For each sessile droplet analyzed, the average CA between the left and right side of the droplet is reported which could vary by 1-2°. Because this difference is within the error of the measurement, it was determined this variation is insignificant.

This APF technique has proven to be accurate to $\pm 2°$ in comparison to the axisymmetric drop shape analysis (ADSA) methodology. The ADSA is generally accepted as the standard and most accurate method to measure the CA of axisymmetric droplets [91]. However, on SH surfaces composed of rib patterns, the method is invalid because the rib patterns cause the droplet to have an elliptical base line. Because of this, the APF technique is used and the larger range of error is unavoidable.

2.3.2 Sliding Angle

A tilting stage was constructed to measure the sliding angle of each surface. As seen in Figure 2.8, this tilting stage had two plates connected together via a hinge. The bottom plate was attached to a large block that could be held starionary to prevent any external motion. The top plate attached to the bottom plate via a hinge and had one degree of freedom in which it could rotate. The top plate also had a slot cut out which the SH surface could be placed and not slide off the plate when tilted. A long bolt threaded through the bottom plate raised and lowered the top plate. Finally, an *Angle Cube*® was secured to the tilting stage which measures the angle of the top plate from horizontal.

To measure the sliding angle, a SH surface was placed on the tilting stage in the premade slot when the top plate was horizontal. A 2 mm droplet was gently placed on the surface. Then the bolt attached to the bottom plate was slowly rotated until the droplet began to roll off the surface.

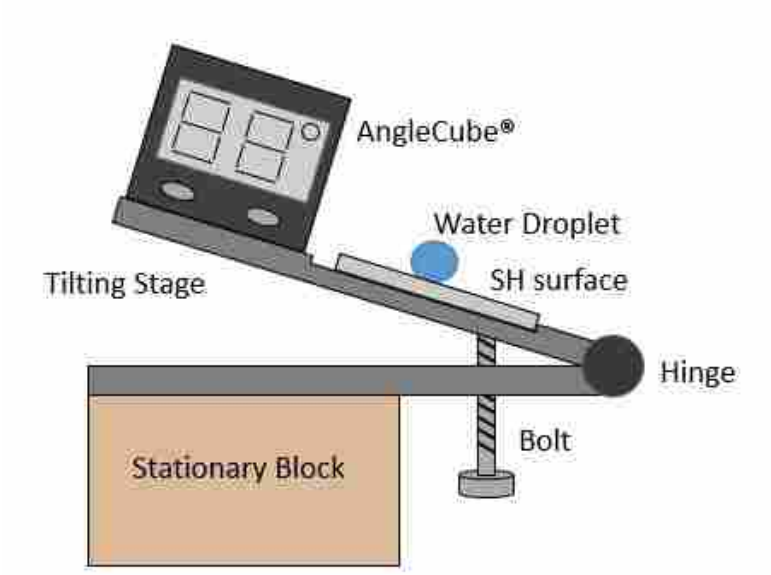

Figure 2.8: Tilting stage used to measure the SA on each surface.

The angle of the top plate measured by the *Angle Cube*® was then recorded. The *Angle Cube*® has a accuracy of $\pm 0.2°$ and a resolution of $0.05°$. Additionally, the *Angle Cube*® was tared on a flat, horizontal optics table which has had extensive testing to ensure it is level so as to assume there is no variability in the zero-ing of the measuring device. The user would twist the bolt which rotated the tilting stage by $0.73 \pm 0.24°$. This is based on 67 data points, with three different users simply twisting the bolt. Using a root-sum-squares method, this results in an overall uncertainty of $\pm 0.76°$. However, to account for any additional human error, this uncertainty is increased to be $\pm 1°$.

The size of the droplet is critical to the accuracy of the SA and CA measurements. For both measurements, a 2 mm diameter droplet was used. This droplet size was chosen based on the Bond number (equation 2.2)

$$B_o = \Delta\rho g L^2/\sigma \tag{2.2}$$

which represents the ratio between gravitational and surface tension forces. For the B_o number, $\Delta\rho$ is the difference in density between the water droplet and the surrounding air, g represents the gravitational constant, σ_{LV} is liquid-vapor surface tension, and L is the characteristic length. In the case of water droplets, the characteristic length is the diameter of the droplet. For a B_o equal to 1, which is used throughout this study, droplets must have a 2 mm diameter. A B_o equal to 1 implies

the effects of gravity and surface tension are of the same order. To create 2 mm diameter droplets, a 27 gage needle was held slightly above the SH surface and water was slowly released until the weight of the droplet exceeded the surface tension's hold between the droplet and the needle. At this point the droplet would fall onto the surface, creating a 2 mm droplet. This process proved to be both accurate and repeatable.

2.4 Metric For Contaminate Removal

One of the biggest challenges of this work was to define to what degree the surface was contaminated with salt, tobacco, and pollen and how that degree of contamination changed as the surfaces were cleaned, either via rolling droplets or condensation. Multiple approaches were considered including counting the number of particles on the surface at the macroscopic and microscopic levels as other researches have done [1,3,12]. However, counting the number of particles visible to the naked eye did not satisfy the desired outcomes of this study and counting the number of particles on the surface at a microscopic scale proved to be too time and resource intensive to acquire statistically significant data. A system focusing on droplet behavior and surface hydrophobicity was chosen which satisfies both time and financial constraints. Specifically, this system focuses on how the CA and SA improve as a contaminated surface is cleaned. This answers the fundamental question as to how the hydrophobicity of the surface, as indicated by the CA and SA, is affected by the presence of contaminates.

The averages for the CA and SA before and after each surface is contaminated is presented in Table 2.1. This table represents the initial conditions for each clean and contaminated surface. SH surfaces in Table 2.1 include micro-structured surfaces with a Teflon® coating and nano-structured surfaces with a proprietary coating. Smooth surfaces coated with Teflon® or a proprietary, hydrophobic coating are also shown Table 2.1. Notice that for both nano-structured surfaces and micro-structured surfaces, the CA for a clean surface is clearly higher than any of the contaminated surfaces. Additionally, the SA of a clean surface is notably smaller than any of the contaminated surfaces. This leads to the initial conclusion that the presence of each contaminate can greatly affect the overall hydrophobicity of the surface, as indicated by the CA and SA.

Operating on the basis that the contaminates cause the reduction in hydrophobicity, the CA and SA are measured both before and after a surface is cleaned. Great care was taken to ensure

Table 2.1: Tabulated values for average static CA and SA on clean and contaminated SH surfaces are shown here. Surfaces included micro-structured surfaces, nano-structured surfaces, smooth surfaces with a Teflon® coating, and smooth surfaces with a proprietary coating. The number of surfaces tested for each surface structure is reported in Table 2.2.

	Nano-structured Surfaces		Micro-structured Surfaces		Smooth surfaces, Teflon Coating		Smooth Surfaces, Proprietary Coating	
Contaminate	Contact Angle	Sliding Angle	Contact Angle	Sliding Angle	Contact Angle	Sliding Angle	Contact Angle	Sliding Angle
Clean	144°	10°	150°	7°	122°	32°	112°	Did Not Roll
Salt	135°	13°	140°	10°	114°	39°	102°	Did Not Roll
Tobacco	131°	40°	142°	18°	107°	71 °	96°	Did Not Roll
Pollen	45°	Did Not Roll	65°	Did Not Roll	-	-	-	-

the CA and SA were measured in areas that had been cleaned on the surface such as within the droplet path after the surface was cleaned by rolling droplets. As contaminates are removed from the surface, the CA and SA of the surface will approach that of a clean surface. Conversely, if contaminates are still present after the surface is cleaned, a reduction in the overall hydrophobicity of the surface from a clean surface will be apparent due to the CA and SA still being disparate from the clean surfaces.

2.5 Test Procedures Summary

In summary, this study evaluates the cleaning efficiency of water droplets on four surfaces including a SH micro-structured surface, SH nano-structured surface, a smooth hydrophobic surface consisting a Teflon® coating, and a smooth hydrophobic surface consisting of a proprietary hydrophobic coating used on the nano-structured surfaces. Each surface is contaminated with one of three contaminates including sea salt build up, tobacco residue, and pollen deposits. The CA and SA of each surface is measured on the contaminated surface. Then, the surface is cleaned either by rolling droplets over the surface or by condensing water on the surface. Afterwards, the CA and SA are again measured on each surface to determine the change in the hydrophobicity of the surface. Increased CA and decreased SA indicate that contaminates have been removed from

Table 2.2: The following table shows the number of surfaces tested for each contaminate. Pollen was not tested on either smooth surface.

	Clean		Salt		Tobacco		Pollen	
	Rolling Droplets	Condensed Droplets	Rolling Droplets	Condensed Droplets	Rolling Droplets	Condensed Droplets	Rolling Droplets	Condensed Droplets
Micro-Structured SH Surfaces	9	6	10	7	6	6	3	2
Nano-Structured SH Surfaces	8	8	8	7	8	6	3	2
Smooth Surface, Teflon Coating	6	4	7	4	6	4	-	-
Smooth Surface, Proprietary Coating	6	4	6	4	6	4	-	-

the surface. Additionally, the same cleaning and test procedures were performed on clean surfaces to establish a base line to compare the difference between the contaminated surfaces and clean surface. Table 2.2 shows the total number of surfaces tested for each case. The results for all CA and SA changes will be presented in the following chapter.

CHAPTER 3. RESULTS AND DISCUSSION

This chapter presents the results for the self-cleaning experiments performed in this study. First, the results for the CA and SA tests after the SH surfaces are cleaned of salt, tobacco, and pollen via rolling droplets are presented and the cleaning dynamics related to rolling water droplets are discussed. Following this, a similar discussion presents the results of the CA and SA tests after the SH surfaces are cleaned via condensation and describes the cleaning dynamics associated with cleaning via condensation. The next section presents a non-dimensional CA and SA to compare the two cleaning methods in this study. A full comparison between cleaning via rolling droplets and cleaning via condensation is reserved for this section. Finally, the effects of the surface structure will be examined by comparing the micro-structured and nano-structured surfaces to the cleaning efficiencies of smooth surfaces with the same hydrophobic coatings.

3.1 Cleaning Via Rolling Droplets

The first cleaning method tested was rolling water droplets over each contaminated surface. As is discussed in Section 2.2.1, contaminated surfaces were cleaned by one to four water droplets rolling over the surface. The CA and SA were then measured in the droplet path (See Figure 2.4). This section discusses the effects salt, tobacco, and pollen have on the overall hydrophobicity of the surface. The cleaning efficiency for each contaminate was tested on both the micro-structured and nano-structured surfaces.

3.1.1 SH Surfaces Contaminated with Salt and Cleaned via Rolling Droplets.

Salt was deposited on each surface using an atomizing spray bottle to spray the surface with salt saturated micro-droplets as described in Section 2.1.1. Small, micro-scale salt crystals formed as the micro-water droplets evaporated from each surface. SEM images of these salt crystals are shown on the micro-structured surfaces in Figure 3.1a and the nano-structured surfaces in Figure

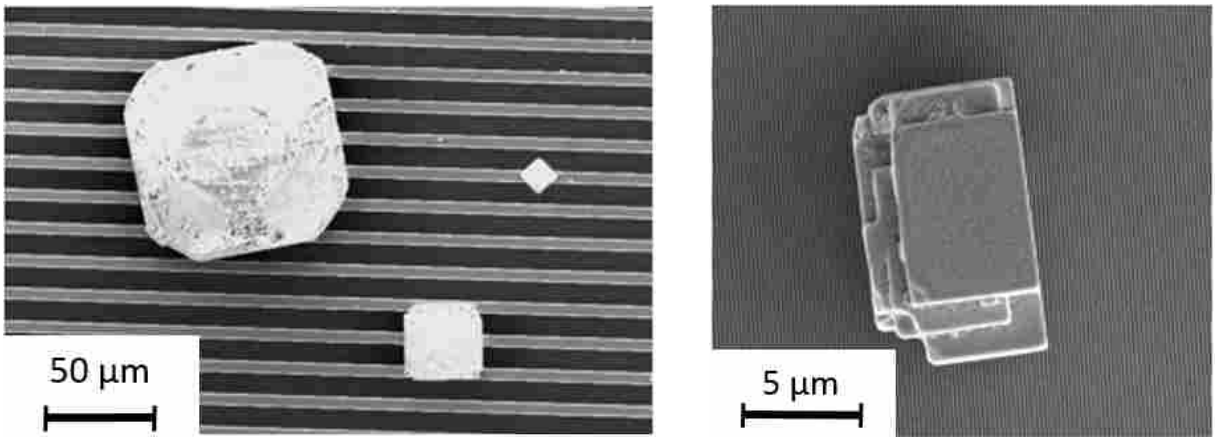

(a) (b)

Figure 3.1: SEM images of salt particles deposited on top of a micro-structured SH surface (a) and a nano-structured SH surface (b). Note the difference in scales between the two images.

3.1b. Note the difference in scales between the two images which emphasizes the salt crystals' location and size with repect to the surface structures. In both these images, the salt particles sit on top of the rib structures. Because the initial salt water droplets are not forcibly placed on the surface, which would cause a high stagnation pressure and possibly wetting the surface, it is expected that the these droplets sit primarily in the Cassie-Baxter state. The salt particles sitting on top of the surface confirms that atomized droplets prefer the Cassie-Baxter state as opposed to the Wenzel state. If these atomized droplets settled in the Wenzel state when deposited on the surface, the salt crystals may have formed in between the rib structures. Note also that the largest salt crystal on the micro-structured surface in Figure 3.1a spans eight ribs but the smallest salt crystal is nearly the same size as the rib structure. On the nano-structured surface, the salt crystal in Figure 3.1b (which is about half the same size as the smallest salt crytal on the micro-structured surface) spans approximately 50 rib structures.

In terms of self-cleaning surfaces, the position of the salt particles has two effects on the cleaning water droplet's ability to remove the contaminates from the surface. First, the salt has minimal contact area with the surface, resulting in a decreased amount of force holding the particles to the surface. Because of this, minimal force between the water droplet and the salt particles is required to remove the salt particles from the surface. Second, because the salt particles are sitting on top of the surface, they can easily be completely engulfed by the cleaning water droplet as

it rolls over the surface. If the salt particles were sitting in between the ribs, the cleaning water droplet rolling over the surface in the Cassie-Baxter state would have minimal contact with the salt particles or not come in contact with them at all. As will be seen, these two factors result in the majority of the salt particles being removed from the surface after two to three cleaning water droplets roll over the surface.

Using the CA and SA tests, both micro-structured and nano-structured surfaces show tremendous self-cleaning properties with regards to removing salt buildup from both micro-structured and nano-structured surfaces when water droplets roll over the surface. Figure 3.2 shows the results of the CA and SA after the rolling droplet cleaning tests were performed on the SH surfaces contaminated with salt. The x-axis represents the number of droplets that rolled over the surface and the y-axis represents the CA (Figure 3.2a) or the SA (Figure 3.2b). Data points representing the CA and SA for surfaces contaminated with salt are offset by 0.1 from the clean surface to enhance clarity of the data. However, by nature of this study, the x-axis can only represent a whole number of droplets and so each data point is associated with the closest integer. The solid data points in Figure 3.2 represent the micro-structured surfaces and the open data points represent the nano-structured surfaces. Clean surfaces are represented by data points shown as circles and salt contaminated surfaces are represented by data points shown as triangles.

As discussed in Section 2.4, an increase in CA and decrease in SA indicates that some of the contaminates on the surface have been removed. The surface is considered completely clean when the CA and SA of a contaminated surface matches the CA and SA of a clean surface. To account for measurement uncertainty and variations between the surfaces, the standard deviations are heavily considered as a method to determine how closely the contaminated surfaces match the clean surfaces after being cleaned.

As indicated in Table 2.1 and seen in Figure 3.2, The initial CA is reduced by approximately 10° and the initial SA is increased by approximately 4° on both the micro-structured and nano-structured surfaces due to salt contamination. Table 2.2 shows the number of surfaces used for each test and the raw data is included in Appendix A.3-4. In general, Figure 3.2 shows that as the number of droplets thats have rolled over the surface increases, the CA increases and the SA decreases due to the cleaning effect of the droplet. After two to three droplets rolling over the surface, the hydrophobic characteristics of the contaminated surface matches that of a clean

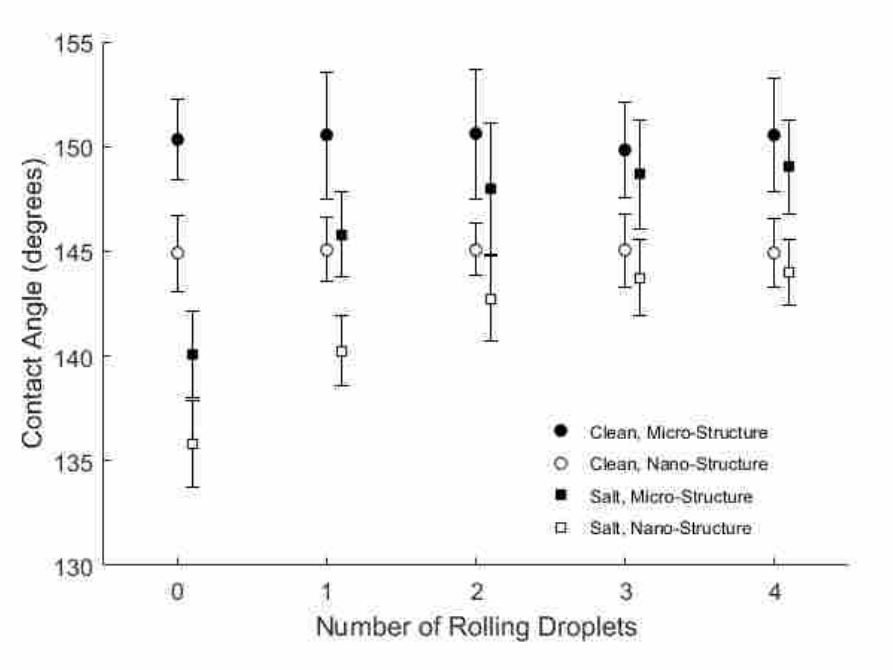

(a)

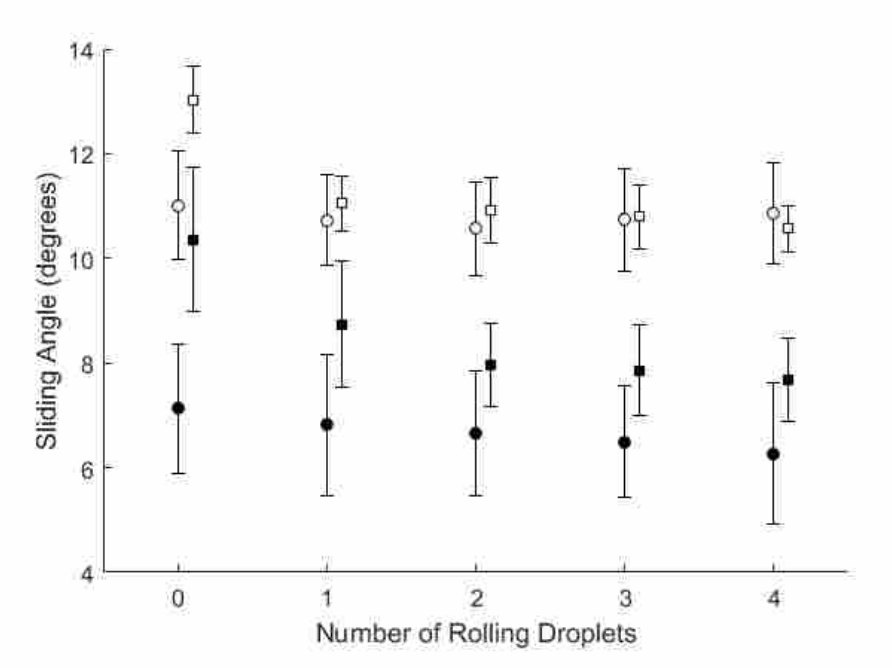

(b)

Figure 3.2: SH surfaces contaminated with salt were cleaned by rolling 1-4 water droplets over the surface. After the surface was cleaned, the CA and SA were measured in the droplet path. In this figure, open data points represent micro-structures and closed data points represent nano-structured surfaces. The legend given in Figure (a) also applies to Figure (b).

surface. Once the surface has been fully cleaned, the CA and SA stays consistent, even with additional droplets rolling over the surface.

On the micro-structured surfaces (solid markers), the lower standard deviations for the clean surfaces and upper stand deviation of the salt surfaces begin to overlap after a single droplet rolls over the surface in Figure 3.2a. This indicates that the cleanest contaminated surfaces exhibit the same CA as the lowest CA measured on the clean surface and could be considered clean. After a second droplet rolls over the the surface, the upper bound of the standard deviation for the salt surfaces is greater than the average CA of the clean surface and the average CA of the salt surfaces is greater than the lower standard deviation bound for the clean surface. This implies that most of the salt has been removed from the surface and the majority of the surfaces have a CA which behaves as clean surfaces.

This same trend is shown in the SA data on the micro-structured surfaces in Figure 3.2b. After the first droplet rolls over the surface, the standard deviations of the salt surfaces and clean surfaces intersect. The SA again improves after the second droplet cleans the surface. After this, however, little improvement is seen as additional droplets roll over the surface. The average resulting SA on these salt surfaces is approximately the same as the upper limit of the standard deviation of the clean surfaces. This implies that about half of the contaminated surfaces match the SA of their clean counterparts, while half the contaminated surfaces exhibited a SA up to 2° greater than the clean surfaces. While this small effect on the hydrophobicity is consistently noticeable, this difference is within the error of the tilting stage ($\pm 1°$). Results of both the CA and SA on salt contaminated micro-structured SH surfaces show that the majority of salt deposited on the surface can be removed via rolling droplets and that no lasting effects on the hydrophobicity of the surface are found as additional droplets roll over the surface.

The CA and SA of nano-structured SH surfaces contaminated with salt are also shown in Figure 3.2. As mentioned, the CA increases by 10° and the SA decreases by 2°. A significant increase in the average CA of 5° is apparent on the nano-structured surfaces after one droplet is rolled over the surface, cutting the difference between the clean and contaminated CA in half. After the second droplet rolls over the surface the average CA of the contaminated surfaces is still approximately 2° lower than the lower standard deviation of the clean surface. Since the upper standard deviation bound of the contaminated surfaces intersects with the clean surface standard

deviation bounds, it can be seen that some of the contaminated surfaces begin to behave as clean surfaces. However, only after a third droplet rolls over the surface does the average CA on the salt contaminated surface become greater than the lower standard deviation of the clean surface, implying that the majority of the surfaces have been cleaned.

Interestingly, after the first cleaning droplet rolls over the surface, the average SA on the contaminated nano-structured surface nearly matches the average SA of the clean nano-structured surface. Furthermore, the spread of the standard deviation for the contaminated surfaces was within than the standard deviation spread of the clean surface. Subsequent droplets improve this as the average SA's nearly match after four droplets. Thus, in terms of SA, the surface was able to recapture the majority of its hydrophobicity after a single droplet rolled over the surface. Based on the CA and SA tests, the majority of the contaminated surfaces regained their full SH properties and matched the hydrophobic properties of the clean surfaces after three droplets rolled over surface.

The implication with regards to these experimental results is that multiple droplets are required for all the salt particles to be completely removed from the surface. As shown in Figure 2.4, a single droplet can remove the majority of the visible particulates creating a distinct droplet path. However, as the experimental results in this section shows , two to three droplets are required to roll over the surface to reclaim its full hydrophobicity.

One limitation to this study is that the experimental setup does not confidently explain why some particles do not adhere to the cleaning droplet the first time it rolls over the surface. The particles not picked up by the first droplet appear to be random. This most likely is due to the concentration of the particles on the surface. When more particles are present in a centralized location on the surface, less particles could potentially be picked up by the droplet. Because a droplet path is formed the entire length of the surface, droplet saturation does not appear to be a possible cause.

3.1.2 SH Surfaces Contaminated with Tobacco and Cleaned via Rolling Droplets.

Unlike salt, tobacco residue was not easily removed from the SH surfaces via rolling droplets. Figure 3.3 shows SEM images of tobacco residue on a micro-structured surface (Figure 3.3a) and nano-structured surface (Figure 3.3b). Again, note the difference in scale on each surface. As discussed in Section 2.1.2, surfaces are contaminated with tobacco residue by burning

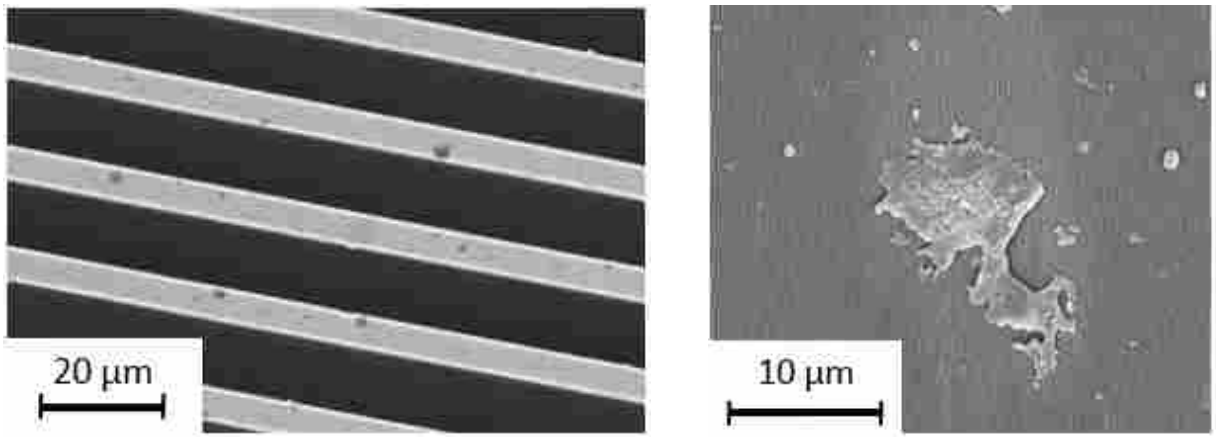

(a) (b)

Figure 3.3: SEM images of tobacco particles sitting on top of a micro-structured SH surface (a) and a nano-structured SH surface (b).

a cigarette in an enclosed chamber. The contained smoke then adheres to the SH surfaces. One of the biggest factors affecting the hydrophobicity of the surfaces is the size of the particulates with regards to the surface structures. In Figure 3.3a, tobacco is seen as the black spots on the micro-structured surfaces . The size of the tobacco particles is small relative to the size of the rib and cavity structures. Consequently, large portions of these tobacco particles could fall in-between the ribs and into the cavities of the surface during the contamination process. A droplet in the Cassie-Baxter state, sitting on top of the rib-structures, would not be in contact with and consequently unaffected by any tobacco particles in-between the rib-structures. Thus the initial reduction in CA and increase in SA would not be as great as if all the tobacco residue was sitting on top of the surface. This also reduces the percentage of tobacco capable of being removed by the cleaning droplet as it rolls over the surface.

On the nano-structured surface, shown in Figure 3.3b, some of the tobacco particles span the length of several nano-rib structures. Thus a larger portion of the tobacco deposited on the surface adheres to the top of the rib structures and therefore significantly affects the initial CA and SA of a water droplet in the Cassie-Baxter state more than the micro-structured surfaces. Because the tobacco proves to greatly affect the hydrophobicity of the surface, the more tobacco in contact with the droplet, the greater the effect the tobacco has on the droplet's behavior and overall hydrophobicity of the surface. Additionally, unlike the salt particles that seemingly "sit" on top

of the rib structures, the tobacco particles appear to have a much firmer bond between with the surface.

The CA and SA tests were again used to show the effect tobacco has on the self-cleaning properties of SH surfaces as it was cleaned via rolling water droplets. The results of these test are shown in Figure 3.4. In this figure, solid data points represent micro-structured surfaces and open data points represent nano-structured surfaces. Additionally, clean surfaces are represented by circles and tobacco contaminated surfaces are represented by triangles. Similar to Figure 3.2, the x-axis represents the number of droplets rolled over the surface and the y-axis represents the CA (Figure 3.4a) or SA (Figure 3.4b). Again, data points representing surfaces contaminated with tobacco are offset along the x-axis by 0.1 to more clearly present the data but still associate with the closest whole number.

As noted in Table 2.1 and seen in Figure 3.4, tobacco residue has a significant impact on the CA and SA for both the micro-structured and nano-structured surfaces. For the micro-structured surfaces, the CA was reduced by 8° and the SA increased by 11°. Similarly, the CA decreased by 13° and the SA increased by 30°on the nano-structured surfaces. Table 2.2 shows the number of surfaces used for each test and the raw data points collected for this portion of the study are shown in Appendix A.5-6. Figure 3.4 shows that surfaces contaminated with tobacco have substantial improvement as the first couple water droplets roll over the surface, but reach a limit where the CA and SA plateaus with additional droplets. Unlike the salt contaminated surfaces, the tobacco contaminated surfaces are never able to reclaim their full hydrophobicity even after being cleaned with up to four cleaning droplets rolling over the surface.

First, focusing on the micro-structured surfaces, the presence of tobacco reduces the CA by about 8°. The average CA after the first cleaning droplet rolls over the surface improves by 3°, but subsequent droplets show little further improvement with additional droplets rolling over the surface. One important observation is that the upper standard deviation begins to overlap with the lower standard deviation of the clean surfaces after the first droplet rolls over the surface. This implies that the cleanest contaminated surfaces behave similar to those clean surfaces with the lowest CA and therefore, by definition, could be considered clean. However, the average CA of the contaminated surfaces is still less than the lower bound of the clean surface standard deviation meaning that the majority of the surfaces do not exhibit the same hydrophobicity as the clean

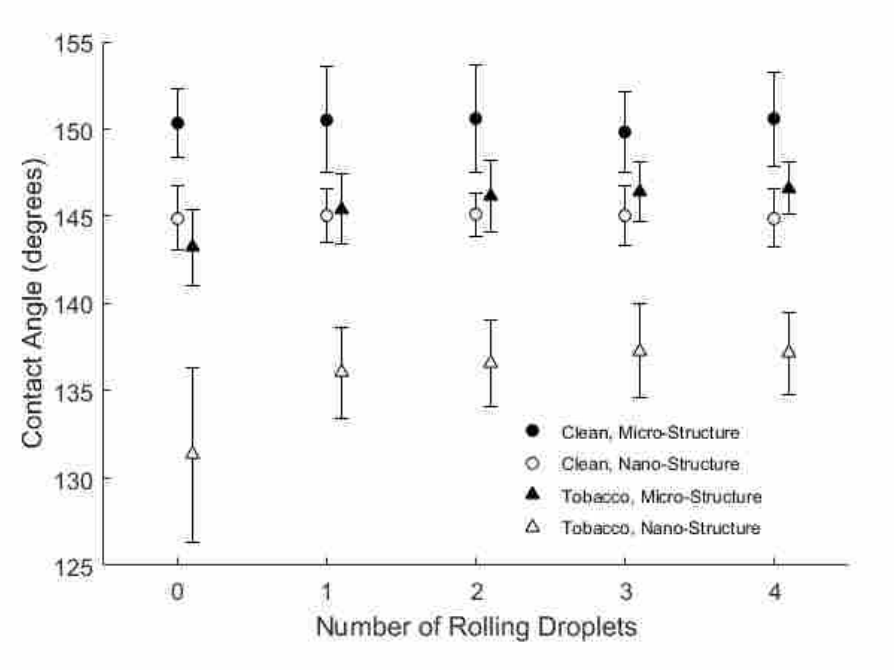

(a)

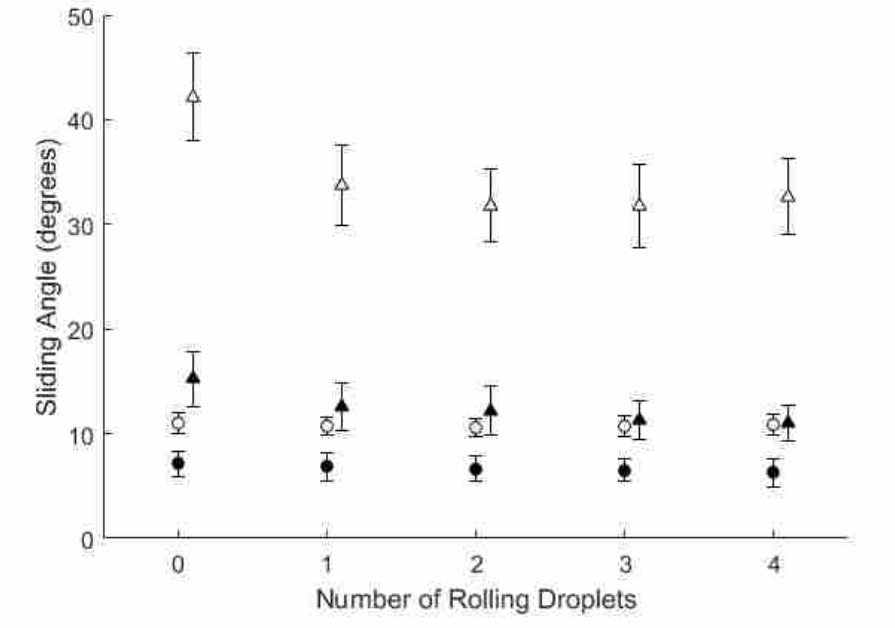

(b)

Figure 3.4: SH surfaces contaminated with tobacco were cleaned by rolling 1-4 water droplets over the surface. After the surface was cleaned, the CA and SA were measured in the droplet path. In this figure, closed data points represent micro-structures and open data points represent nano-structured surfaces.

surface. This implies that tobacco residue has a lasting effect on the majority of the contaminated surfaces.

SA data in Figure 3.4b further shows the lasting effect tobacco has on the micro-structured SH surface. Initially, the tobacco causes the SA to increase by about 8°. Like the CA measurements on contaminated micro-structured surfaces, the SA improves by 3° after the first droplet but then plateaus with subsequent droplets. However, unlike the CA measurements, the standard deviations of the SA on the contaminated surfaces does not cross with the standard deviation of the SA on the clean surfaces. Even though the cleanest of the contaminated surfaces exhibit a CA that matches the lowest CA's of clean surfaces, the fact that the lower standard deviation of contaminated surface SA remains 2° greater than the upper standard deviation of the clean surfaces SA emphasizes the long lasting affect tobacco has on the overall hydrophobicity of the micro-structured surfaces. This leads to the conclusion that the micro-structured surfaces can not be fully cleaned of tobacco residue via rolling water droplets.

The effects of tobacco are even more extreme on nano-structured surfaces. This is because the tobacco residue primarily sits on top of the rib structures, as shown in Figure 3.3b, as opposed to falling in between the cavities as was hypothesized to occur on the micro-structured surfaces. The consequence of this is that the water droplets are in contact with more tobacco residue, causing a greater reduction in the overall hydrophobicity of the surface relative to the micro-structured surfaces. The average CA on nano-structured surfaces contaminated with tobacco is 15° less than the average CA on the clean surfaces. The large standard deviation of the initial CA ($\pm 5°$) on surfaces contaminated with tobacco is caused by two different factors. First, there is variability in the amount of tobacco that adheres to the surface during the contamination process. Second, the static CA of a sessile droplet, as used in the goniometer setup to measure the CA, can be any angle between the advancing and receding angles. For SH surfaces, this difference between the advancing and receding angle, known as the hysteresis, is typically very small, thus explaining the small standard deviations of the clean surfaces (see Section 1.2.1 for further details). However, as a surface loses its hydrophobicity such as what happens when tobacco is present on the surface, the hysteresis increases, resulting in the large standard deviation in CA measurements on the tobacco surfaces.

After the first droplet rolls over the contaminated nano-structured surface, the CA increases by about 5° as can be seen in Figure 3.4a. This is the same increase in CA on the salt surfaces. However, because of the difference in the initial CA on the contaminated surfaces, about 14°, a significant gap still remains between the contaminated surfaces and clean surface. Very little improvement is seen with additional droplets rolling over the surface.

Similarly, the SA on the nano-structured surfaces (Figure 3.4b) is greatly affected by the tobacco residue, increasing the average SA by 30°. Because the SA is a function of the hysteresis of the surface (Equation 1.1), this significant increase on the tobacco contaminated surfaces is not surprising when considering the significant reduction of the initial CA on the tobacco contaminated surfaces. [11, 93, 94]. After the first cleaning droplet rolls over the surface, the SA decreases by 10°. However, it does not improve with any additional cleaning droplets rolling over the surface. Despite the large reduction in SA on the tobacco contaminated surfaces after one cleaning droplet rolling over the surface, the average SA is 22°greater than that of a clean surface, implying a lack of cleaning capability of the water droplet on the tobacco contaminated, nano-structured surfaces. Even after four droplets roll over the surface, the contaminated SA and clean SA remain separated. Like the micro-structured surfaces, these results imply that tobacco has a long lasting effect on the SH surfaces and can only partially be cleaned via rolling droplets.

3.1.3 Water Droplets Rolling Over SH Surfaces Contaminated with Pollen

Pollen particles had the greatest impact on the hydrophobicity of the surface. As indicated in Table 2.1, the CA of water droplets in contact with pollen particles on the surface reduced the CA from 150° to 65° on micro-structured surfaces and from 144° to 45° on nano-structured surfaces, altering the surface to behave as hydrophilic surface. Furthermore, water droplets in contact with pollen particles on the surface do not roll off either micro-structured or nano-structured surfaces, even if the surface is tilted to 90° (vertical). Larger droplets, up to 6 mm in diameter were placed on the surface and would not roll off once in contact with any pollen particles.

A water droplet's behavior on a SH surface contaminated with pollen is best seen in Figure 3.5. In this figure, a nano-structured surface was contaminated with pollen as described in Section 2.1.3. As noted, the pollen particles were not evenly distributed across the surface and are larger than either the salt or tobacco particles. Consequently, there are areas on the surface that are not

(a) (b)

Figure 3.5: A water droplet was placed on a clean portion of a SH surface contaminated with pollen and rolled off the surface (a). As the water droplet came in contact with the pollen particles (as indicated by the black particles on the surface), the water droplet pinned to the surface, rendering the surface hydrophilic (b). Notice the large difference in CA between the two images.

contaminated with pollen particles. In Figure 3.5a, a water droplet was placed on a clean portion of the surface and the surface was tilted to the SA so that the water droplet began to roll off the surface. When the water droplet came in contact with pollen particles, the droplet immediately stopped and pinned to the surface. When this happens, the CA is reduced to $45\pm3^\circ$ as shown in Figure 3.5b. Once the droplet was in contact with the pollen it would not roll again, even when the surface was raised to a vertical position.

Another notable affect of pollen is the permanent damage it causes to the surface after a water droplet comes in contact with it, as shown in Figure 3.6. In this figure, water droplets came in contact with pollen particles and wetted the surface, similar to what is shown in Figure 3.5b. Two different attempts were then made at then removing the droplets from the surface. The first attempt included using compressed air to blow the droplet off the surface. Because the droplet behaved as if in contact with a hydrophilic surface in the areas that the water droplet was in contact with pollen particles, the droplet did not roll across the surface as expected. Instead, it slowly slid across the surface, leaving a trail of water as is often seen on hydrophilic surfaces when a droplet experiences a shear stress. After the water had been completely blown off the surface, a splatter pattern was left on the surface, represented by the white areas on the surface shown in Figure 3.6a. Throughout this study, this area will be referred to as a pollen stain.

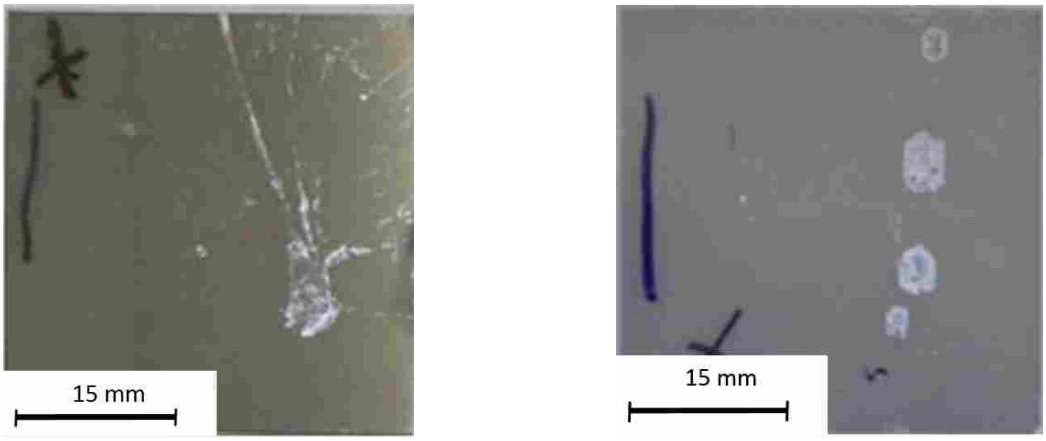

(a) (b)

Figure 3.6: A water droplet was placed on a clean portion of a SH surface contaminated with pollen (a). As the water droplet came in contact with the pollen particles (as indicated by the black particles on the surface), the water droplet pinned to the surface, rendering the surface hydrophilic (b). Notice the large difference in CA between the two images.

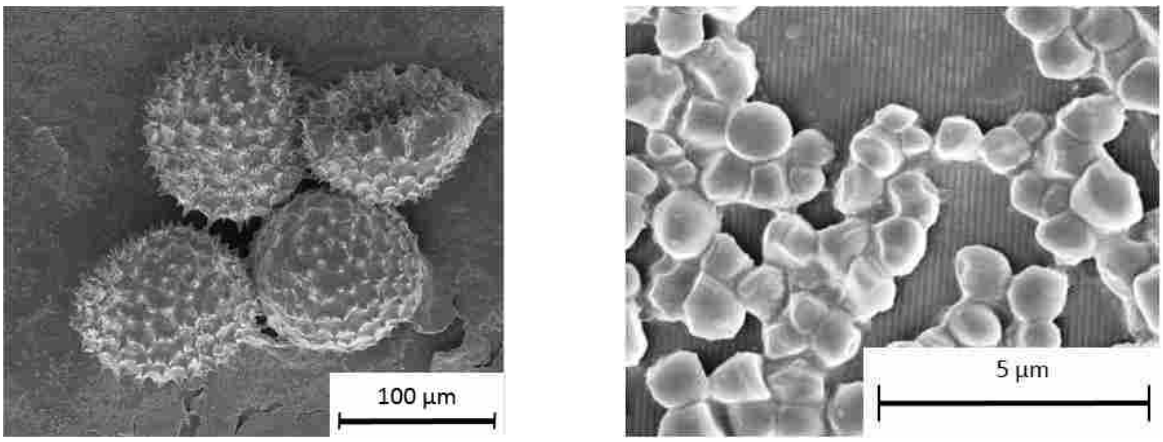

(a) (b)

Figure 3.7: SEM images of the pollen stains shown in Figure 3.6. Cellular organelles covers the surface due to pollen bursting when the pollen particles were exposed to too much water at one time.

A second method to remove the water droplets from the surface after they had come in contact with pollen particles was by natural, convective evaporation. Figure 3.6b shows four pollen stains on the surface where four water droplets had come in contact with pollen particles. Note the four distinct round white spots left on the surface; here is where the water droplets in contact with the pollen particles were positioned. These droplets were evaporated by simply exposing the droplets to the dry surrounding air (about 20-25% relative humidity). No additional heat was applied to the surface to aid in the evaporation process. Once the droplets were evaporated, a second droplet was rolled over the surface. This droplet and all additional droplets also pinned to the surface when it came in contact with these pollen stains. This leads to the conclusion that the pollen can not be removed from the surface via rolling droplets.

The primary cause of rolling water droplets pinning to the surface is the structural integrity of pollen particles. Many pollen particles are susceptible to large osmotic differences between the surrounding water and the pollen cytoplasm. This means that for many pollen particles, water will flood the cell, increasing the hydrostatic pressure of the cell and eventually causing the cell wall to burst. When this happens, the cellular organelles (parts of a cell) spreads out across the surface. This primarily occurs when the pollen particles are exposed to too much water [95]. Figure 3.7 shows two SEM images of the pollen stains on the surfaces shown in Figure 3.6. Figure 3.7a shows the pollen particles from a morning glory flower still present on the surface within the pollen stain. This also shows that the rib structures are entirely covered by what is believed to be the the cellular organelles released from the pollen particles after the pollen particles experienced bursting. Figure 3.7b zooms in further to the pollen stain and shows what is believed to be the cellular organelles sitting on top of the rib structures. Because this cellular organelles are "sticky" and creates a strong adhesive bond to the surface, the water droplets are unable remove the particles from the surface. Additionally, the cellular organelles and pollen particles cover the hydrophobic coating and surface structure, rendering that area of the surface hydrophilic. Because of this, the CA of a water droplet within the pollen stain is dramatically reduced and the droplet is unable to roll off the surface.

3.1.4 Summary of Cleaning via Rolling Droplets

Rolling water droplets over a contaminated surface, similar to what occurs during a rain shower, is the most common way researchers have considered the self-cleaning efficiency of SH

surfaces [1, 3, 12]. This portion of the study has shown that rolling droplets is a viable method to removing contaminates from SH surface composed of micro-structured surfaces or nano-structured surfaces, as long as the contaminate is loosely bound to the surface, such as salt. Tobacco contaminated surfaces could be partially cleaned, but the hydrophobicity of the surface was permanently damaged as indicated by the CA and SA plateauing prior to matching the CA and SA of the clean surfaces. Also, pollen particles ruined the hydrophobicity of the surface because of cell bursting upon contact with the water droplet. Consequently these pollen particles could not removed from the surface via rolling water droplets. This section confirms the conclusions of other researchers that the adhesive force between the surface and the contaminate must be overcome in order for the SH surface to exhibit self-cleaning properties [67, 69, 70].

3.2 Cleaning Via Condensation

The second cleaning method tested in this study was removal of contaminates from the SH surfaces via condensation. As described in Section 2.2.2, the contaminated surfaces were placed vertically in a humid environment and cooled 3° to 5° below the dew point temperature, causing micro-droplets to form on the surface via condensation. With time, these droplets grew large enough to roll off the surface, ideally removing any contaminates in its path. The cyclic pattern of the droplets growing and rolling off the surface is referred to as a condensation cycle. Between each condensation cycle, the CA and SA were measured. This section discusses how effective condensation is at removing salt, tobacco, and pollen from a SH surface over the course of 4 condensation cycles. Both the micro-structured and nano-structured surfaces were tested is this portion of the study.

3.2.1 SH Surfaces Contaminated with Salt and Cleaned via Condensation

Similar to the rolling droplet tests, salt showed excellent potential to be removed from the surface via condensation. Figure 3.8 shows the CA and SA between each condensation cycle. In this figure, the x-axis represents the number of condensation cycles the surface has experienc and the y-axis represents the CA (Figure 3.8a) or SA (Figure 3.8b). Solid data points represent the CA and SA on micro-structured surfaces and the open data points represent the CA and SA on

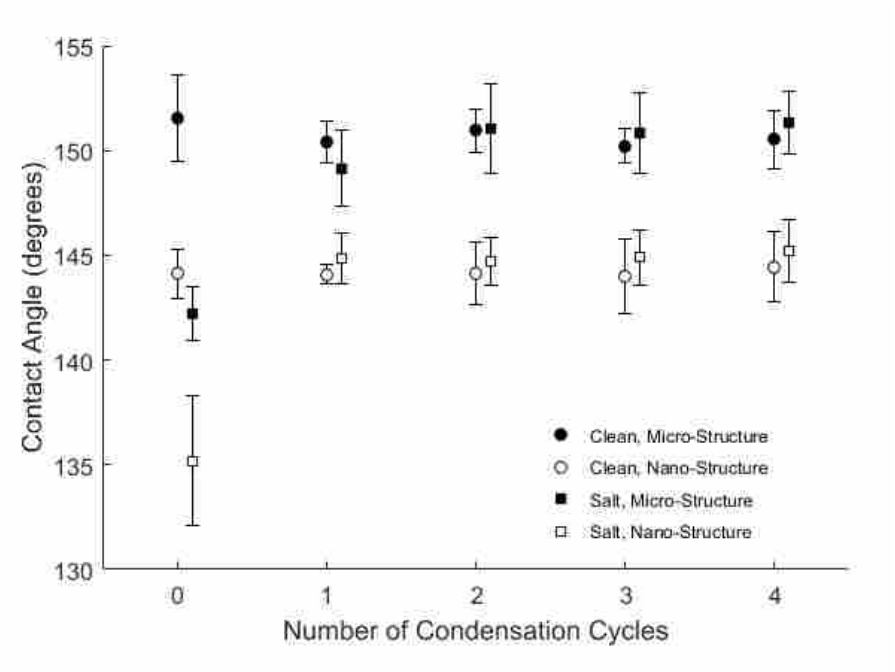

(a)

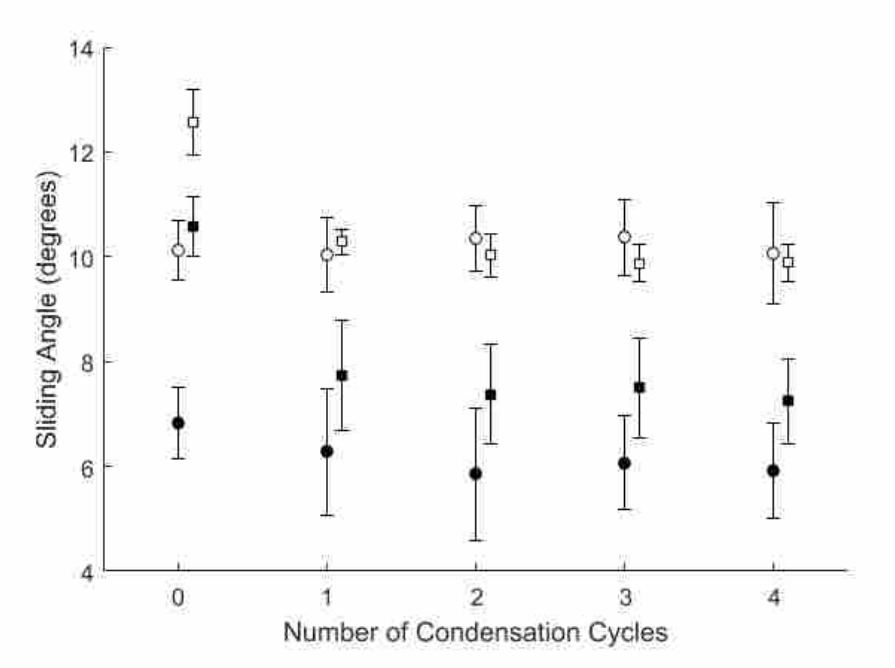

(b)

Figure 3.8: SH surfaces contaminated with salt were cleaned via condensation on the surface. The CA and SA were measured between each condensation cycle. In this figure, open data points represent micro-structures and closed data points represent nano-structured surfaces.

nano-structured surfaces. Clean surfaces are represented by circles and salt contaminated surfaces are represented by squares. An offset of 0.1 is applied to the contaminated data points to better present the data, but still associates with the nearest whole number. As indicated in Table 2.1 and seen in Figure 3.8, the presence of salt particles causes the CA to drop by approximately 10° and the SA to increase by approximately 3° on both the micro-structured and nano-structured surfaces. The raw data collected for this portion of the study are shown in Appendix A.9-10.

Figure 3.8 shows that both micro-structured and nano-structured surfaces are nearly completely cleaned after the first condensation cycle. For example, the salt particles cause the CA on the micro-structured surface to drop from 150$\pm$1.9°to 142$\pm$1.3°. After a single condensation cycle, the average CA on the contaminated surface increases to be within 2° of the average CA on the clean surface, which is equal to the error of the goniometer used to measure the CA. Furthermore, the upper limit of the contaminated surface standard deviation is greater than the average CA on the clean surface, implying that the CA on several of the contaminated surfaces are approximately the same or better than their clean surface counterparts. Additional condensation cycles cause the average CA on the contaminated surfaces to be equal to or greater than the average CA on the clean surfaces.

However, the SA on the micro-structured surface, unlike the CA, is not fully recovered. Similar to the CA tests on the micro-structured surfaces, the only significant improvement for the SA occurs after the first condensation cycle. Additional condensation cycles show no meaningful change. The challenge with these results is determining if the standard deviation of the contaminated surface SA overlaps with the clean surface SA sufficiently to claim the surface is clean. After each condensation cycle, the standard deviation bars for the clean and contaminated surfaces overlap implying that several of the contaminated surfaces exhibit a lower SA than several of the clean surfaces. However, the average SA for the contaminated surfaces is consistently greater than the upper standard deviation bound of the clean surfaces by about 1.3° to 1.5°. This is slightly larger than the error of the tilting stage ($\pm$1°) suggesting a small degree of contamination is still present on the surface. Despite this, the CA on the contaminated surfaces matches the clean surface so well that we conclude the surface must be fully cleaned with minimal lasting effects on the SA of the droplet.

For nano-structured surfaces, the CA behaves in the exact same pattern described for the micro-structured surfaces. Specifically, the salt initially reduces the CA by 10° and after the first condensation cycle, the average CA is within the standard deviation bounds of the clean surface. In fact, the average SA is greater on the contaminated surface than the clean surface. This is acceptable assuming the CA and SA of the SH surfaces contaminated with salt in their clean state is slightly better than the CA and SA of the SH surfaces used as the clean surfaces. A variety of factors can cause this including impurities in the surface during production and slightly inconsistent amounts of hydrophobic coatings applied to the surface. Regardless, because the surfaces are completely cleaned after the first condensation cycle, no further improvement is possible.

The SA of the nano-structured surfaces contaminated with salt behaves in a similar manner. The presence of the salt causes the SA of the surface to increase by approximately 3°. After a single condensation cycle, the entire standard deviation of the SA on the contaminated surface is within the bounds of the standard deviation for the clean surface, implying that all the surfaces have been completely cleaned. Additional condensation cycles did not improve the SA because no more salt particles are present to be removed from the surface. Consequently, the SA on the contaminated surface matches the SA on the clean surface nearly perfectly for all additional condensation cycles.

Later in this report two non-dimensional numbers, CA^* and SA^*, will be presented which creates a ratio between the current CA and SA of the surface after each cleaning iteration and the initial CA and SA of each contaminated surfaces. The purpose of CA^* and SA^* will be to compare the cleaning efficiency of both cleaning methods and surface structures and the effects each contaminate has on the cleaning efficiency. Because of this, a comparison between cleaning salt contaminated surfaces via rolling water droplets and via condensation is reserved for this later section (See Section 3.3).

An interesting observation made during this study is the location of the condensed droplets' nucleation sites when a contaminate was present on the surface. Figure 3.9 shows images from six different time intervals during a condensation cycle on a nano-structured surface contaminated with salt. Initially (0 min), the surface is dry and the salt deposits are evenly spread out across the surface, represented by the white dots in Figure 3.9. The blue elliptical dot is a marking on the back of the surface which is used to determine the scale of the image (the nano-structured surfaces were transparent). The width of this dot is 1.5 mm. As condensation commences on the surface in Figure

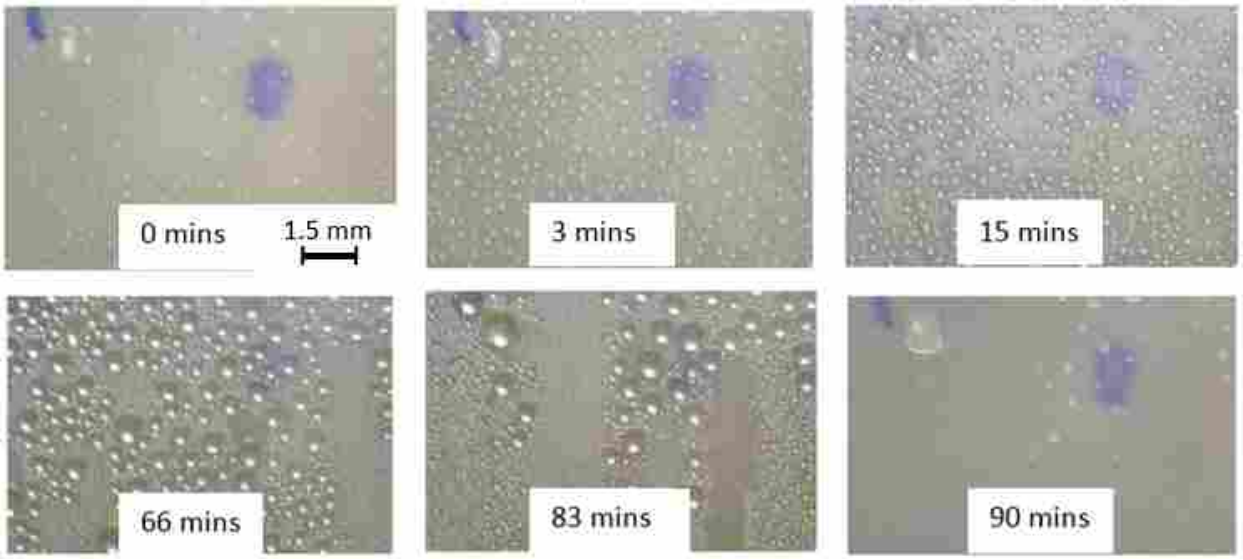

Figure 3.9: Sequence of images showing a condensation cycle occurring on a nano-structured SH surface contaminated with salt particles. When droplets roll off the surface, the salt particles are removed with the droplets. Also, this figure shows that after 3 mins, the salt particles served as the primary nucleation sites for the condensed droplets.

3.9, the salt particles serve as the primary nucleation sites for the condensing droplets (3 mins). Xu et. al observed that contaminates on a surface frequently serve as the preferred nucleation site during condensation [96]. Additionally, salt particles are hydrophilic and are hypothesized to naturally attract the water vapor molecules as opposed to other areas on the SH surface. After several minutes, the salt appears to be entirely engulfed by the condensed droplets and the droplets begin forming at other nucleation sites across the surface (15 mins). As time passes, these droplets coalesce and reach the critical diameter (1.1 ± 0.2 mm on a nano-structured surface), after which they roll off the surface (66 mins). Secondary droplets immediately begin to form in the droplet path, beginning a second condensation cycle. After the majority of the droplets have rolled off the surface, completing a condensation cycle (83 mins), the surface is removed from the humid environment and the remaining condensed droplets are evaporated from the surface into the dry surrounding air via natural convection (90 mins). Note the salt deposits left behind coincide with the locations of the droplets which did not roll off the surface and were instead evaporated.

With regards to exhibiting self-cleaning properties via condensation, note the reduction in salt particles on the surface in Figure 3.9 as indicated by the white areas from to 0 mins and to 90 mins. There are significantly fewer salt particles present on the surface after the condensation

Figure 3.10: Sequence of images showing an abbreviated condensation cycle occurring on a surface contaminated with salt, where the droplets do not reach the critical diameter to roll off the surface. Because the droplets do not roll off the surface, the surface does not exhibit self-cleaning properties. Note: time=55 mins is the same image as time = 0 mins in Figure 3.9.

cycle at 90 mins. This reduction is due to the droplets rolling off the surface, removing the salt particles and thus demonstrating the self-cleaning property.

Prior to the full condensation cycle shown in Figure 3.9, the same surface underwent a portion of a condensation cycle where water droplets condensed on the surface for 45 mins so that distinct individual droplets formed, but not long enough for any condensed droplet to reach the critical diameter and begin rolling off the surface. This abbreviated condensation cycle is shown in Figure 3.10. Because the droplets did not reach the critical diameter and roll off the surface, the salt particles were not removed from the surface. This is seen in Figure 3.10 where salt is present both before (0 mins) and after the abbreviated condensation cycle (55 mins). While seemingly obvious, this observation emphasizes an important point that the condensed droplets must be physically removed from the surface in order for the SH surface to exhibit self-cleaning. Also note the salt is again left in the droplet evaporation area. In this study, droplets rolling off the surface due to the gravitational force was the only droplet removal mechanism. Many researches have observed jumping droplets as an alternative form of droplet removal in which a particulate could be removed from the surface. Wisdom et. al. and Watson et. al even showed that self-cleaning is possible via jumping droplets (see section 1.2.6) [2, 85]. This phenomena, however, was not observed in this study as these jumping droplets are generally observed on two tiered surfaces.

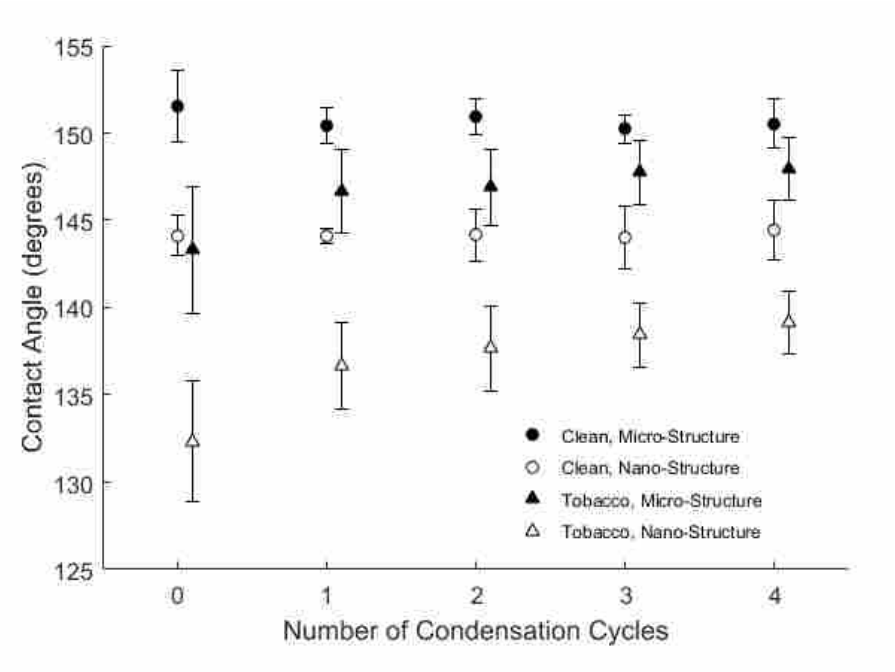

(a)

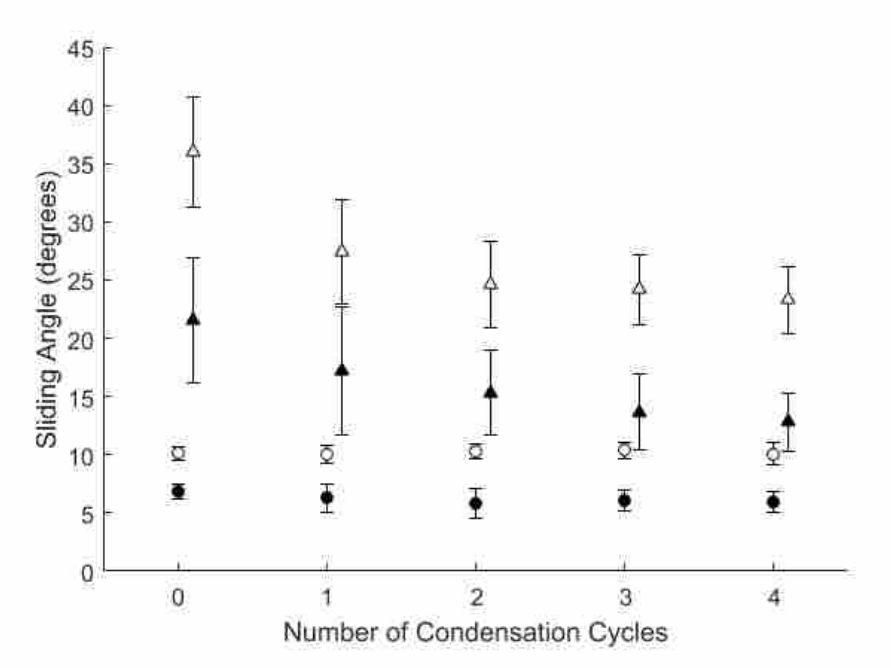

(b)

Figure 3.11: SH surfaces contaminated with tobacco were cleaned via condensation on the surface. The CA and SA were measured between each condensation cycle. In this figure, open data points represent micro-structures and closed data points represent nano-structured surfaces.

3.2.2 SH Surfaces Contaminated with Tobacco and Cleaned via Condensation

Similar to the rolling droplet test, tobacco could only partially be removed from the surface via condensation. Figure 3.11 shows the measured CA and SA on tobacco contaminated surfaces between each condensation cycle. The axes and markers are similar to the Figure 3.4, except the x-axis represents condensation cycles. Data for these test are included in Appendix A.11-12. As has been discussed previously, tobacco has a significant impact on the overall hydrophobicity of the SH surface. Because of the tobacco, the CA is reduced on average by approximately 13° on nano-structured surfaces and 7° on micro-structured surfaces. The SA was also greatly affected, increasing by 30° on nano-structured surfaces and by 11° on micro-structured surfaces.

The majority of the cleaning on tobacco contaminated surfaces occurs after the first condensation cycle. On the micro-structured surfaces, for instance, the CA saw the greatest improvement of 4° after the first condensation. Additional condensation cycles resulted in small improvements in the average CA totaling approximately 2° over the next 3 condensation cycles. However, because the accuracy of the goniometer is $\pm 2°$, this improvement is not substantial enough to claim any further significant improvement in the cleanliness of the surface. Interestingly, the upper bound of the contaminated surface begins to intersect with the lower standard deviation bounds of the clean surface, suggesting that some of the contaminated surfaces behave similarly to the lowest CA of the clean surfaces. This small intersection of standard deviations was also seen when the tobacco contaminated surfaces were cleaned with rolling water droplets. Since the intersection of the standard deviations is minimal and only small increases in the average CA occurs over multiple condensation cycles, we can conclude that the tobacco still has a lasting effect on the hydrophobicity of the surface when cleaned via condensation.

This conclusion is further sustained by the results of the SA on the micro-structured surfaces. As seen in Figure 3.11b, the presence of tobacco residue also greatly affects the SA on the micro-structured surfaces. Similar to the CA, the SA experiences the greatest improvements after the first condensation cycle. However, unlike surfaces contaminated with salt, the SA data points continue to improve with additional condensation cycles. After both the second and third condensation cycles, the SA decreases by about 2° per condensation cycle. This continual cleaning is most likely due to the tobacco particles serving as the preferential nucleation sites and could not

be seen on salt surfaces because all the salt was removed after the first condensation cycle. Unfortunately, the SA after the third and fourth condensation cycles are the same, suggesting that the surface has reached its maximum cleaning potential and will experience the plateauing effect. To confirm this though, additional condensation cycles would be required. Despite the continued improvement in the surface hydrophobicity after multiple condensation cycles, the standard deviation of the SA measurements on the contaminated surfaces does not cross the standard deviation of the clean surfaces. Consequently, it is apparent that notwithstanding the continual improvement in the SA and CA after the first three condensation cycles, the surface is not ever capable of recapturing the original hydrophobicity of a clean surface.

On the nano-structured surfaces, the CA improved the most during the first condensation cycle in which the average CA increased by 4°. Additional condensation cycles saw small but further improvements, in which the average CA improved by 3° over the course of three additional condensation cycles. However, the upper standard deviation bound is still substantially greater on the tobacco contaminated surface than the the lower standard deviation bound on the clean nano-structured surface. After four condensation cycles on the surface, the standard deviation bounds between the contaminated and clean surfaces remain separated by 4° implying that there is still significant lasting effects on the surfaces due to the tobacco.

Finally, the SA on the nano-structures surfaces remains greatly affected by the tobacco even after four condensation cycles. Like the micro-structured surface, the nano-structured surface saw the greatest improvement in the SA after the first condensation cycle. Here, the average SA decreases by 9°. The second condensation cycle further reduces the SA by an additional 3°. However, after this, the surfaces experience the same plateauing effect seen during the rolling droplet tests (see Figure 3.4). Specifically, the average SA on the contaminated surfaces does not decrease any further after two condensation cycles occur on the surface. Furthermore, like the CA measurements in Figure 3.11, a significant difference of 9° remains between the SA standard deviation bounds of the contaminated and clean, nano-structured surfaces after the fourth condensation cycle.

Observations of condensation on tobacco contaminated surfaces show that like salt, tobacco particles serve as the preferred nucleation site of condensing droplets. Figure 3.12 shows the early stages of a condensation cycle on a surface contaminated with salt (Figure 3.12a) and tobacco (Figure 3.12b) in which the initial condensed droplets forms around the contaminating particulates

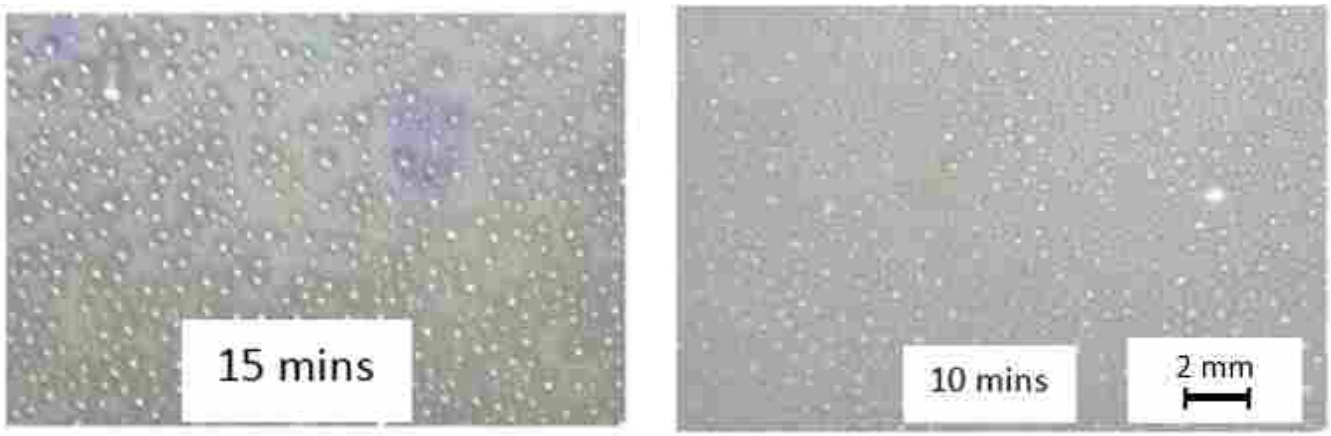

(a) (b)

Figure 3.12: Condensation on two nano-structured surfaces contaminated with salt particles (a) and tobacco residue (b). As can be seen in this image, the particles on the surface initially serve as the primary nucleation sites for condensing droplets.

on a nano-structured surface. The condensation cycle and cleaning dynamics are similar to the the condensation cycle on a surface contaminated with salt as discussed in Figure 3.9. As the droplets on a tobacco surface reaches the critical diameter and roll off the surface, they sweep away any condensed droplet in its path. These condensed droplets would have also condensed around the tobacco particles and ideally partially peeled the particles away from the surface and absorbed them in to the condensed droplet. Because the tobacco particles serve as the preferred nucleation site, this could potentially happen for every condensation cycle that tobacco particles are present. However, as the CA and SA have shown, there is a limit as to how much tobacco can be removed from the surface.

3.2.3 Condensation on SH Surface Contaminated with Pollen

As discussed previously in Section 3.1.3, water droplets were not able to remove pollen particles from the surface via rolling droplets. Unfortunately, this is also the case for cleaning via condensation. In this section, both micro-structured and nano-structured surfaces were contaminated with with pollen by shaking stamin and pistil portions of the flower as described in Section 2.1.3. This causes several pollen particles to fall onto the surface as shown in Figure 3.13 (cycle

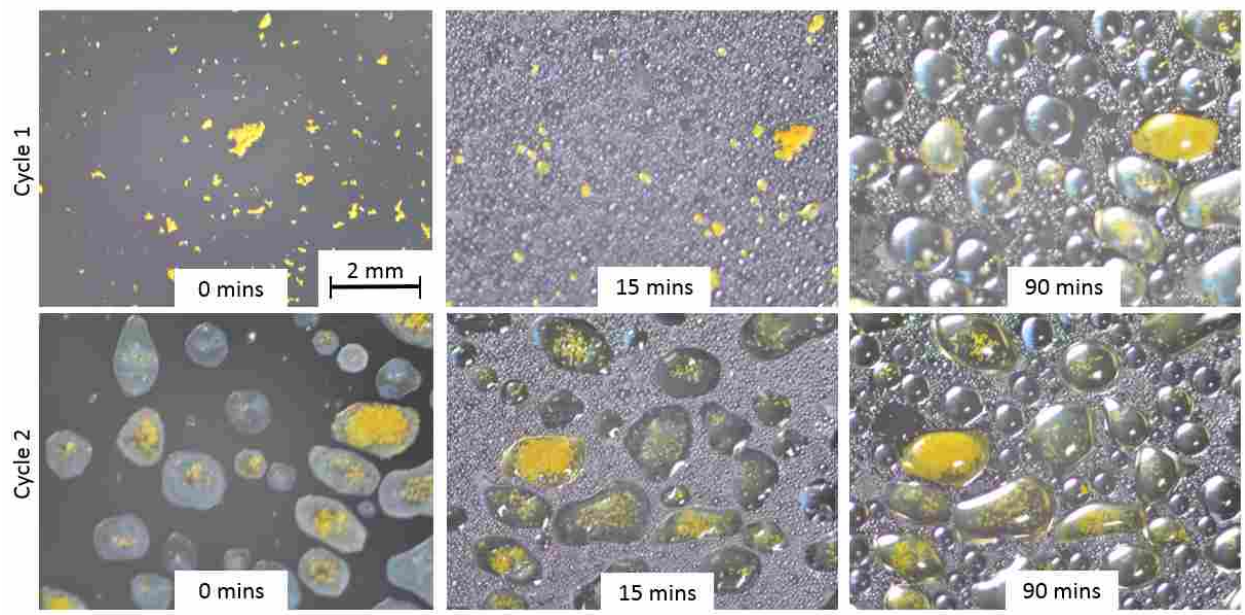

Figure 3.13: Sequence of images showing a condensation cycle occurring on a micro-structured SH surface contaminated with pollen particles. At 0 mins in cycle 1, the surface has just been contaminated with pollen. After 90 mins, the pollen particles have experience cell bursting and the condensed droplets have become pinned to the surface. These droplets are evaporated from the surface, which is shown in 0 mins of cycle 2. A second condensation cycle occurs where the pollen stains become the primary nucleation sites across the surface.

1, 0 mins). The surfaces were then placed in the humidity environment and cooled below the dew point temperature.

A series of images in which two condensation cycles occur on a micro-structured surface contaminated with pollen is shown in Figure 3.13. The rib patterns are vertical in this figure. Unlike surfaces contaminated with salt and tobacco, the condensed droplets first form randomly across the pollen contaminated surface, as shown after 15 mins in cycle 1. However, as the condensation cycle continues and the pollen particles are continually exposed to the condensed water droplets, the water droplets are osmotically absorbed into the cell creating a high hydrostatic pressure within the cell. This causes the cell wall to fail and the cellular organelles to spread out across the surface, similar to what was observed in Figure 3.5. When this happens, the condensed droplets are pinned to the surface as observed after 90 mins in cycle 1. Note that a full condensation cycle was not achieved in this part of the study because no droplets ever rolled off the surface. Furthermore, the condensed droplets behave similar to filmwise condensation in the areas in which the condensed

droplets are in contact with the pollen particles. Consequently, no droplet roll off is observed on this surface resulting in no self-cleaning properties.

After 90 mins of the condensing droplet not rolling off the surface in cycle 1 of Figure 3.13, the surface was removed from the humid environment and the condensed droplets allowed to naturally evaporate with no additional heat applied to the surface. This resulted in the pollen stains seen at 0 mins of cycle 2 in Figure 3.13. These pollen stains are similar to the pollen stains shown in Figure 3.6 in that they are entirely composed of the cellular organelles. Once all the water droplets are evaporated from the surface, the surface was placed back in the humid environment to experience a second condensation cycle. This is referred to as cycle 2 in Figure 3.13. After 15 mins of the second condensation cycle, it is evident that the pollen stains serve as the preferential nucleation sites for the condensing droplets. Furthermore, within these pollen stains, filmwise condensation occurs. After 90 mins, the filmwise condensation continues to expand across the majority of the surface. Again, no droplet roll off is observed on this surface and so the SH surface could not exhibit any self-cleaning properties. Also, because no droplet roll off occurred after 90 mins, no full condensation cycle was ever achieved.

The CA was also measured in between condensation cycles 1 and 2 of Figure 3.13. On both micro-structured and nano-structured surfaces, the hydrophobicity of the surface was ruined. The CA was reduced to 45°on the nano-structured surface and 65°on a micro-structured surface. Furthermore, because both surface types behaved as a hydrophilic surface, any droplet placed on the surface would not roll off meaning the SA was unmeasurable. These same results were found on both surfaces after the second condensation cycle.

Like the rolling droplet tests, the condensed droplets in contact with the pollen particles causes hydrodynamic osmosis leading to cell bursting. Figure 3.14 shows two SEM images of the pollen stains which were caused by the cell bursting. The pollen in these images come from Daylily flowers. The first SEM image, Figure 3.14a shows that the cellular organelles have spread out across the nano-structured surface and is the direct cause of the pollen stains. Figure 3.14b displays the pollen stain on a micro-structured surface. Interestingly, because the size of the rib structures in relation to the cellular organelles is so much larger, the cellular organelles fall in between the rib structures. The cellular organelles spread across the surface is the cause of the destruction of the hydrophobicity of the surface.

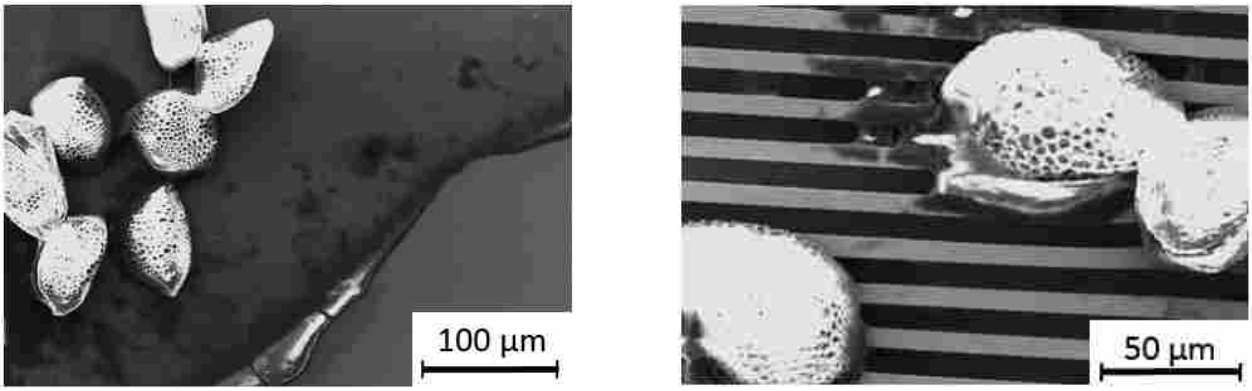

(a) (b)

Figure 3.14: SEM images of the pollen stains on micro-structured surfaces (a) and nano-structured surfaces (b). Due to cell bursting, the cellular organelles spread out across the SH surface, ruining the hydrophobicity of the surface.

3.2.4 Summary of Self-Cleaning via Condensation

From this study of cleaning via condensation, it has been shown that condensation is viable means to clean SH surfaces for certain contaminates loosely bound to the surface such as salt in a single condensation cycle. Other contaminates that have a stronger adhesive force to the surface like tobacco can be partially removed from the surface over multiple condensation cycles, but leaves a lasting affect on the overall hydrophobicity of the surface. And finally, contaminates such as pollen can be devastating to the surface's hydrophobicity due to hydrodynamic osmosis and cell bursting. Like cleaning via rolling droplets, the type of contaminate significantly effects the overall self-cleaning efficiency of a SH surface.

3.3 Non-Dimensional Contact Angle and Sliding Angle

One of the primary questions this study has strived to answer is how the hydrophobicity of a SH surface improves as the surface is cleaned either via rolling droplets or via condensation. Using the CA and SA tests, this objective boils down to the difference in the hydrophobic properties between the clean surfaces and contaminated surfaces. To answer this question, this study has tracked the CA and SA and their improvements as the surfaces are cleaned by both cleaning methods.

Two challenges arrive with this approach in order to make the best comparisons between the cleaning efficiencies on all contaminated surfaces. First, the clean micro-structured surfaces and nano- structured surfaces have different CA and SA making it difficult to compare the cleaning efficiency across them. Second, the initial CA and SA on the contaminated surfaces can vary significantly, especially on surfaces contaminated with tobacco as indicated by the large standard deviations seen on these surfaces in Figures 3.4 and 3.11. This is primarily caused by varying degrees of contaminates settling on the surface during the contamination process and the contaminated surface exhibiting a large hysteresis. Because the presence of the contaminates reduces the overall hydrophobicity of the surface, surfaces that accumulate more salt particles and tobacco residue generally exhibit lower CAs and higher SAs. This further adds to the difficulty of comparing the cleaning efficiencies of the different types of contaminates.

To address these issues, two non-dimensional numbers, CA^* and SA^*, have been created as shown in equations 3.1 and 3.2

$$CA^* = \frac{CA_i - CA_{clean}}{CA_{initial} - CA_{clean}} \tag{3.1}$$

$$SA^* = \frac{SA_i - SA_{clean}}{SA_{initial} - SA_{clean}} \tag{3.2}$$

where CA_i represents the CA after i number of droplets have rolled over the surface or i number of condensation cycles the surface has experienced, CA_{clean} represents the average CA across several clean surfaces (exact number of surfaces tested is shown in Table 2.2), and $CA_{initial}$ is the initial CA on each individual surface. The variables of SA^* in equation 3.2 are similar. The numerator of CA^* and SA^* represents the difference between the current CA and SA and the average clean CA and SA. This difference represents how far the current surface is from a clean surface. The difference in the denominator represents the degree to which the surface was initially contaminated. The ratio of these two differences allows all surfaces to be compared regardless of initial contamination conditions, hydrophobicity of the clean surface, and surface structure or contaminate. The CA^* and SA^* were calculated for each surface.

Figure 3.15 shows the average CA^* and SA^* on micro-structured and nano-structured surfaces. Each surface is contaminated with salt or tobacco and cleaned either via rolling droplets or condensation. The y-axis represents the CA^* (Figure 3.15a) or SA^* (Figure 3.15b). The x-axis represents the number of droplets that have rolled over the surface or the number of condensation

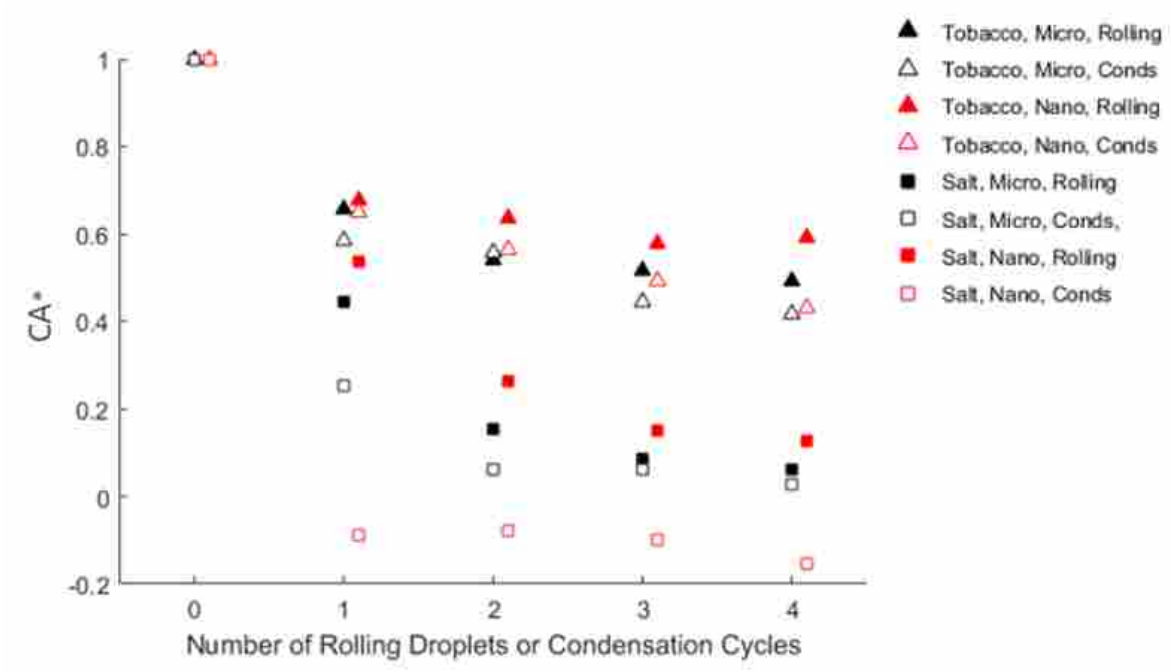

(a)

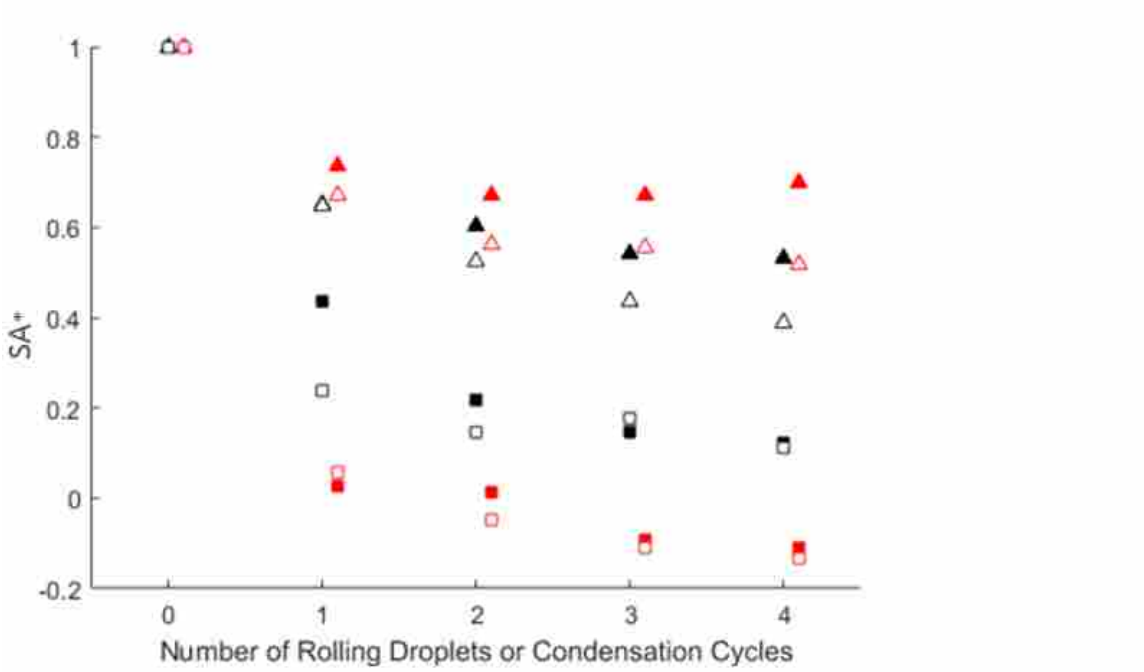

(b)

Figure 3.15: Average non-dimensional contact angle, CA^* (a), and sliding angle, SA^* (b), as a function of droplets rolling over the surface or condensation cycles. All data points are equal to 1 at 0 water droplets or 0 condensation cycles. Condensation is abbreviated to "Conds" in the legend.

cycles the surface has experienced. Surfaces contaminated with salt and tobacco are represented by squares and triangles respectively. Pollen was excluded because it showed no potential to be removed from the surface. Micro-structured surface data correspond to the black data points and nano-structured surfaces to the red data points. The purpose of Figure 3.15 is to compare the general trends observed throughout this study across all surface types, contaminates, and cleaning methods. Consequently, only the average CA^* and SA^* are presented in Figure 3.15 without the standard deviation bars.

As can be seen in Figure 3.15, the overall cleaning efficiency of each surface is primarily contaminate dependent and not surface or cleaning method dependent. For example, in Figure 3.15 it is apparent that regardless of the cleaning method, salt particles are removed from the surface much more easily than tobacco particles as all square markers are below the triangle makers. Generally speaking, surfaces contaminated with salt were able to reclaim the fullness of their hydrophobicity after two to three water droplets rolled over the surface or after the surface experienced one to two condensation cycles. This is seen as the CA^* and SA^* approach zero. where CA^* and SA^* equal to zero implies that the difference between CA_i and CA_{clean} or SA_i and SA_{clean} is minimal. On the other hand, CA^* and SA^* for surfaces contaminated with tobacco plateaus between 0.4-0.6 after two droplets roll over the surface and two to three condensation cycles. Beyond this, all of the tobacco contaminated surfaces show only small improvement, irrespective of surface size and cleaning method. This means that the average tobacco contaminated surfaces only reclaims approximately 50% of their original hydrophobicity over the range of droplets and condensation cycles tested in this study. This observation was confirmed in Sections 3.1.2 and3.2.2 when the individual cases were analyzed.

One of the primary factors to consider when determining if a particulate can be removed is the surface area the particulate is in contact with on the surface. In order for any particle to be removed, the water droplet must overcome the force between the particle and the surface [1, 70]. Recalling Figure 3.1, salt particles primarily sit on top of the mico-rib and nano-rib structures. Sitting on top of the rib structures reduces the amount of surface area the particles is in contact with on the surface. By minimizing this contact area, the surface energy between the droplet and salt particles is also minimized. Thus, little force is required to overcome the surface adhesive force between the salt and the surface. Conversely, the contact area between the tobacco and the

surface is much greater as seen in Figure 3.3 where the entirety of the tobacco particles appear to be in contact with the rib structures. Additionally, tobacco has a greater adhesive force to the surface than does salt. Thus neither rolling droplets nor condensing droplets to provide the required amount of force needed to remove the bulk of the tobacco residue from the surface.

With regards to the SH structure size, CA^* and SA^* shows that the surface structure does not significantly impact the cleaning efficiency of the surface. For instance, the CA^* and SA^* for tobacco surfaces is essentially the same regardless of surface structure size. This was unexpected due to the severe negative effect tobacco had on the overall hydrophobicity of the nano-structured surfaces compared to the micro-structured surfaces. Similarly, results of micro-structured and nano-structured surfaces contaminated with salt align nearly the same as well. The largest discrepancy appears to be in the average SA^*, which the nano-structured surfaces contaminated with salt is notably lower than the average SA^* for micro-structured surfaces. However, the CA^* of the micro-structured and nano-structured surfaces are still about the same. The difference in the SA^* is perhaps due to some salt particles potentially falling in between the ribs of the micro-structured surfaces which would not be removed by either cleaning method but may still have an affect on the CA and SA measurements. Bhushan et. al similarly showed that the cleaning efficiency on micro-structured surfaces contaminated with SiC particles is similar to that on nano-structured surfaces in an artificial rain shower. [3]. They also showed, however, that the cleaning efficiency on two-tiered surfaces was superior to both micro-structured surfaces and nano-structured surfaces.

Finally, Figure 3.15 addresses one of the overarching questions of this study: is condensation as effective at cleaning SH surfaces as rolling droplets over the surface? In many cases presented in Figure 3.15, the CA^* and SA^* of surfaces cleaned via condensation are nearly the same as the CA^* and SA^* of the counterpart surfaces cleaned via rolling droplets. However, with that said, there are some notable differences between surfaces cleaned via condensation and surfaces cleaned via rolling droplets.

First, the CA^* on surfaces contaminated with salt is consistently higher for the rolling droplet scenario. As discussed in Section 3.2.1, many of the salt surfaces tested in this study required only one condensation cycle to fully clean the surface. This is seen as the red open data points in Figure 3.15a level out below zero after the first condensation cycle. This is most likely because the salt particles have a longer time in contact with the condensing droplets as these droplets

grow around the salt particles on the surface (see Figure 3.9). This allows the salt to dissolve into and diffuse through the condensing droplets and remove the bulk of the salt particles in a single condensation cycle. Conversely, two to three droplets rolling over the surface are required for CA^* and SA^* to approach zero, as indicated by the solid red dots in Figure 3.15a . Because the droplet is moving, the salt does not have the same amount of time to dissolve into and diffuse through the droplet, but must instead simply adhere to the surface of the droplet. Because of this, not all salt particles may be picked up by the first or second rolling droplet. There is minimal difference between the SA^* data points for condensation and rolling droplets in Figure 3.15b.

Second, surfaces contaminated with tobacco showed only a small but notable difference between surfaces cleaned via rolling droplets and surfaces cleaned via condensation. In Section 3.2.2 it was noted that the CA and SA on tobacco contaminated surfaces decreased for the first three condensation cycles but showed evidence of plateauing after the fourth condensation cycle. In Section 3.1.2 it was observed that the CA and SA plateau after the second or third droplet rolls over the surface. These pattern are again seen in Figure 3.15a where the open data points diverge slightly from the solid data points between the third and fourth rolling droplets and condensation cycles. These lower CA^* and SA^* suggest that more tobacco was removed from the surface after being cleaned via condensation. The difference between these two sets of data is believed to be in relation to how the water droplets come in contact with the tobacco particles and is similar to the way salt particles come in contact with the cleaning droplets. Recall from Figure 3.12b that the condensing droplets prefer to condense around the tobacco particles. While tobacco may not dissolve into the the droplet like salt, condensing around the tobacco particles can assist in separating the tobacco from the surface. Conversely, as water droplets roll over the surface, they only have a limited time in which the tobacco particles can adhere to the droplet and pull these particles away from the surface. Consequently, the CA^* and SA^* on surfaces cleaned via condensation are slightly lower than theCA^* and SA^* on surfaces cleaned via rolling droplets. Thus, condensation proves to be more effective at cleaning tobacco particulates from SH surfaces given sufficient time for the condensed droplets to roll off the surface.

In Figure 3.15, CA^* and SA^* may be less than zero, essentially implying that when cleaned the contaminated surfaces become more hydrophobic than the clean surfaces. This is acceptable because the data reported are average values of the CA^* and SA^* on each surface. Recalling equa-

tions 3.1 and 3.2, we see that the CA and SA are respectively normalized by the average CA and SA of several clean surfaces. Because of this, it is possible for the clean state of the contaminated surfaces to be more hydrophobic than the reported average values of the clean surface and thus result in a negative CA^* and SA^* when the entire surface is cleaned. Another approach that could be used for future studies would be to measure the CA and SA on each surface prior to contaminating the each surface. These CA and SA values could then be used in place of the average CA_{clean} and SA_{clean} values which would avoid negative CA^* and SA^* values.

3.4 Self- Cleaning on Smooth, Hydrophobic Surfaces

The final section of this thesis discusses the difference between smooth and structured surfaces. As defined previously in Section 1.2, the difference between hydrophobic and SH surfaces is that SH surfaces are composed of micro-structures or nano-structures. Recall from Chapter 2 that a Teflon® hydrophobic coating was applied to the micro-structured surfaces and a proprietary coating was applied to the nano-structured surfaces. These same coatings have been applied to smooth surfaces without the rib structures to create a smooth, hydrophobic surface. The purpose of this section is to isolate the effect surface structures have on the self-cleaning properties and elucidate the effect of surface chemistry on the particulate bonding.

Each smooth surface underwent the same contamination processes explained in Section 2.1 (except pollen since it adhered to the surface). Once contaminated, half the surfaces were cleaned via rolling droplets and the other half were cleaned via condensation. The number of surfaces tested in this section is presented in Table 2.2. The CA^* and SA^* for each smooth surface was calculated to directly compare the cleaning efficiency of the smooth surfaces to that of the structured surfaces. During this portion of this thesis, note that the CA on smooth, hydrophobic surfaces is less than on structured, SH surfaces and the SA on smooth, hydrophobic surfaces is greater than on structured, SH surfaces .

3.4.1 Cleaning via Rolling Droplets on Smooth, Hydrophobic Surfaces

Figure 3.16 shows the results of the rolling droplet test over smooth surfaces contaminated with salt and tobacco. The x-axis represents the number of droplets that cleaned the surface and

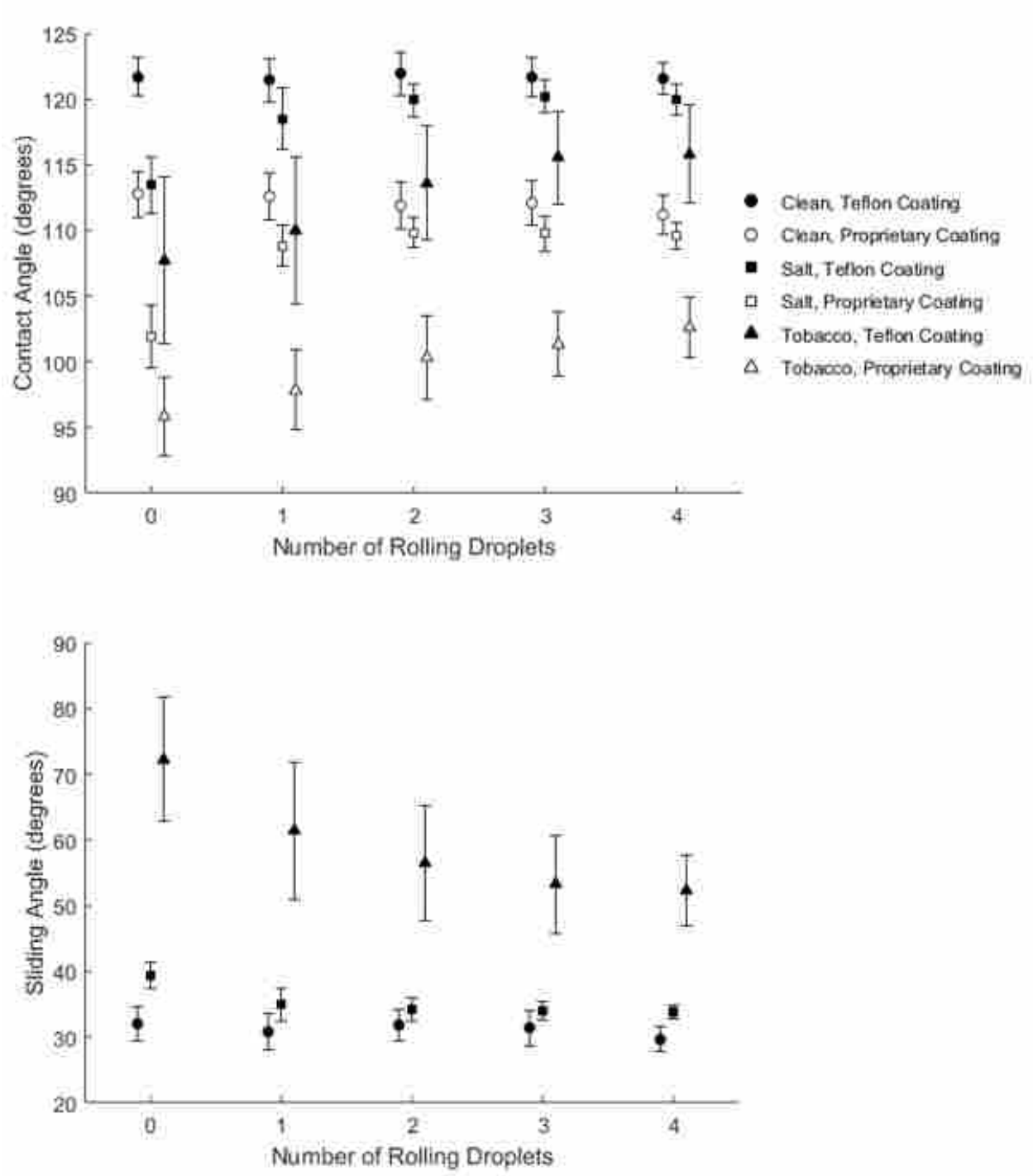

Figure 3.16: Smooth, hydrophobic surfaces contaminated with salt and tobacco were cleaned via rolling droplets. The CA (a) and SA (b) were measured after each droplet rolled over the surface. Droplets did not roll off smooth surfaces coated with the proprietary coating used in this study. Consequently, the SA on these surfaces are omitted from this figure.

the y-axis represent the CA (Figure 3.16a) and SA (Figure 3.16b). Surfaces coated with Teflon® are represented with solid data points and the surfaces coated with the proprietary coating are open data points. Clean surfaces are represented by circles; salt contaminated surfaces are represented by squares, and tobacco contaminated surfaces are represented by triangles. The SA for the smooth surfaces coated with the proprietary coating was approximately 90° on a clean surface. Consequently, the SA could not be used to determine the cleaning efficiency on these surfaces and is omitted from Figure 3.16b and subsequent figures discussing the SA.

As can be seen in Figure 3.16, the presence of contaminates on the surface greatly affects the hydrophobicity of the smooth surface. The data collected for individual surfaces is presented in Appendix A.13-18. On the Teflon® coated surfaces, the salt and tobacco reduced the average CA by 8° and 15° respectively and increased the average SA by 7° and 39°. Comparatively, salt and tobacco decreased the average CA on the micro-structured surfaces by 10° and 7° and increased the average SA by 4° and 15° respectively. The smooth surface coated with the proprietary coating saw a reduction in CA of 10° and 16° due to the presence of salt and tobacco on the surface, where as the nano-structured surfaces, the CA was reduced by 10° and 15°. Thus the alterations in CA and SA due to contamination are nearly the same as on the nano-structured surfaces. Recalling Figure 3.1b and Figure 3.3b, the contaminates primarily sit on top of the surface structures and thus similar effects salt and tobacco have on the structured surfaces versus smooth surfaces is not surprising.

The cleaning patterns observed on the structured surfaces in Section 3.1 are also seen on the smooth, hydrophobic surfaces in Figure 3.16. On surfaces contaminated with salt, two to three water droplets are required to roll over the surface in order to clean the surface. Specifically, after two water droplets roll over the surface on Teflon® coated surfaces and three droplets roll over the proprietary coated surfaces, the average CA is approximately equal to the lower standard deviation bound of their respective clean surfaces. This would imply that approximately half the surfaces match the hydrophobic behavior of the clean surfaces while half are slightly less than that of the clean surface. Because the standard deviation for both the Teflon® surfaces and the proprietary coated surfaces is small after three to four droplets rolling over the surface, we conclude that these surfaces are essentially cleaned. The average SA of the Teflon® surfaces is within the standard

deviation bounds of the clean surface after the second droplet rolls over the surface and therefore supports this conclusion.

The cleaning patterns shown in Figure 3.16 on the smooth surfaces contaminated with tobacco are similar to those discussed in Section 3.1.2. Like the SH surfaces contaminated with tobacco, the hydrophobicity of the smooth surfaces improves as the first two to three droplets roll over the surface before plateauing. This is true for both hydrophobic coatings. The SA of the Teflon® surfaces contaminated with tobacco remains substantially higher than the average SA on a clean surface. This again implies that regardless of how many droplets roll over the surface, the tobacco has a lasting effect on the hydrophobicity of the surface.

To best compare the effects of surface structures, CA^* and SA^* are shown in Figure 3.17 for both types of smooth surfaces (solid markers) and the associated structured surfaces (open markers). Red data points in Figure 3.17 coincide with surfaces coated with Teflon® and black data points are associated with surfaces coated with the proprietary coating. On Teflon® coated surfaces, structured surfaces achieved a slightly lower CA^* than smooth surfaces after three to four droplets rolling over the surface when contaminated with salt, but resulted in slightly higher CA^* than smooth surfaces when the surface was contaminated with tobacco. The SA^* on these surfaces was consistently lower for structured surfaces than smooth surfaces. Similarly, surfaces coated with the proprietary coating and contaminated with salt also achieved slightly lower CA^* than smooth surfaces. No significant difference between the smooth and structured proprietary coated surfaces was measured in the CA^* when contaminated with tobacco.

These results suggest that more salt will be removed from structured surfaces because the salt crystals sit on top of the surface structures. This minimizes the contact area and consequently the force between the salt particles and the surface. The tobacco on the other hand could easily fall between the ribs of the micro-structured surfaces, creating a larger contact area and force between the tobacco particles and surface. Because the cleaning droplets are in the Cassie-Baxter state, these tobacco particles would have minimal contact between the droplet and the particle, not sufficient enough to over come the adhesive force between the particle and surface. However, in general, the CA^* and SA^* between the smooth and structured surfaces are close enough to claim that the surface structure does not have a significant effect on the self-cleaning properties of the SH surface.

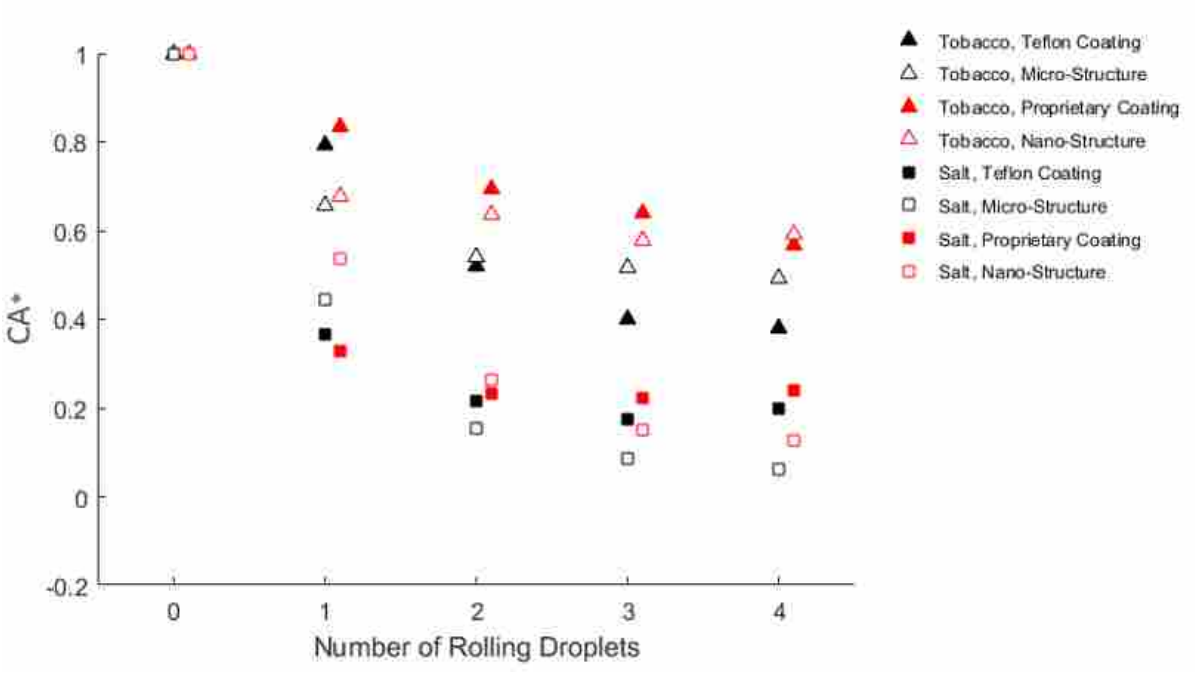

(a)

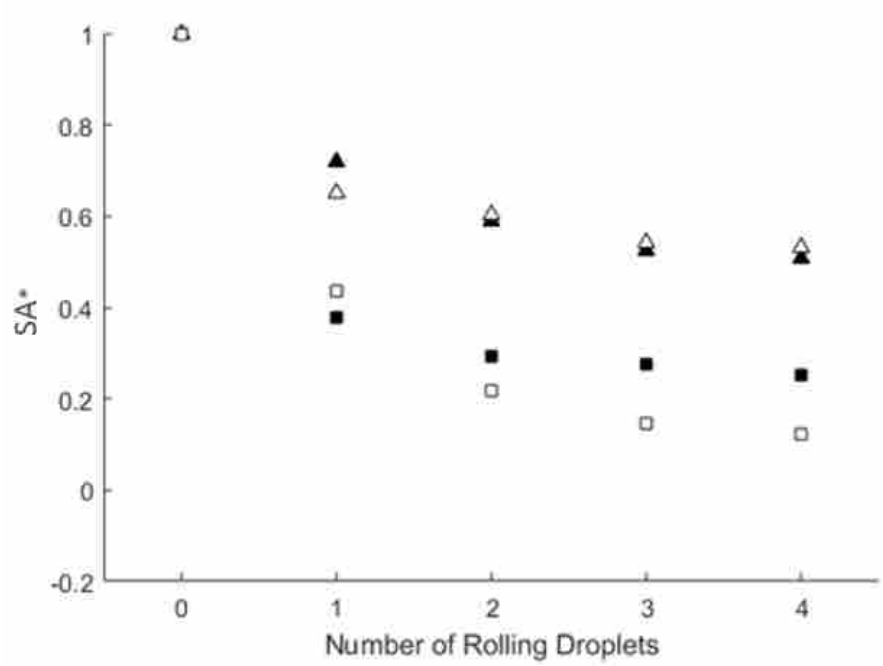

(b)

Figure 3.17: CA^* (a) and SA^* (b) on smooth and structured surfaces. These surfaces were contaminated with salt and tobacco and then cleaned via rolling droplets.

Since Figure 3.17 shows the surface structures do not significantly affect the overall cleaning efficiency of a surface , it may seem there is no motivation to spend the time and production resources to manufacture SH surfaces for the purpose of creating a self-cleaning surface. However, the initial SA has been normalized and thus the advantage of a lower SA is missing in Figure 3.17. The droplet mobility on a SH surface due to the low SA can be a crucial factor in a surface's ability to clean itself. The low SA of a SH surface promotes droplet roll off at very low angles. Consequently, the likelihood of droplets rolling off the surface is substantially higher on a SH surface. Subsequently, the likelihood of the surface cleaning itself is much higher on SH surfaces.

3.4.2 Cleaning via Condensation on Smooth, Hydrophobic Surfaces

Figure 3.18 shows the results of cleaning smooth, hydrophobic surfaces via condensation. The CA and SA were measured after each condensation cycle. The formatting scheme of this figure is the same as Figure 3.16 with the exception that the x-axis represents the number of condensation cycles experienced by the surface. Again, the SA for the smooth surfaces coated with the proprietary coating was approximately 90° on a clean surfaces and so is omitted from Figure 3.18b. The data collected for this portion of the study is reported in Appendix A.19-24.

Similar to the rolling droplets, the cleaning pattern via condensation on the smooth, hydrophobic surfaces are very similar to the cleaning patterns on a structured surface described in Section 3.2 in that the majority of the cleaning occurs during the first condensation cycle. For instance, the average CA of salt surfaces improves by 6° for Teflon® coated surfaces contaminated with salt. This is sufficient for the upper standard deviation bound of the salt surfaces to be equal to the lower standard deviation bound of the clean surface. A second condensation cycle increases the average CA by only 1°, but is sufficient enough that the average CA of the contaminated surfaces is approximately equal to the lower standard deviation bound of the clean surface. Furthermore, the upper standard deviation of the salt surface is approximately equal to the average CA of the clean surface after the second condensation cycle. Considering this increase is less than the error of the goniometer, we can conclude that the Teflon® coated surfaces required one to two condensation cycles to fully clean the surface. Additional condensation cycles do not make a significant difference in the average CA. After the first condensation cycle, the SA of the Teflon® coated surfaces contaminated with salt also match the SA of the clean surface, again suggesting the surface

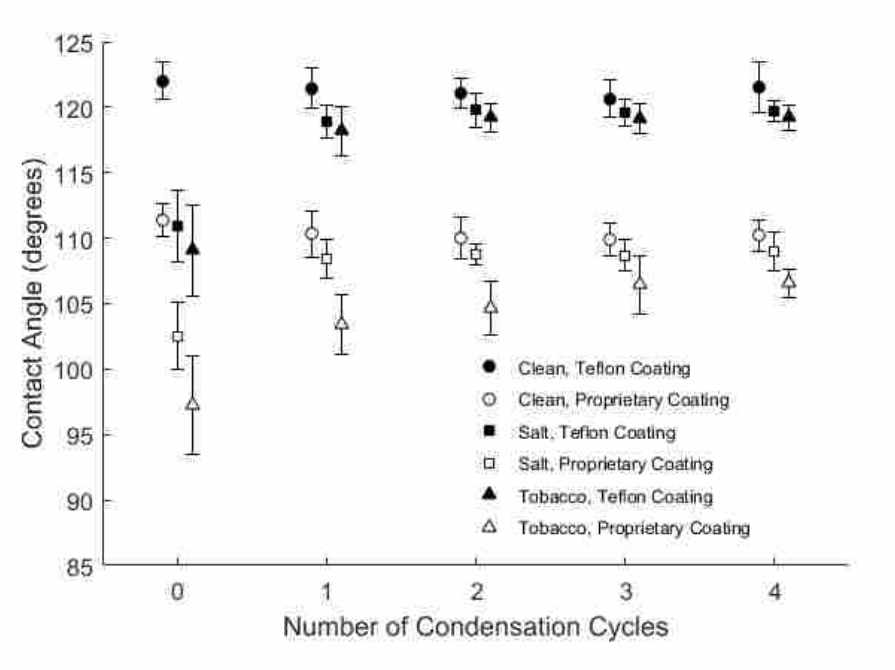

(a)

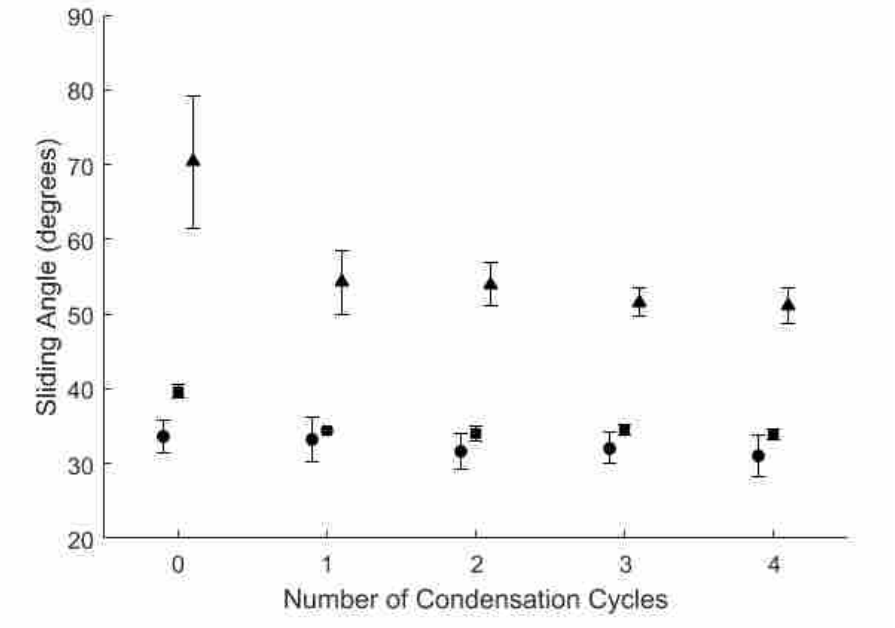

(b)

Figure 3.18: Hydrophobic surfaces contaminated with salt and tobacco were cleaned via condensation. The CA (a) and SA (b) were measured after each condensation cycle. Droplets did not roll off smooth surfaces coated with the proprietary coating used in this study. Consequently, the SA on these surfaces are omitted from this figure.

is fully cleaned. This same cleaning pattern is also seen for the smooth, hydrophobic surfaces contaminated with salt and coated with the proprietary coating.

The CA of Teflon® coated surfaces contaminated with tobacco increased significantly after the first condensation cycle. Interestingly, like the salt surfaces, the the upper standard deviation bound is about equal to the lower standard deviation bound of the clean surfaces after the first condensation cycle. With a small increase of 1°, which is within the error of the goniometer, the average CA of surfaces contaminated with tobacco is equal to the lower standard deviation bound of the clean surface after two to three condensation cycles. This implies that about half the tobacco contaminated surfaces match the CA of the clean surfaces. However, Figure 3.18b shows that the SA of the tobacco contaminated surfaces is significantly higher than the SA of a clean surface, thus implying that the tobacco still leaves a significant lasting effect on the overall hydrophobicity of the surfaces.

The CA of the tobacco contaminated surfaces coated with the proprietary hydrophobic coating improved over the course of three to four condensation cycles. While the greatest improvement occurred after the first condensation cycle, the continual improvement is significantly different than the Teflon® coated surfaces which saw the majority of its cleaning after in the first two condensation cycles. Likely, most the tobacco particles that could be removed via condensation were released during the first condensation cycle. However, while a lot of the loosely bound particles were swept away from the surface during the first condensation cycle, tobacco particles more tightly bound to on the proprietary coated surface continued to be removed over the course of several condensation cycles. This was also seen in Figure 3.11 on the nano-structured surfaces which has the same surface chemistry but plateaued after three condensation cycles.

Normalized values CA^* and SA^* for the smooth, hydrophobic surfaces cleaned via condensation are shown in Figure 3.19. This figure has a similar formatting scheme to Figure 3.17 except the x-axis represents the number of condensation cycles the surface experienced. Similar to Figure 3.17, the primary purpose of Figure 3.19 is to compare CA^* and SA^* of the smooth, hydrophobic surfaces in relation to the structured surface coated with the same hydrophobic coating; or in essence, to compare each solid data point to the accompanying open data point. In most cases, the structured surfaces, or open data points, exhibit a lower CA^* than the equivalent smooth, hydrophobic surfaces. This is particularly true for surfaces coated with Teflon® and contaminated with salt,

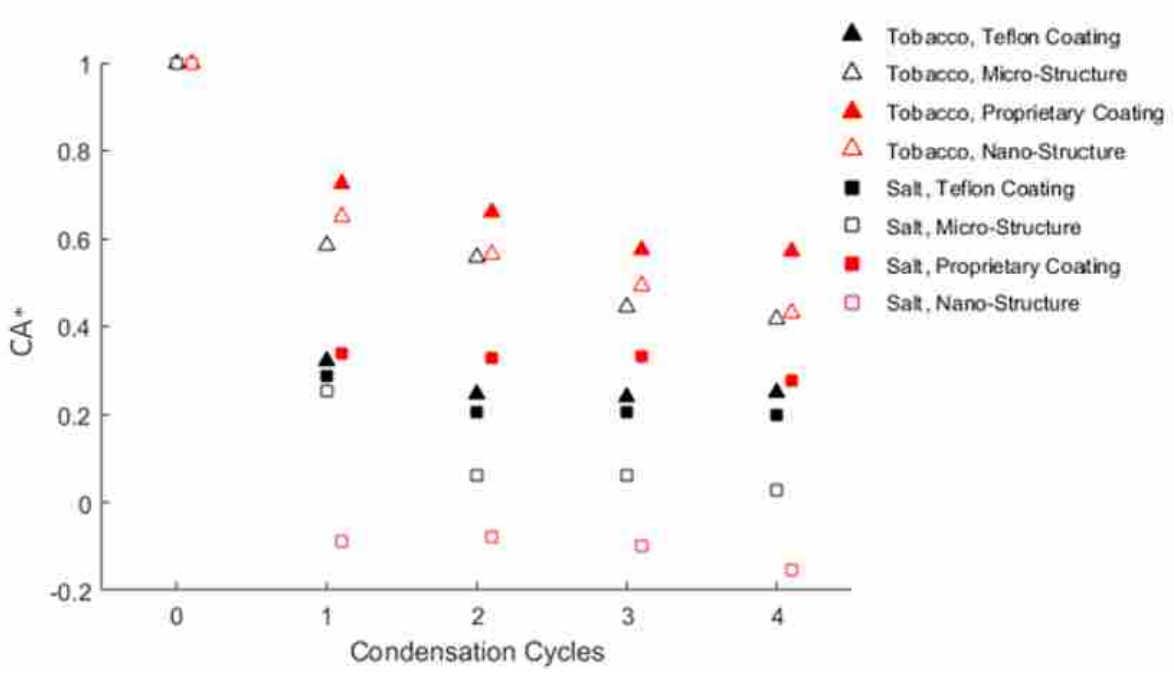

(a)

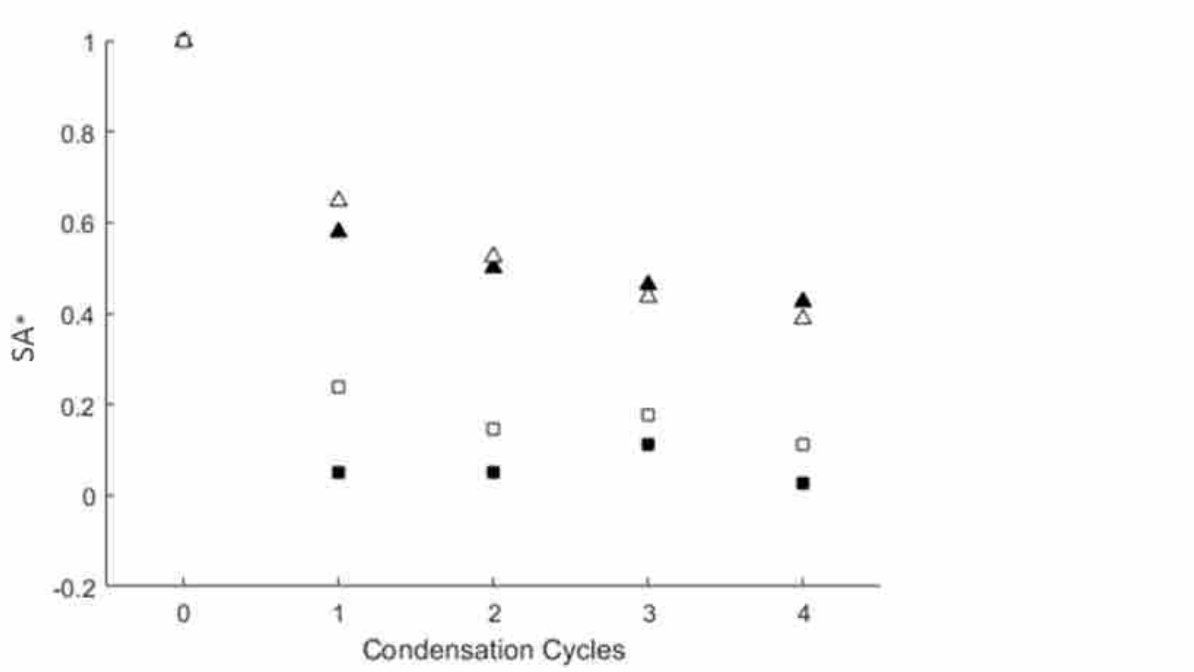

(b)

Figure 3.19: CA^* (a) and SA^* (b) on smooth and structured surfaces. These surfaces were contaminated with salt and tobacco and then cleaned via condensation.

surfaces coated with the proprietary coated and contaminated with salt, and surfaces coated with the proprietary coating and contaminated with tobacco, thus implying that structured surfaces are beneficial to self cleaning via condensation.

The only case in which this pattern does not apply is on surfaces coated with Teflon® and contaminated with tobacco. In this case, the smooth, hydrophobic surfaces exhibited a significantly lower CA^* after each condensation cycle relative to the micro-structured surface coated with Teflon®. This is explained as tobacco particles can fall in between the micro-structures where condensing droplets preferentially form due to the higher heat transfer rates at the corners of the rib structures [64]. Consequently, these particles inside the rib structures are the particles that will be removed during condensation. The tobacco particles on top of the rib structures may not be removed as the condensed droplets may not nucleate around them. Since the CA is measured by a droplet in the Cassie-Baxter state, these tobacco particles on top of the rib structures have the most influence on the CA measurement. Conversely, on a smooth surface, there are no rib structures for the droplets to nucleate in-between or for tobacco to collect within. Consequently, all the tobacco particles on the surface become the preferred nucleation site and more of these tobacco particles can be removed from the surface when the condensed droplets roll off. This is not the case for nano-structured surfaces because the majority of the tobacco particles sit on top of the surface structures as they are too big to fit into the cavities.

Lastly, in Figure 3.19 the CA^* for micro-structured surfaces equals approximately zero after the second condensation cycle and the CA^* for the nano-structured surface equals zero after the first condensation cycle implying that the average CA on the structured surfaces after being cleaned is approximately equal to the average CA on the clean surfaces. However, both the smooth structured surfaces had a final CA^* after four condensation cycles between 0.2 and 0.3, implying that the salt had some residual affects on the overall hydrophobicity of the surface. These results are intriguing since in Figure 3.18 it was determined that these contaminated surfaces were clean after four condensation cycle since the average CA was greater than the lower standard deviation bound of the clean surfaces. However, in examining Figure 3.18 a second time, it is evident that while declared "clean" for the purposes of this thesis, the average CA on the contaminated surfaces after being cleaned via condensation was still lower than the average CA on the clean surfaces. This small difference is expressed in a higher CA^* in Figure 3.19. Again, the difference between the

structured surfaces and smooth surfaces with regards to the cleaning efficiency on each surface comes down to the contact area between the salt particles and the surface. Because the structured surfaces minimize this contact area between the salt particle and surface, significantly less force is required to over come the adhesion between salt particles and the surface. This reduced adhesive force evidently makes a significant difference in the overall cleaning efficiency on SH surfaces.

From the results of this section, it is evident that for most cases structured SH surfaces are beneficial for promoting self-cleaning properties via condensation. In nature, most contaminates; such as salt, dust and dirt; that settle on a surface have a very low adhesive force to the surface. Consequently, minimizing the area the particles are in contact with the surface via the rib structures increases the likelihood that condensation will remove the particles from the surface. In cases where the particles are small enough to fall between the ribs which creates a stronger adhesion to the surface, such as tobacco in this study, a smooth, hydrophobic surface will be more beneficial for removing contaminates. Although this study only considered condensation on vertical surfaces, in order for the droplets to roll off and clean the surface, it must be tilted at an angle greater than the SA. For these reasons, SH can be much more beneficial in applications seeking to utilize self-cleaning properties via condensation as the SA is lower.

CHAPTER 4. CONCLUSION

Mimicking the Lotus Effect by the use of SH surfaces has many potential benefits in improving the efficiency of a variety of industrial applications. Consequently, several researchers have pursued developing a durable SH surface which can exhibit self-cleaning properties [33, 37]. In all cases, SH surfaces have a combination of a high CA and low SA causing water droplets on a SH surface to bead up like a marble and roll off the surface at very low SA. When tilted above the SA, a droplet on a contamianted SH surface will roll off the surface and remove any contaminating particles in its path, thus creating a self-cleaning effect. Researchers have sought to understand the capability of these self-cleaning properties by using a variety of cleaning methods including simulated rain showers and condensation on SH surfaces composed of micro-structures, nano-structures, and two-tiered structures [1–3, 12, 85].

In this thesis, the self-cleaning efficiency of SH surfaces was considered as each surface was cleaned by individual water droplets rolling over the surface or as condensed water droplets rolled off the surface. Three different contaminates were considered including salt, tobacco, and pollen on SH surfaces composed of micro-rib structures or nano-rib structures. To determine the cleaning efficiency of each surface, the CA and SA were measured before and after the surface was cleaned. It was observed that the hydrophobicity of the surface, indicated by the CA and SA, was greatly effected by each contaminate on the surface, but improved as contaminates were removed and the surfaces were cleaned by water droplets. The contaminated surface was considered clean when its CA and SA were equal to the CA and SA of a clean surface. This study makes three key observations which further the understanding of self-cleaning surfaces.

First, this study shows that the cleaning efficiency is dependent upon the surface adhesion between the contaminate and the surface. For instance, both the micro-structured and nano-structured surfaces were very effective at removing salt particles from the surface via rolling droplets and condensation. This is because the salt particles sat on top of the surface structures,

minimizing the contact area and subsequently the adhesive force between the salt crystals and the surface. Conversely, however, a much stronger adhesive force between the tobacco particles and surface was created such that only a partial cleaning was ever achieved when cleaning the surface either via rolling droplets or condensation. SEM images showed that tobacco residue would spread out across the surface, even falling in between the micro-rib structures, forming a very strong bond between the surface and particles in some locations. Although loosely bound tobacco particles could be removed from the surface, causing an overall improvement in the hydrophobicity of the surface, no surface contaminated with tobacco ever matched the hydrophobicity of a clean surface after being cleaned by rolling droplets or condensation. This permanent reduction in the hydrophobicity of the surface is due to some of the tobacco particles continually sticking to the surface. Finally, pollen particles ruined the hydrophobicity of the surfaces in this study. When exposed to water, hydrodynamic osmosis occurred in which the water was absorbed into the pollen cells until the hydrostatic pressure reached a limit which would cause cell bursting to occur. During cell bursting, the cell walls would fail and the cellular organelles would spread across and attach to the surface rendering the surface hydrophilic in those regions. No self-cleaning was ever seen on these surfaces. While the contaminates tested in this study vary from previous studies, these results agree with and emphasize the accepted understanding that the adhesive force between the contaminates and the surface is a significant factor in the potential for a SH surface to exhibit self-cleaning properties [1, 71]

Second, self-cleaning via condensation proved to be just as effective as self-cleaning via rolling droplets. This was shown using a non-dimensional contact angle, CA^*, and a non-dimensional sliding angle, SA^*, which is a ratio between the current hydrophobic state of the surface and the initial hydrophobic state of the contaminated surface. In nearly all cases, CA^* and SA^* of surfaces cleaned via condensation match the respective CA^* and SA^* of surfaces cleaned via rolling droplets after four condensation cycles or four water droplets rolling over the surface. The primary difference in the two cleaning methods is that only one to two condensation cycles as opposed to two to three rolling droplets were required to reach the cleanest possible state for each contaminate. This is believed to be because the contaminates serve as the preferential nucleation site during condensation and so the contaminate has substantially more time to diffuse through the water droplets prior to droplet roll off. When cleaned by rolling droplets, the droplet is only in contact with the

particulate for a limited amount of time and so the particulate does not have the time to diffuse throughout the droplet, but instead may remain adhered to the surface. This limits the overall number of particulates any one droplet can remove. To date, no research articles other than this thesis have made such a comparison between cleaning via rolling droplets and cleaning via condensation.

The third significant observation made in this study is that the self-cleaning efficiency of each surface is similar for both micro-structured and and nano-structured surfaces. This is indicated by CA^* and SA^* equaling similar values for both micro-structured and nano-structured surfaces, regardless of cleaning method or contaminate. Because the self-cleaning is independent of the size of surface structures, a range of manufacturing possibilities are available to achieve self-cleaning surfaces with similar cleaning efficiencies. Additionally, the CA^* and SA^* of smooth, hydrophobic surfaces similarly match that of structured surfaces after cleaning via rolling droplets or cleaning via condensation, thus implying that the smooth, hydrophobic surfaces exhibit the same cleaning efficiency as their structured counterparts. However, in considering the droplet mobility of the surface, the high CA and low SA are very beneficial in promoting droplet roll off and so seem to be a critical part of the self-cleaning process.

4.1 Proposed Future Work

Over the past several decades, the possibility of mimicking the Lotus Effect and utilizing SH surfaces for their self-cleaning properties has been widely accepted and multiple articles have been dedicated to developing self-cleaning surfaces. However, as alluded to in the introduction of this thesis, very few articles have been published which analyze the cleaning efficiency of specific SH surfaces. This leaves a range of possibilities for future researchers to investigate the overall efficiency of self-cleaning surfaces. This section presents just three ideas for future work.

The first possible direction is to considered the self cleaning properties of SH surfaces which exhibit spontaneous jumping droplets during condensation. Wisdom et. al and Watson et. al have reported that spontaneous jumping droplets can effectively remove contaminates from the surface [2,85]. However, this cleaning mechanism has yet to be compared to the cleaning efficiency of rolling water droplets over the surface. Additionally, it is anticipated that the cleaning dynamics of spontaneous jumping droplets differ from the cleaning dynamics of condensed droplets that roll off the surface, as seen during condensation in this thesis. This is primarily because at the

time of departure from the surface, the spontaneous jumping droplets are significantly smaller than the condensed droplets that roll off the surface. Thus, it is suggested that similar studies to this thesis ought to be done on surfaces that exhibit jumping droplets to determine the optimal cleaning method of SH surfaces.

Second, the current understanding of which particulates can be removed and which ones can not is still limited. A variety of contaminates including dried soil, siliconcarbide dust, titanium dioxide, and quartz dust and more have been removed from SH surfaces in various self-cleaning research articles [1–3, 12, 85]. This study adds salt, tobacco, and pollen to that list. However, as this study has shown, not all contaminates can be removed from the surface, such as tobacco residue and pollen particles. Expanding our understanding of which contaminates can be removed from self-cleaning surfaces will greatly assist in implementing self-cleaning surfaces as a feasible reality. To best classify and predict contaminates that can and can not be removed from the surface, a comprehensive study of the surface chemistry of each SH surface and molecular bonds between the contaminates and SH surface in relation to self-cleaning surfaces may be required.

Finally, to date all self-cleaning tests on artificial SH surfaces have been focused in a laboratory setting with very controlled parameters. Because the end goal is to create self-cleaning surfaces which can be utilized in a variety of environments, studies analyzing self-cleaning surfaces behavior in natural environments can be very beneficial in improving the manufacturing process of SH surfaces for the purpose of self-cleaning. Factors that occur in natural environments and not laboratory settings can include irregular cleaning cycles, a large range of contaminates all settling on the surface at the same time, varying temperatures and humidity, and other realistic situations. Taking a step back and looking at the big picture by considering how the current state of the art SH surfaces behave in the real world can greatly assist in understanding what further developments are needed to truly accomplish durable, robust, self-cleaning surfaces.

REFERENCES

[1] W. Barthlott and C. Neinhuis, "Purity of the sacred lotus, or escape from contamination in biological surfaces," *Planta*, vol. 202, no. 1, pp. 1–8, 1997. viii, 1, 14, 15, 16, 17, 34, 51, 66, 80, 81, 83

[2] G. S. Watson, M. Gellender, and J. A. Watson, "Self-propulsion of dew drops on lotus leaves: a potential mechanism for self cleaning," *Biofouling*, vol. 30, no. 4, pp. 427–434, 2014. viii, 18, 19, 56, 80, 82, 83

[3] B. Bhushan, Y. C. Jung, and K. Koch, "Self-cleaning efficiency of artificial superhydrophobic surfaces," *Langmuir*, vol. 25, no. 5, pp. 3240–3248, 2009. 1, 3, 14, 16, 18, 20, 34, 51, 67, 80, 83

[4] N. A. Patankar, "Mimicking the lotus effect: influence of double roughness structures and slender pillars," *Langmuir*, vol. 20, no. 19, pp. 8209–8213, 2004. 1, 6

[5] A. Marmur, "Wetting on hydrophobic rough surfaces: to be heterogeneous or not to be?" *Langmuir*, vol. 19, no. 20, pp. 8343–8348, 2003. 2

[6] K.-Y. Law, "Definitions for hydrophilicity, hydrophobicity, and superhydrophobicity: Getting the basics right," *The Journal of Physical Chemistry Letters*, vol. 5, no. 4, pp. 686–688, 2014. 2

[7] K. Smyth, A. Paxon, H. m. Kwon, T. Deng, and K. K. Varanasi, "Dynamic wetting on superhydrophobic surfaces: Droplet impact and wetting hysteresis," in *Thermal and Thermomechanical Phenomena in Electronic Systems (ITherm), 2010 12th IEEE Intersociety Conference on*, Conference Proceedings, pp. 1–8. 2

[8] Z. Yoshimitsu, A. Nakajima, T. Watanabe, and K. Hashimoto, "Effects of surface structure on the hydrophobicity and sliding behavior of water droplets," *Langmuir*, vol. 18, no. 15, pp. 5818–5822, 2002. 2, 3

[9] L. Gao and T. J. McCarthy, "Contact angle hysteresis explained," *Langmuir*, vol. 22, no. 14, pp. 6234–6237, 2006. 3

[10] J. P. Rothstein, "Slip on superhydrophobic surfaces," *Annual Review of Fluid Mechanics*, vol. 42, no. 1, pp. 89–109, 2010. 3, 9, 10

[11] K. A. Wier and T. J. McCarthy, "Condensation on ultrahydrophobic surfaces and its effect on droplet mobility: ultrahydrophobic surfaces are not always water repellant," *Langmuir*, vol. 22, no. 6, pp. 2433–2436, 2006. 3, 13, 47

[12] R. Frstner, W. Barthlott, C. Neinhuis, and P. Walzel, "Wetting and self-cleaning properties of artificial superhydrophobic surfaces," *Langmuir*, vol. 21, no. 3, pp. 956–961, 2005. 3, 14, 16, 17, 34, 51, 80, 83

[13] L. Mahadevan and Y. Pomeau, "Rolling droplets," *Physics of Fluids*, vol. 11, no. 9, pp. 2449–2453, 1999. 3, 15

[14] J. F. Prince, "The influence of superhydrophobicity on laminar jet impingement and turbulent flow in a channel with walls exhibiting riblets," Dissertation, 2013. 4, 6, 22

[15] A. B. D. Cassie and S. Baxter, "Wettability of porous surfaces," *Transactions of the Faraday Society*, vol. 40, no. 0, pp. 546–551, 1944. 4

[16] A. Lafuma and D. Quere, "Superhydrophobic states," *Nat Mater*, vol. 2, no. 7, pp. 457–460, 2003. 5

[17] A. Nakajima, A. Fujishima, K. Hashimoto, and T. Watanabe, "Preparation of transparent superhydrophobic boehmite and silica films by sublimation of aluminum acetylacetonate," *Advanced Materials*, vol. 11, no. 16, pp. 1365–1368, 1999. 6

[18] B. He, N. A. Patankar, and J. Lee, "Multiple equilibrium droplet shapes and design criterion for rough hydrophobic surfaces," *Langmuir*, vol. 19, no. 12, pp. 4999–5003, 2003. 6

[19] K. Y. Suh and S. Jon, "Control over wettability of polyethylene glycol surfaces using capillary lithography," *Langmuir*, vol. 21, no. 15, pp. 6836–6841, 2005. 6

[20] D. Oner and T. J. McCarthy, "Ultrahydrophobic surfaces. effects of topography length scales on wettability," *Langmuir*, vol. 16, no. 20, pp. 7777–7782, 2000. 6

[21] P. Chen, "Tunable superhydrophobic surfaces by colloidal lithography," in *ABSTRACTS OF PAPERS OF THE AMERICAN CHEMICAL SOCIETY*, vol. 226. AMER CHEMICAL SOC 1155 16TH ST, NW, WASHINGTON, DC 20036 USA, Conference Proceedings, pp. U382–U383. 6

[22] Y. Wu, M. Kuroda, H. Sugimura, Y. Inoue, and O. Takai, "Nanotextures fabricated by microwave plasma cvd: application to ultra water-repellent surface," *Surface and Coatings Technology*, vol. 174, pp. 867–871, 2003. 6

[23] J. Fresnais, L. Benyahia, and F. Poncin-Epaillard, "Dynamic (de)wetting properties of superhydrophobic plasma-treated polyethylene surfaces," *Surface and Interface Analysis*, vol. 38, no. 3, pp. 144–149, 2006. 6

[24] S. Minko, M. Mller, M. Motornov, M. Nitschke, K. Grundke, and M. Stamm, "Two-level structured self-adaptive surfaces with reversibly tunable properties," *Journal of the American Chemical Society*, vol. 125, no. 13, pp. 3896–3900, 2003. 6

[25] M. Ma, Y. Mao, M. Gupta, K. K. Gleason, and G. C. Rutledge, "Superhydrophobic fabrics produced by electrospinning and chemical vapor deposition," *Macromolecules*, vol. 38, no. 23, pp. 9742–9748, 2005. 7

[26] H. Liu, L. Feng, J. Zhai, L. Jiang, and D. Zhu, "Reversible wettability of a chemical vapor deposition prepared zno film between superhydrophobicity and superhydrophilicity," *Langmuir*, vol. 20, no. 14, pp. 5659–5661, 2004. 7

[27] M. Li, J. Zhai, H. Liu, Y. Song, L. Jiang, and D. Zhu, "Electrochemical deposition of conductive superhydrophobic zinc oxide thin films," *The Journal of Physical Chemistry B*, vol. 107, no. 37, pp. 9954–9957, 2003. 7

[28] A. Nakajima, C. Saiki, K. Hashimoto, and T. Watanabe, "Processing of roughened silica film by coagulated colloidal silica for super-hydrophobic coating," *Journal of Materials Science Letters*, vol. 20, no. 21, pp. 1975–1977, 2001. 7

[29] G. Zhang, D. Wang, Z.-Z. Gu, and H. Mhwald, "Fabrication of superhydrophobic surfaces from binary colloidal assembly," *Langmuir*, vol. 21, no. 20, pp. 9143–9148, 2005. 7

[30] T. Soeno, K. Inokuchi, and S. Shiratori, "Ultra-water-repellent surface: fabrication of complicated structure of sio2 nanoparticles by electrostatic self-assembled films," *Applied Surface Science*, vol. 237, no. 1, pp. 539–543, 2004. 7

[31] L. Zhai, F. . Cebeci, R. E. Cohen, and M. F. Rubner, "Stable superhydrophobic coatings from polyelectrolyte multilayers," *Nano Letters*, vol. 4, no. 7, pp. 1349–1353, 2004. 7

[32] R. M. Jisr, H. H. Rmaile, and J. B. Schlenoff, "Hydrophobic and ultrahydrophobic multilayer thin films from perfluorinated polyelectrolytes," *Angewandte Chemie International Edition*, vol. 44, no. 5, pp. 782–785, 2005. 7

[33] C.-H. Xue and J.-Z. Ma, "Long-lived superhydrophobic surfaces," *Journal of Materials Chemistry A*, vol. 1, no. 13, pp. 4146–4161, 2013. 7, 8, 80

[34] D. Shchukin and H. Mhwald, "Self-repairing coatings containing active nanoreservoirs," *Small*, vol. 3, no. 6, pp. 926–943, 2007. 7

[35] Y. Li, L. Li, and J. Sun, "Bioinspired self-healing superhydrophobic coatings," *Angewandte Chemie*, vol. 122, no. 35, pp. 6265–6269, 2010. 7

[36] F.-C. Wang, F. Yang, and Y.-P. Zhao, "Size effect on the coalescence-induced self-propelled droplet," *Applied Physics Letters*, vol. 98, no. 5, p. 053112, 2011. 7

[37] X.-M. Li, D. Reinhoudt, and M. Crego-Calama, "What do we need for a superhydrophobic surface? a review on the recent progress in the preparation of superhydrophobic surfaces," *Chemical Society Reviews*, vol. 36, no. 8, pp. 1350–1368, 2007. 8, 80

[38] J. Ou and J. P. Rothstein, "Direct velocity measurements of the flow past drag-reducing ultrahydrophobic surfaces," *Physics of Fluids*, vol. 17, no. 10, p. 103606, 2005. 8, 9

[39] R. Perkins, "Piv measurements of turbulent flow in rectangular channel over superhydrophobic surfaces with riblets," Thesis, 2014. 9

[40] M. Xu, G. Sun, and C.-J. C. Kim, "Wetting dynamics study of underwater superhydrophobic surfaces through direct meniscus visualization," in *Micro Electro Mechanical Systems*

(MEMS), 2014 IEEE 27th International Conference on. IEEE, Conference Proceedings, pp. 668–671. 10

[41] R. Poetes, K. Holtzmann, K. Franze, and U. Steiner, "Metastable underwater superhydrophobicity," *Physical Review Letters*, vol. 105, no. 16, p. 166104, 2010. 10

[42] C. Lee and C.-J. Kim, "Wetting and active dewetting processes of hierarchically constructed superhydrophobic surfaces fully immersed in water," *Journal of Microelectromechanical Systems*, vol. 21, no. 3, pp. 712–720, 2012. 10

[43] S. Nath, S. F. Ahmadi, and J. B. Boreyko, "A review of condensation frosting," *Nanoscale and Microscale Thermophysical Engineering*, pp. 1–21, 2017. 10

[44] M. J. Kreder, J. Alvarenga, P. Kim, and J. Aizenberg, "Design of anti-icing surfaces: smooth, textured or slippery?" *Nature Reviews Materials*, vol. 1, p. 15003, 2016. 10

[45] T. M. Schutzius, S. Jung, T. Maitra, P. Eberle, C. Antonini, C. Stamatopoulos, and D. Poulikakos, "Physics of icing and rational design of surfaces with extraordinary icephobicity," *Langmuir*, vol. 31, no. 17, pp. 4807–4821, 2014. 10

[46] P. Kim, T.-S. Wong, J. Alvarenga, M. J. Kreder, W. E. Adorno-Martinez, and J. Aizenberg, "Liquid-infused nanostructured surfaces with extreme anti-ice and anti-frost performance," *ACS nano*, vol. 6, no. 8, pp. 6569–6577, 2012. 11

[47] K. Rykaczewski, S. Anand, S. B. Subramanyam, and K. K. Varanasi, "Mechanism of frost formation on lubricant-impregnated surfaces," *Langmuir*, vol. 29, no. 17, pp. 5230–5238, 2013. 11

[48] Y. Zhang, X. Yu, H. Wu, and J. Wu, "Facile fabrication of superhydrophobic nanostructures on aluminum foils with controlled-condensation and delayed-icing effects," *Applied Surface Science*, vol. 258, no. 20, pp. 8253–8257, 2012. 11

[49] L. Mishchenko, B. Hatton, V. Bahadur, J. A. Taylor, T. Krupenkin, and J. Aizenberg, "Design of ice-free nanostructured surfaces based on repulsion of impacting water droplets," *ACS nano*, vol. 4, no. 12, pp. 7699–7707, 2010. 11

[50] T. Maitra, M. K. Tiwari, C. Antonini, P. Schoch, S. Jung, P. Eberle, and D. Poulikakos, "On the nanoengineering of superhydrophobic and impalement resistant surface textures below the freezing temperature," *Nano letters*, vol. 14, no. 1, pp. 172–182, 2013. 11

[51] J. B. Boreyko and C. P. Collier, "Delayed frost growth on jumping-drop superhydrophobic surfaces," *ACS nano*, vol. 7, no. 2, pp. 1618–1627, 2013. 11

[52] J. B. Boreyko, R. R. Hansen, K. R. Murphy, S. Nath, S. T. Retterer, and C. P. Collier, "Controlling condensation and frost growth with chemical micropatterns," *Scientific reports*, vol. 6, 2016. 11

[53] A. Kim, C. Lee, H. Kim, and J. Kim, "Simple approach to superhydrophobic nanostructured al for practical antifrosting application based on enhanced self-propelled jumping droplets," *ACS applied materials and interfaces*, vol. 7, no. 13, pp. 7206–7213, 2015. 11

[54] Q. Hao, Y. Pang, Y. Zhao, J. Zhang, J. Feng, and S. Yao, "Mechanism of delayed frost growth on superhydrophobic surfaces with jumping condensates: more than interdrop freezing," *Langmuir*, vol. 30, no. 51, pp. 15 416–15 422, 2014.

[55] K. R. Murphy, W. T. McClintic, K. C. Lester, C. P. Collier, and J. B. Boreyko, "Dynamic defrosting on scalable superhydrophobic surfaces," *ACS Applied Materials and Interfaces*, vol. 9, no. 28, 2017. 11

[56] C. Antonini, M. Innocenti, T. Horn, M. Marengo, and A. Amirfazli, "Understanding the effect of superhydrophobic coatings on energy reduction in anti-icing systems," *Cold Regions Science and Technology*, vol. 67, no. 1, pp. 58–67, 2011. 12

[57] R. Enright, N. Miljkovic, J. L. Alvarado, K. Kim, and J. W. Rose, "Dropwise condensation on micro- and nanostructured surfaces," *Nanoscale and Microscale Thermophysical Engineering*, vol. 18, no. 3, pp. 223–250, 2014. 12, 14

[58] J. B. Boreyko and C.-H. Chen, "Self-propelled dropwise condensate on superhydrophobic surfaces," *Physical Review Letters*, vol. 103, no. 18, p. 184501, 2009. 13

[59] C.-H. Chen, Q. Cai, C. Tsai, C.-L. Chen, G. Xiong, Y. Yu, and Z. Ren, "Dropwise condensation on superhydrophobic surfaces with two-tier roughness," *Applied Physics Letters*, vol. 90, no. 17, p. 173108, 2007. 13

[60] C. Dietz, K. Rykaczewski, A. G. Fedorov, and Y. Joshi, "Visualization of droplet departure on a superhydrophobic surface and implications to heat transfer enhancement during dropwise condensation," *Applied Physics Letters*, vol. 97, no. 3, p. 033104, 2010. 13

[61] R. Enright, N. Miljkovic, A. Al-Obeidi, C. V. Thompson, and E. N. Wang, "Condensation on superhydrophobic surfaces: The role of local energy barriers and structure length scale," *Langmuir*, vol. 28, no. 40, pp. 14 424–14 432, 2012. 13

[62] K. Rykaczewski, "Microdroplet growth mechanism during water condensation on superhydrophobic surfaces," *Langmuir*, vol. 28, no. 20, pp. 7720–7729, 2012. 13

[63] N. Miljkovic, R. Enright, and E. N. Wang, "Effect of droplet morphology on growth dynamics and heat transfer during condensation on superhydrophobic nanostructured surfaces," *ACS Nano*, vol. 6, no. 2, pp. 1776–1785, 2012. 13

[64] R. D. Narhe and D. A. Beysens, "Nucleation and growth on a superhydrophobic grooved surface," *Physical Review Letters*, vol. 93, no. 7, p. 076103, 2004. 13, 78

[65] X. Qu, J. B. Boreyko, F. Liu, R. L. Agapov, N. V. Lavrik, S. T. Retterer, J. J. Feng, C. P. Collier, and C.-H. Chen, "Self-propelled sweeping removal of dropwise condensate," *Applied Physics Letters*, vol. 106, no. 22, p. 221601, 2015. 13

[66] C. Dorrer and J. Rhe, "Condensation and wetting transitions on microstructured ultrahydrophobic surfaces," *Langmuir*, vol. 23, no. 7, pp. 3820–3824, 2007. 13

[67] Y.-Y. Quan, L.-Z. Zhang, R.-H. Qi, and R.-R. Cai, "Self-cleaning of surfaces: the role of surface wettability and dust types," *Scientific reports*, vol. 6, 2016. 14, 16, 51

[68] W. Barthlott and N. Ehler, "Raster-elektronen-mikroskopie der epidermis-oberflachen von spermatophyten," *Scanning electron microscopy of epidermal surfaces of Spermatophyta.) Abh. Akad. Wiss. Lit. Mainz, Math.-Naturwiss. Klasse, Trop. Subtrop. Pflanzenwelt*, vol. 19, pp. 367–467, 1977. 16

[69] P. Sharma, M. Flury, and J. Zhou, "Detachment of colloids from a solid surface by a moving airwater interface," *Journal of colloid and interface science*, vol. 326, no. 1, pp. 143–150, 2008. 16, 51

[70] A. W. Adamson and A. P. Gast, "Physical chemistry of surfaces," 1997. 16, 51, 66

[71] M. Yu, S. Chen, B. Zhang, D. Qiu, and S. Cui, "Why a lotus-like superhydrophobic surface is self-cleaning? an explanation from surface force measurements and analysis," *Langmuir*, vol. 30, no. 45, pp. 13 615–13 621, 2014. 16, 81

[72] R. Blossey, "Self-cleaning surfaces–virtual realities," *Nature materials*, vol. 2, no. 5, p. 301, 2003. 16

[73] S. Nishimoto and B. Bhushan, "Bioinspired self-cleaning surfaces with superhydrophobicity, superoleophobicity, and superhydrophilicity," *Rsc Advances*, vol. 3, no. 3, pp. 671–690, 2013. 16

[74] Y. Lu, S. Sathasivam, J. Song, C. R. Crick, C. J. Carmalt, and I. P. Parkin, "Robust self-cleaning surfaces that function when exposed to either air or oil," *Science*, vol. 347, no. 6226, pp. 1132–1135, 2015. 16

[75] I. P. Parkin and R. G. Palgrave, "Self-cleaning coatings," *Journal of Materials Chemistry*, vol. 15, no. 17, pp. 1689–1695, 2005. 16

[76] J. Zhu, C.-M. Hsu, Z. Yu, S. Fan, and Y. Cui, "Nanodome solar cells with efficient light management and self-cleaning," *Nano letters*, vol. 10, no. 6, pp. 1979–1984, 2009. 16

[77] Y. C. Jung and B. Bhushan, "Mechanically durable carbon nanotube composite hierarchical structures with superhydrophobicity, self-cleaning, and low-drag," *ACS nano*, vol. 3, no. 12, pp. 4155–4163, 2009. 16

[78] V. A. Ganesh, H. K. Raut, A. S. Nair, and S. Ramakrishna, "A review on self-cleaning coatings," *Journal of Materials Chemistry*, vol. 21, no. 41, pp. 16 304–16 322, 2011. 16

[79] J. Huang, S. Li, M. Ge, L. Wang, T. Xing, G. Chen, X. Liu, S. Al-Deyab, K. Zhang, and T. Chen, "Robust superhydrophobic tio 2@ fabrics for uv shielding, self-cleaning and oil-water separation," *Journal of Materials Chemistry A*, vol. 3, no. 6, pp. 2825–2832, 2015. 16

[80] I. Sas, R. E. Gorga, J. A. Joines, and K. A. Thoney, "Literature review on superhydrophobic self-cleaning surfaces produced by electrospinning," *Journal of Polymer Science Part B: Polymer Physics*, vol. 50, no. 12, pp. 824–845, 2012. 16

[81] K. Liu and L. Jiang, "Bio-inspired self-cleaning surfaces," *Annual Review of Materials Research*, vol. 42, no. 1, pp. 231–263, 2012. 16

[82] A. Nakajima, K. Hashimoto, T. Watanabe, K. Takai, G. Yamauchi, and A. Fujishima, "Transparent superhydrophobic thin films with self-cleaning properties," *Langmuir*, vol. 16, no. 17, pp. 7044–7047, 2000. 16

[83] T. Kamegawa, Y. Shimizu, and H. Yamashita, "Superhydrophobic surfaces with photocatalytic selfcleaning properties by nanocomposite coating of tio2 and polytetrafluoroethylene," *Advanced Materials*, vol. 24, no. 27, pp. 3697–3700, 2012. 16

[84] C. Neinhuis and W. Barthlott, "Characterization and distribution of water-repellent, self-cleaning plant surfaces," *Annals of Botany*, vol. 79, no. 6, pp. 667–677, 1997. 17

[85] K. M. Wisdom, J. A. Watson, X. Qu, F. Liu, G. S. Watson, and C.-H. Chen, "Self-cleaning of superhydrophobic surfaces by self-propelled jumping condensate," *Proceedings of the National Academy of Sciences*, vol. 110, no. 20, pp. 7992–7997, 2013. 18, 56, 80, 82, 83

[86] J. Stoddard, "Jet and droplet impingement on superhydrophobic surfaces," Thesis, 2015. 22

[87] J. C. Maxwell, "Year end and fourth quarter 2016 cigarette industry," *The Maxwell Report*, 2017. 25

[88] "Tobacco brand preferences," March 3, 2017 2017. [Online]. Available: https://www.cdc.gov/tobacco/data_statistics/fact_sheets/tobacco_industry/brand_preference/index.htm 25

[89] M. G. Lawrence, "The relationship between relative humidity and the dewpoint temperature in moist air: A simple conversion and applications," *Bulletin of the American Meteorological Society*, vol. 86, no. 2, pp. 225–233, 2005. 29

[90] O. A. Alduchov and R. E. Eskridge, "Improved magnus form approximation of saturation vapor pressure," *Journal of Applied Meteorology*, vol. 35, no. 4, pp. 601–609, 1996. 29

[91] A. Bateni, S. S. Susnar, A. Amirfazli, and A. W. Neumann, "A high-accuracy polynomial fitting approach to determine contact angles," *Colloids and Surfaces A: Physicochemical and Engineering Aspects*, vol. 219, no. 1, pp. 215–231, 2003. 32

[92] E. Atefi, J. A. Mann, and H. Tavana, "A robust polynomial fitting approach for contact angle measurements," *Langmuir*, vol. 29, no. 19, pp. 5677–5688, 2013. 32

[93] E. B. Dussan V and R. T.-P. Chow, "On the ability of drops or bubbles to stick to non-horizontal surfaces of solids," *Journal of Fluid Mechanics*, vol. 137, pp. 1–29, 2006. 47

[94] A. ElSherbini and A. Jacobi, "Liquid drops on vertical and inclined surfaces; i. an experimental study of drop geometry," *J Colloid Interface Sci*, vol. 273, no. 2, pp. 556–65, 2004. 47

[95] Y. Mao and S. Huang, "Pollen resistance to water in 80 angiosperm species: flower structures protect rainsusceptible pollen," *New Phytologist*, vol. 183, no. 3, pp. 892–899, 2009. 50

[96] N. Xu, L. Zhao, C. Ding, C. Zhang, R. Li, and Q. Zhong, "Laboratory observation of dew formation at an early stage of atmospheric corrosion of metals," *Corrosion Science*, vol. 44, no. 1, pp. 163–170, 2002. 55

APPENDIX A. RAW DATA COLLECTED DURING CA AND SA TESTS

This Appendix is dedicated to including the raw data collected during the CA and SA test performed in this study. The CA and SA were measured twice on each surface. The average and standard deviation of the CA and SA are also reported in this section. The "-" symbol implies that specific data point was not recorded for use in the study. The data tables are presented as follows:

1. Surfaces Cleaned via Rolling Droplets
    - Clean, Micro-structured Surfaces (Table A.1)
    - Clean, Nano-structured Surfaces (TableA.2)
    - Salt, Micro-structured Surfaces (Table A.3)
    - Salt, Nano-structured Surfaces (Table A.4)
    - Tobacco, Micro-structured Surfaces (Table A.5)
    - Tobacco, Nano-structured Surfaces (Table A.6)
2. Surfaces Cleaned via Condensation
    - Clean, Micro-structured Surfaces (Table A.8)
    - Clean, Nano-structured Surfaces (Table A.8)
    - Salt, Micro-structured Surfaces (Table A.9)
    - Salt, Nano-structured Surfaces (Table A.10)
    - Tobacco, Micro-structured Surfaces (Tables A.11)
    - Tobacco, Nano-structured Surfaces (Tables A.12)
3. Smooth Surfaces cleaned via Rolling Droplets
    - Clean, Teflon® Surfaces (Table A.13)

- Clean, Proprietary Coating Surfaces (Table A.14)
- Salt, Teflon® Surfaces (Table A.15)
- Salt, Proprietary Coating Surfaces (Table A.16)
- Tobacco, Teflon® Surfaces (Table A.17)
- Tobacco, Proprietary Coating Surfaces (Table A.18)

4. Surfaces Cleaned via Condensation

- Clean, Teflon® Surfaces (Table A.19)
- Clean, Proprietary Coating Surfaces (Table A.20)
- Salt, Teflon® Surfaces (Table A.21)
- Salt, Proprietary Coating Surfaces (Table A.22)
- Tobacco, Teflon® Surfaces (Table A.23)
- Tobacco, Proprietary Coating Surfaces (Table A.24)

Table A.1: Contact angles and sliding angles on clean, micro-structured surfaces after being cleaned via rolling droplets

	Contact Angle					Sliding Angle				
Number of Drops	0	1	2	3	4	0	1	2	3	4
Surface 1	153.50	149.47	150.68	147.36	152.91	7.40	8.80	7.05	6.55	6.30
	152.10	148.26	152.06	151.17	151.33	7.70	7.40	8.55	6.65	7.35
Surface 2	151.22	153.87	154.96	152.60	153.60	5.95	6.55	5.10	4.50	3.85
	153.03	151.79	154.82	151.91	151.41	4.90	5.00	4.95	4.75	6.50
Surface 3	152.95	155.05	152.21	150.40	152.76	8.00	8.50	8.15	7.55	8.40
	150.30	154.50	153.01	152.41	154.23	5.70	5.25	6.95	6.30	5.25
Surface 4	153.15	152.34	152.99	150.51	151.73	6.30	6.95	6.45	6.70	5.65
	149.62	152.85	150.38	151.17	151.70	6.95	8.55	7.65	6.65	6.20
Surface 5	149.19	154.61	151.50	152.44	152.44	6.50	6.45	5.75	5.35	5.25
	152.71	153.37	155.45	154.64	151.76	8.30	6.95	5.65	6.30	6.15
Surface 6	147.70	148.75	147.37	148.04	147.61	7.70	7.45	6.80	6.75	4.85
	149.06	153.48	154.66	149.93	153.83	6.70	5.15	6.60	8.90	8.20
Surface 7	149.41	147.34	147.95	147.85	147.20	7.65	6.15	6.30	7.80	7.25
	149.76	146.56	146.66	147.96	147.50	7.85	8.40	7.80	7.30	7.55
Surface 8	149.28	147.58	147.92	146.03	149.16	7.00	5.80	4.95	7.15	5.20
	147.80	146.61	146.45	146.63	146.69	5.90	4.35	5.75	5.70	4.85
Surface 9	147.52	146.21	147.50	149.32	148.80	7.30	7.10	8.85	6.50	8.50
	149.60	149.06	150.49	149.25	150.57	10.50	8.05	6.40	5.60	5.50
Surface 10	148.87	148.57	148.51	147.69	151.54	-	-	-	-	-
	149.88	150.44	146.56	149.46	144.57	-	-	-	-	-
Average	144.90	145.08	145.09	145.03	144.91	11.01	10.73	10.56	10.74	10.86
Standard Deviation	1.82	1.54	1.26	1.73	1.66	1.03	0.86	0.90	0.98	0.96

Table A.2: Contact angles and sliding angles on clean, nano-structured surfaces after being cleaned via rolling droplets

	Contact Angle					Sliding Angle				
Number of Drops	0	1	2	3	4	0	1	2	3	4
Surface 1	144.59	145.13	144.19	143.92	145.14	11.97	12.50	11.78	11.55	12.05
	143.52	144.33	143.14	143.45	143.16	11.43	11.80	11.30	11.75	10.85
Surface 2	143.365	143.12	144.2	143.57	142.57	10.79	11.35	10.80	10.50	10.50
	143.6375	144.6	143.94	142.71	143.3	10.73	11.10	10.00	10.10	11.70
Surface 3	142.47	143.01	144.65	143.56	143.90	12.55	11.45	12.50	12.40	11.80
	143.78	143.26	144.21	143.36	145.28	11.60	10.55	11.25	11.25	10.15
Surface 4	146.83	146.40	145.58	145.83	144.85	11.35	10.95	10.40	11.15	10.60
	146.46	144.80	144.52	146.78	147.66	11.50	10.80	9.80	10.60	10.55
Surface 5	143.01	144.23	144.57	142.93	143.24	12.10	10.90	11.70	11.50	12.40
	142.90	143.88	143.84	143.99	142.87	11.90	10.63	10.45	12.15	12.15
Surface 6	144.07	144.61	145.29	146.25	146.23	9.10	9.25	9.90	10.25	10.05
	145.07	147.2	146.73	147.5	146.13	10.70	10.65	9.70	9.40	10.15
Surface 7	146.5	146.92	146.21	146.19	144.51	11.55	10.35	10.10	9.50	9.60
	147.12	144.84	147.01	146.535	145.41	9.75	9.10	10.10	10.10	11.60
Surface 8	147.89	147.67	147.32	147.53	147.67	9.50	10.00	9.40	9.20	10.15
	147.25	147.25	146.07	146.38	146.66	9.70	10.35	9.85	10.45	9.40
Average	144.90	145.08	145.09	145.03	144.91	11.01	10.73	10.56	10.74	10.85
Standard Deviation	1.81	1.54	1.25	1.72	1.65	1.02	0.86	0.89	0.97	0.95

Table A.3: Contact angles and sliding angles on salt contaminated, micro-structured surfaces after being cleaned via rolling droplets

	Contact Angle					Sliding Angle				
Number of Drops	0	1	2	3	4	0	1	2	3	4
Surface 1	141.78	146.70	148.35	149.42	149.23	9.85	7.13	7.20	7.10	7.00
	142.00	145.70	149.30	152.27	152.07	8.00	7.80	7.65	7.10	7.35
Surface 2	139.72	147.78	150.89	150.80	149.65	10.20	7.75	7.50	6.90	7.30
	142.72	145.79	150.03	151.24	150.50	10.15	8.90	6.90	6.50	6.55
Surface 3	142.64	150.29	150.78	150.53	150.23	10.05	7.90	8.15	7.20	6.50
	142.30	146.16	150.34	149.67	150.88	11.70	8.70	6.90	7.51	7.80
Surface 4	142.71	145.02	150.51	150.33	149.95	13.50	11.50	8.35	8.15	7.30
	140.81	146.29	148.86	147.55	148.50	11.22	9.25	9.05	8.80	9.15
Surface 5	141.83	144.67	148.44	148.81	149.29	10.90	9.80	9.20	8.95	8.40
	140.02	146.98	151.42	150.43	150.56	10.70	9.05	8.10	8.90	7.10
Surface 6	136.25	148.49	151.87	149.32	150.84	9.90	8.95	7.20	7.35	7.95
	139.20	145.92	151.22	150.70	151.59	9.95	8.35	7.83	7.65	7.50
Surface 7	136.41	144.79	144.53	149.63	150.32	8.35	7.90	7.75	7.50	7.75
	139.43	143.22	145.64	149.16	149.15	10.50	7.10	6.40	6.50	6.30
Surface 8	138.55	143.33	143.72	144.84	145.90	10.25	8.25	7.65	8.10	7.90
	138.74	144.92	142.99	145.67	146.64	12.00	8.50	8.60	8.70	7.95
Surface 9	137.56	141.19	142.52	142.68	143.73	10.50	9.40	8.80	9.25	9.25
	138.20	145.85	143.22	143.70	144.59	12.45	11.65	8.50	8.10	7.90
Surface 10	141.57	147.99	148.71	149.14	149.30	10.55	9.00	8.85	8.25	8.25
	138.99	145.09	146.84	147.49	147.46	11.00	8.00	8.62	9.00	8.25
Average	140.07	145.81	148.01	148.67	149.02	10.59	8.74	7.96	7.88	7.67
Standard Deviation	2.08	2.01	3.14	2.59	2.27	1.25	1.21	0.79	0.86	0.79

Table A.4: Contact angles and sliding angles on salt contaminated, nano-structured surfaces after being cleaned via rolling droplets

	Contact Angle					Sliding Angle				
Number of Drops	0	1	2	3	4	0	1	2	3	4
Surface 1	135.88	140.36	140.92	140.88	142.54	12.85	11.10	11.15	10.20	10.40
	135.88	139.46	140.61	141.80	142.34	13.30	11.35	11.70	10.30	10.20
Surface 2	135.88	141.26	143.78	143.39	142.53	12.95	11.25	11.35	10.85	10.35
	135.88	141.30	142.97	141.84	143.46	13.08	10.95	11.25	11.40	11.75
Surface 3	138.81	141.06	142.49	143.19	144.63	12.35	11.25	11.30	11.15	10.75
	134.93	137.07	138.90	144.02	142.88	13.40	10.55	11.75	11.20	11.60
Surface 4	135.99	139.76	141.70	141.60	142.86	13.45	10.35	10.75	10.30	10.90
	138.16	140.84	140.57	143.21	143.43	13.40	11.29	11.10	10.55	10.25
Surface 5	137.40	140.62	141.40	144.76	143.70	13.60	10.30	9.80	10.55	10.80
	136.28	138.97	144.39	144.44	143.41	13.40	11.25	10.65	10.55	10.90
Surface 6	134.71	136.73	145.98	143.60	147.60	12.50	10.85	10.95	10.95	10.70
	136.49	139.50	145.17	147.72	145.95	11.85	11.05	11.01	11.25	11.30
Surface 7	131.77	143.26	142.80	146.95	144.83	12.60	11.15	10.80	10.55	10.40
	130.89	140.41	143.28	143.94	146.74	14.35	12.50	11.35	11.90	11.20
Surface 8	137.62	141.50	143.02	144.14	143.42	12.95	10.65	10.20	10.40	10.55
	136.53	141.73	145.94	144.44	143.25	13.50	11.50	11.55	10.90	10.50
Average	135.82	140.24	142.75	143.75	143.97	13.10	11.08	11.04	10.81	10.78
Standard Deviation	2.07	1.67	2.02	1.81	1.57	0.59	0.52	0.52	0.47	0.47

Table A.5: Contact angles and sliding angles on tobacco contaminated, micro-structured surfaces after being cleaned via rolling droplets

	Contact Angle					Sliding Angle				
Number of Drops	0	1	2	3	4	0	1	2	3	4
Surface 1	145.81	146.97	147.99	147.54	148.55	17.55	15.70	14.50	13.60	13.25
	144.47	148.00	147.50	147.22	147.64	13.10	12.10	11.00	10.30	9.50
Surface 2	145.14	147.48	148.48	148.48	148.03	19.35	16.75	16.40	13.75	11.55
	143.98	144.28	146.99	147.52	147.53	15.30	12.35	12.30	11.60	11.40
Surface 3	143.02	145.57	147.66	147.96	147.80	14.75	10.50	10.40	10.15	11.55
	144.35	146.42	147.39	147.94	147.90	19.35	14.40	14.50	14.50	15.50
Surface 4	140.61	141.86	143.50	144.44	144.59	13.05	10.45	10.50	10.90	10.45
	144.06	146.92	147.04	147.02	146.52	16.75	13.10	14.80	13.55	14.35
Surface 5	142.76	146.99	146.96	146.06	146.03	14.25	10.60	10.90	11.60	10.75
	141.23	143.44	144.48	145.44	144.41	15.30	13.50	12.10	10.50	11.10
Surface 6	139.94	143.79	143.11	143.47	145.47	17.80	15.70	11.80	11.85	11.50
	140.09	143.21	142.84	143.74	144.91	18.15	12.10	12.70	12.10	12.75
Average	142.96	145.41	146.16	146.40	146.62	16.23	13.10	12.66	12.03	11.97
Standard Deviation	2.03	2.01	2.06	1.74	1.48	2.24	2.16	1.96	1.49	1.70

Table A.6: Contact angles and sliding angles on tobacco contaminated, nano-structured surfaces after being cleaned via rolling droplets

	Contact Angle					Sliding Angle				
Number of Drops	0	1	2	3	4	0	1	2	3	4
Surface 1	131.71	134.81	134.29	134.74	134.08	41.25	33.70	32.20	33.70	34.00
	127.19	131.06	133.77	134.25	134.73	43.50	33.70	31.90	33.15	32.70
Surface 2	119.32	132.51	132.67	132.73	132.61	41.25	33.70	32.20	33.70	34.00
	129.52	135.56	135.02	134.48	137.24	43.50	33.70	31.90	33.15	32.70
Surface 3	124.05	134.67	134.38	134.09	134.12	40.05	36.40	34.00	35.50	35.25
	126.91	133.74	133.54	138.73	136.23	47.05	33.40	32.80	33.25	33.60
Surface 4	133.58	136.97	136.01	138.33	138.00	40.20	37.35	34.15	32.75	34.85
	130.77	135.63	138.47	138.61	139.43	40.20	31.60	30.48	29.35	32.24
Surface 5	131.74	137.88	138.64	138.89	137.78	43.25	36.40	38.70	37.55	34.30
	136.79	140.64	140.03	140.43	139.26	46.30	41.20	34.25	36.65	37.40
Surface 6	136.24	137.15	139.75	141.28	139.73	40.25	32.15	31.25	25.65	26.40
	134.24	136.94	137.07	138.92	138.34	40.25	36.90	33.00	30.25	34.00
Surface 7	137.30	139.28	139.24	140.27	140.25	34.15	28.25	25.75	26.20	26.20
	135.30	136.03	137.27	137.37	137.88	45.35	31.10	28.90	29.60	35.90
Surface 8	134.88	139.74	139.21	138.69	139.50	36.15	24.70	23.70	23.60	25.15
	131.72	134.25	135.64	134.77	135.43	51.45	36.10	33.30	34.05	33.68
Average	131.33	136.05	136.56	137.29	137.16	42.13	33.77	31.78	31.76	32.65
Standard Deviation	4.96	2.60	2.46	2.68	2.36	4.19	3.87	3.48	3.99	3.58

Table A.7: Contact angles and sliding angles on clean, micro-structured surfaces after being cleaned via condensation

	Contact Angle					Sliding Angle				
Condensation Cycles	0	1	2	3	4	0	1	2	3	4
Surface 1	153.14	148.78	150.23	150.84	149.75	6.50	4.45	4.20	6.70	6.20
	148.82	149.87	151.41	149.21	150.21	5.90	4.96	5.15	5.30	5.00
Surface 2	153.77	150.03	152.17	149.23	151.87	6.50	4.35	4.70	4.70	4.40
	151.95	150.67	149.77	151.19	150.53	7.90	4.65	4.55	6.70	5.67
Surface 3	151.21	150.94	152.62	149.94	153.24	6.50	7.20	7.20	5.75	5.90
	150.74	148.55	150.45	149.83	149.58	7.45	7.20	6.90	6.40	5.75
Surface 4	154.79	151.61	151.79	150.85	150.92	6.20	4.70	4.35	5.25	6.10
	153.85	151.75	152.09	151.57	152.75	5.60	6.85	5.10	4.90	4.75
Surface 5	148.84	150.55	149.46	149.88	149.93	7.45	7.20	7.15	6.60	5.90
	151.30	150.61	149.99	149.21	149.39	7.15	7.30	6.75	6.90	7.10
Surface 6	148.87	150.43	150.98	149.93	149.02	6.55	6.30	7.00	7.60	7.20
	151.00	151.27	150.39	150.97	149.14	7.00	7.00	7.15	6.05	7.10
Average	151.52	150.42	150.95	150.22	150.53	6.83	6.28	5.85	6.07	5.92
Standard Deviation	2.06	1.00	1.05	0.83	1.40	0.69	1.22	1.26	0.90	0.91

Table A.8: Contact angles and sliding angles on clean, nano-structured surfaces after being cleaned via condensation

	Contact Angle					Sliding Angle				
Condensation Cycles	0	1	2	3	4	0	1	2	3	4
Surface 1	145.06	144.74	143.79	141.27	141.25	10.12	10.04	11.05	10.70	10.70
	144.47	143.17	145.36	143.60	143.34	10.12	10.04	11.30	11.60	9.95
Surface 2	145.06	144.57	143.87	144.43	144.53	9.75	9.70	9.90	11.50	9.05
	145.36	143.85	144.18	145.19	145.44	10.55	10.20	9.90	11.00	10.05
Surface 3	145.47	144.55	145.46	144.85	143.73	9.05	9.00	9.50	10.80	9.45
	143.34	143.95	145.46	145.02	146.14	9.80	8.70	10.60	9.30	10.25
Surface 4	144.81	144.04	145.30	144.70	145.46	9.20	9.50	9.20	10.75	9.66
	145.41	144.83	144.25	145.73	145.53	9.70	9.55	10.50	9.60	8.45
Surface 5	145.11	144.44	146.79	146.91	145.59	10.90	11.00	10.20	9.90	9.60
	144.41	144.25	145.43	145.89	146.15	10.15	11.20	10.70	10.45	9.70
Surface 6	142.46	143.76	143.19	145.16	145.35	11.00	10.05	11.20	9.40	10.30
	143.28	143.95	144.76	144.47	146.96	10.25	10.40	9.90	10.00	9.90
Surface 7	141.97	143.87	141.06	141.57	141.62	9.85	9.70	9.70	10.05	9.80
	142.95	143.65	142.12	141.64	143.45	10.70	10.10	10.25	10.15	9.80
Surface 8	143.40	144.22	142.72	141.76	142.63	10.60	10.20	10.50	11.13	12.20
	143.16	143.68	142.87	142.22	143.99	10.20	11.20	11.00	9.65	12.10
Average	144.11	144.09	144.16	144.03	144.45	10.12	10.04	10.34	10.37	10.06
Standard Deviation	1.15	0.45	1.50	1.78	1.67	0.56	0.70	0.63	0.73	0.96

Table A.9: Contact angles and sliding angles on salt contaminated, micro-structured surfaces after being cleaned via condensation

	Contact Angle					Sliding Angle				
Condensation Cycles	0	1	2	3	4	0	1	2	3	4
Surface 1	142.79	149.81	152.04	150.80	149.91	10.85	6.80	7.10	6.50	6.55
	143.57	151.14	150.04	148.86	150.08	11.20	8.07	6.20	7.40	6.85
Surface 2	141.76	148.80	152.88	152.64	152.64	10.50	8.12	6.67	6.05	7.80
	142.83	152.08	153.27	153.59	153.59	10.90	7.20	7.75	7.75	7.22
Surface 3	143.32	149.30	150.87	149.62	149.62	10.30	6.80	8.05	7.70	6.10
	141.87	147.57	150.58	151.67	151.67	11.80	9.50	8.31	9.40	8.10
Surface 4	140.90	149.01	153.05	152.49	152.49	10.30	6.20	6.30	7.60	7.77
	143.10	152.01	152.78	153.08	153.08	10.30	7.30	6.60	6.80	7.60
Surface 5	142.32	150.10	153.04	151.84	151.84	11.25	6.65	6.20	5.90	6.10
	138.59	149.46	153.14	152.89	152.89	9.80	8.10	7.28	7.50	7.50
Surface 6	142.18	146.69	146.84	149.56	151.00	10.70	8.05	7.30	7.59	7.05
	143.78	147.55	147.94	148.73	150.46	10.50	8.50	8.55	8.50	7.95
Average	142.22	149.15	151.05	151.05	151.34	10.58	7.75	7.38	7.50	7.24
Standard Deviation	1.31	1.81	2.17	1.73	1.48	0.57	1.05	0.94	0.96	0.82

Table A.10: Contact angles and sliding angles on salt contaminated, nano-structured surfaces after being cleaned via condensation

	Contact Angle					Sliding Angle				
Condensation Cycles	0	1	2	3	4	0	1	2	3	4
Surface 1	140.58	144.81	144.77	145.38	145.95	14.15	10.35	10.00	10.30	10.40
	139.25	142.76	144.62	143.99	145.92	12.90	10.10	9.85	9.90	10.25
Surface 2	134.43	143.87	145.35	145.73	145.97	13.30	10.35	9.60	10.10	10.10
	133.63	143.09	146.19	145.50	145.03	12.25	10.20	10.40	9.30	9.35
Surface 3	134.77	146.88	145.47	146.41	145.49	13.30	10.40	10.25	10.15	10.15
	136.49	146.96	147.29	147.16	147.53	12.90	10.20	9.65	9.90	9.85
Surface 4	130.64	145.25	144.04	145.01	145.26	13.50	10.40	10.20	10.50	10.00
	132.27	145.09	144.32	143.69	142.99	11.95	10.30	10.00	9.70	9.73
Surface 5	134.98	144.00	143.95	144.74	143.29	12.50	10.55	10.65	9.58	9.60
	130.91	145.26	144.62	145.91	144.64	12.25	10.50	9.80	10.40	10.10
Surface 6	137.60	143.69	143.46	144.48	145.52	13.50	10.40	10.65	9.60	9.30
	137.50	146.80	144.62	144.02	144.54	12.65	10.55	9.75	9.55	9.50
Surface 7	132.08	144.24	143.54	143.88	147.10	11.90	9.95	9.25	9.55	9.25
	137.47	145.41	143.80	142.92	143.62	12.90	9.70	10.35	9.75	9.95
Average	135.19	144.87	144.72	144.92	145.20	12.85	10.28	10.03	9.88	9.82
Standard Deviation	3.09	1.20	1.14	1.32	1.51	0.65	0.24	0.41	0.36	0.37

Table A.11: Contact angles and sliding angles on tobacco contaminated, micro-structured surfaces after being cleaned via condensation

	Contact Angle					Sliding Angle				
Condensation Cycles	0	1	2	3	4	0	1	2	3	4
Surface 1	146.75	147.87	148.38	150.39	150.16	15.23	11.45	10.65	10.75	9.65
	145.80	146.60	148.25	150.61	150.78	21.75	16.30	15.90	13.70	13.10
Surface 2	141.69	149.60	147.39	146.65	148.55	15.50	14.05	12.50	9.75	9.55
	146.76	148.39	147.86	148.53	149.03	21.70	11.80	12.80	10.20	10.80
Surface 3	144.41	149.34	147.65	147.80	150.10	15.50	10.25	10.15	10.70	9.95
	145.01	149.45	148.71	148.26	147.86	19.30	13.75	11.60	11.50	11.10
Surface 4	139.30	143.73	142.51	144.55	145.33	29.00	21.90	19.05	16.95	14.85
	134.12	143.65	145.54	147.53	146.23	28.00	25.85	18.75	14.35	13.65
Surface 5	141.01	143.13	143.01	144.62	145.84	26.75	20.35	21.20	20.20	17.95
	143.25	144.85	146.28	148.62	147.07	27.90	23.50	15.10	15.90	13.20
Surface 6	143.89	146.63	147.96	147.53	147.23	19.50	15.15	13.45	11.80	12.05
	143.65	146.86	149.11	147.93	147.10	20.20	16.95	15.60	15.20	15.65
Average	142.97	146.68	146.89	147.75	147.94	21.69	16.78	14.73	13.42	12.63
Standard Deviation	3.59	2.36	2.17	1.86	1.79	5.12	5.06	3.53	3.21	2.62

Table A.12: Contact angles and sliding angles on tobacco contaminated, nano-structured surfaces after being cleaned via condensation

	Contact Angle					Sliding Angle				
Condensation Cycles	0	1	2	3	4	0	1	2	3	4
Surface 1	125.67	132.59	133.71	135.48	137.25	38.60	33.30	31.63	27.50	27.55
	126.71	133.55	134.68	136.50	136.80	39.50	34.10	34.10	31.50	29.80
Surface 2	138.60	139.42	139.51	140.61	141.70	33.05	32.15	22.70	22.60	20.40
	133.25	134.52	140.99	140.85	140.70	45.40	32.20	23.60	22.40	23.70
Surface 3	133.33	135.90	135.91	139.18	139.95	34.05	28.50	24.40	22.25	20.55
	135.62	138.58	137.46	139.86	139.53	32.35	27.10	22.60	24.70	23.05
Surface 4	133.10	138.98	138.54	137.59	137.87	39.05	24.45	23.08	23.15	22.70
	131.93	138.86	135.93	135.74	135.87	33.55	23.25	22.10	19.70	21.40
Surface 5	132.71	133.95	135.88	137.80	139.88	32.30	28.30	22.59	21.43	22.05
	130.94	136.40	138.64	138.59	140.57	39.10	27.60	23.50	23.48	21.80
Surface 6	133.15	137.80	140.24	139.11	139.21	43.70	29.15	27.65	25.35	25.75
	133.19	139.04	140.69	140.12	140.38	34.10	27.55	24.70	26.50	24.50
Surface 7	-	-	-	-	-	26.30	16.85	19.10	20.90	21.16
	-	-	-	-	-	37.35	22.30	22.60	22.40	19.40
Surface 8	-	-	-	-	-	33.40	27.20	25.40	25.65	21.55
	-	-	-	-	-	33.95	25.20	24.00	27.50	27.00
Average	144.11	144.09	144.16	144.03	144.45	10.12	10.04	10.34	10.37	10.06
Standard Deviation	1.15	0.45	1.50	1.78	1.67	0.56	0.70	0.63	0.73	0.96

Table A.13: Contact angles and sliding angles on clean, Teflon® coated surfaces after being cleaned via rolling droplets

	Contact Angle					Sliding Angle				
Number of Drops	0	1	2	3	4	0	1	2	3	4
Surface 1	124.45	123.71	124.65	124.32	122.23	31.65	28.25	35.25	32.05	31.50
	122.90	124.37	124.71	121.17	119.51	32.20	34.20	33.95	35.20	29.95
Surface 2	121.55	121.94	121.45	121.02	120.82	32.15	33.15	30.35	28.25	29.95
	120.21	119.68	120.93	121.40	122.36	30.60	29.85	28.80	27.40	25.70
Surface 3	122.72	123.35	123.27	122.97	121.67	25.05	30.15	31.65	31.75	29.80
	121.68	122.00	122.85	122.60	123.16	29.65	34.60	32.33	30.75	29.45
Surface 4	121.56	120.96	119.80	123.52	122.63	33.95	32.70	34.70	33.05	29.05
	118.56	119.22	120.98	119.78	121.66	34.95	26.05	27.65	27.30	26.90
Surface 5	121.91	120.39	120.53	121.61	122.58	31.55	30.45	29.75	30.95	29.90
	119.63	120.35	120.26	121.44	121.76	33.25	27.45	31.25	35.25	32.60
Surface 6	122.38	120.37	122.57	120.51	121.47	35.50	29.65	33.40	30.55	29.85
	121.14	121.09	121.01	119.38	119.18	29.65	33.15	32.40	33.85	32.25
Average	121.67	121.45	121.92	121.64	121.59	31.95	30.80	31.79	31.36	29.74
Standard Deviation	1.44	1.64	1.66	1.48	1.22	2.59	2.76	2.35	2.74	1.97

Table A.14: Contact angles and sliding angles on clean, proprietary coated surfaces after being cleaned via rolling droplets. Note that water droplets did not roll off these surfaces at 90°and so no SA was measured

	Contact Angle					Sliding Angle				
Number of Drops	0	1	2	3	4	0	1	2	3	4
Surface 1	111.20	112.52	114.36	112.98	111.37	-	-	-	-	-
	114.64	111.86	112.07	113.34	111.33	-	-	-	-	-
Surface 2	114.82	109.63	112.41	111.66	111.35	-	-	-	-	-
	113.39	113.22	107.92	109.33	108.60	-	-	-	-	-
Surface 3	111.31	113.31	112.46	112.66	111.22	-	-	-	-	-
	111.97	113.95	112.90	110.64	110.86	-	-	-	-	-
Surface 4	111.52	114.69	113.65	112.73	112.71	-	-	-	-	-
	114.70	110.84	110.91	110.10	112.15	-	-	-	-	-
Surface 5	110.75	112.49	113.22	114.16	113.73	-	-	-	-	-
	111.86	110.59	110.01	110.90	111.54	-	-	-	-	-
Surface 6	108.24	115.99	113.68	111.85	108.18	-	-	-	-	-
	114.06	111.80	110.72	114.63	111.21	-	-	-	-	-
Average	112.37	112.57	112.03	112.08	111.19	-	-	-	-	-
Standard Deviation	1.77	1.80	1.80	1.63	1.53	-	-	-	-	-

Table A.15: Contact angles and sliding angles on salt contaminated, Teflon® coated surfaces after being cleaned via rolling droplets

	Contact Angle					Sliding Angle				
Number of Drops	0	1	2	3	4	0	1	2	3	4
Surface 1	111.54	115.78	117.95	118.04	117.48	38.75	37.00	33.00	34.10	34.25
	113.42	117.78	117.90	118.83	119.82	35.80	31.20	31.30	32.65	33.25
Surface 2	115.02	120.44	120.34	121.73	120.34	39.95	38.56	36.45	34.35	34.85
	114.80	120.40	121.71	120.86	120.22	36.90	32.30	34.35	32.55	32.69
Surface 3	110.12	115.65	118.90	118.31	118.38	38.60	35.90	36.25	34.68	34.55
	109.98	113.25	120.30	121.42	119.53	38.80	35.66	34.15	35.35	34.15
Surface 4	115.78	119.92	119.84	120.88	121.45	39.50	33.80	35.75	35.50	32.55
	115.73	118.31	120.13	120.79	121.10	39.65	33.80	34.80	34.25	34.10
Surface 5	111.96	120.92	119.41	121.24	121.85	42.05	32.40	32.20	34.25	34.20
	114.23	118.75	120.62	120.97	119.40	40.35	39.45	32.60	32.65	32.70
Surface 6	116.61	120.15	119.40	120.17	120.57	38.55	34.10	33.85	32.10	33.30
	113.23	118.90	121.40	120.59	119.85	43.15	35.45	36.80	36.90	36.05
Surface 7	112.71	120.28	121.57	118.84	119.77	40.40	34.30	32.95	33.85	33.10
	-	-	-	-	-	-	-	-	-	-
Average	113.47	118.50	119.96	120.21	119.98	39.42	34.92	34.19	34.09	33.83
Standard Deviation	2.14	2.33	1.24	1.25	1.19	1.93	2.42	1.75	1.37	1.01

Table A.16: Contact angles and sliding angles on salt contamianted, proprietary coated surfaces after being cleaned via rolling droplets. Note that water droplets did not roll off these surfaces at 90°and so no SA was measured

	Contact Angle					Sliding Angle				
Number of Drops	0	1	2	3	4	0	1	2	3	4
Surface 1	100.14	108.50	109.52	110.70	110.60	-	-	-	-	-
	101.03	107.10	108.31	107.61	109.76	-	-	-	-	-
Surface 2	102.36	108.01	108.62	109.54	111.24	-	-	-	-	-
	95.54	109.43	111.25	109.05	109.37	-	-	-	-	-
Surface 3	102.13	111.33	109.30	108.22	108.51	-	-	-	-	-
	104.04	107.64	110.85	111.65	110.52	-	-	-	-	-
Surface 4	101.19	110.40	111.34	110.01	109.28	-	-	-	-	-
	104.28	109.50	108.50	109.99	110.00	-	-	-	-	-
Surface 5	103.23	109.74	111.12	108.86	108.63	-	-	-	-	-
	101.53	106.69	108.78	108.64	110.53	-	-	-	-	-
Surface 6	103.70	110.40	110.04	111.94	109.51	-	-	-	-	-
	103.39	107.20	110.17	110.89	108.71	-	-	-	-	-
Average	101.88	108.83	109.82	109.76	109.57	-	-	-	-	-
Standard Deviation	2.39	1.51	1.14	1.36	1.01	-	-	-	-	-

Table A.17: Contact angles and sliding angles on tobacco contaminated, Teflon® coated surfaces after being cleaned via rolling droplets

	Contact Angle					Sliding Angle				
Number of Drops	0	1	2	3	4	0	1	2	3	4
Surface 1	114.22	115.30	115.67	118.63	118.37	65.00	60.00	57.00	57.00	52.00
	114.13	115.01	117.28	119.23	118.13	83.00	77.00	76.00	71.00	64.00
Surface 2	114.75	115.19	119.21	118.69	118.53	57.00	57.00	49.00	48.00	48.00
	112.63	114.15	116.18	118.12	119.48	65.00	49.00	46.00	44.00	47.00
Surface 3	108.29	115.13	118.75	118.89	119.41	73.00	65.00	51.00	49.16	48.65
	109.70	113.64	117.41	118.08	119.30	65.00	54.00	53.00	53.00	52.73
Surface 4	97.06	101.03	110.18	112.41	109.95	90.00	75.00	70.00	62.00	56.55
	99.88	102.03	109.54	111.30	109.82	72.05	54.10	56.45	56.10	46.05
Surface 5	105.70	106.46	107.51	112.23	115.84	65.20	53.40	56.70	50.90	52.75
	102.95	105.42	113.37	114.46	114.12	79.20	62.50	53.35	51.70	59.85
Surface 6	100.61	111.70	108.19	109.13	110.94	80.00	78.75	59.80	48.75	51.35
	101.20	105.12	110.24	115.65	115.81	72.55	50.65	49.15	47.35	49.95
Average	106.76	110.02	113.63	115.57	115.81	72.25	61.37	56.45	53.25	52.41
Standard Deviation	6.36	5.57	4.29	3.55	3.75	9.44	10.47	8.77	7.43	5.37

Table A.18: Contact angles and sliding angles on tobacco contamianted, proprietary coated surfaces after being cleaned via rolling droplets. Note that water droplets did not roll off these surfaces at 90°and so no SA was measured

	Contact Angle					Sliding Angle				
Number of Drops	0	1	2	3	4	0	1	2	3	4
Surface 1	96.97	97.42	102.68	100.06	102.38	-	-	-	-	-
	98.15	100.95	104.41	103.42	105.33	-	-	-	-	-
Surface 2	95.78	98.19	102.75	99.04	103.61	-	-	-	-	-
	98.05	103.37	103.98	105.18	104.57	-	-	-	-	-
Surface 3	94.61	94.99	95.71	101.16	99.73	-	-	-	-	-
	93.26	95.94	97.63	99.64	98.61	-	-	-	-	-
Surface 4	92.91	99.86	102.45	103.96	105.77	-	-	-	-	-
	96.14	96.57	97.24	99.12	103.99	-	-	-	-	-
Surface 5	90.30	94.54	98.52	102.90	102.32	-	-	-	-	-
	94.85	96.27	98.76	100.46	101.17	-	-	-	-	-
Surface 6	97.69	101.96	102.93	104.01	103.70	-	-	-	-	-
	91.92	94.44	96.72	97.40	100.06	-	-	-	-	-
Average	95.13	97.88	100.32	101.36	102.60	-	-	-	-	-
Standard Deviation	2.95	3.01	3.16	2.46	2.30	-	-	-	-	-

Table A.19: Contact angles and sliding angles on clean, Teflon® coated surfaces after being cleaned via condensation

	Contact Angle					Sliding Angle				
Number of Drops	0	1	2	3	4	0	1	2	3	4
Surface 1	121.11	121.30	121.92	120.47	125.23	34.65	33.80	34.55	36.10	31.45
	123.07	121.71	120.96	118.18	122.51	34.95	38.60	29.36	31.15	34.90
Surface 2	124.78	121.77	122.03	119.56	120.82	35.30	34.70	29.30	34.25	27.55
	123.17	118.99	119.74	120.50	120.78	35.40	34.40	30.65	30.00	28.45
Surface 3	121.38	120.22	120.64	122.40	121.68	31.75	31.10	32.20	31.20	34.70
	120.63	121.58	121.58	121.49	118.48	30.10	30.90	33.50	32.10	29.95
Surface 4	122.23	124.36	122.62	120.14	122.37	31.45	33.05	32.65	30.10	32.20
	120.69	121.49	119.41	122.36	120.45	35.35	28.85	30.60	31.75	29.20
Average	122.02	121.43	121.11	120.64	121.54	33.62	33.18	31.67	32.08	31.05
Standard Deviation	1.41	1.52	1.13	1.43	1.96	2.15	2.97	2.42	2.10	2.76

Table A.20: Contact angles and sliding angles on clean, proprietary coated surfaces after being cleaned via condensation. Note that water droplets did not roll off these surfaces at 90°and so no SA was measured

	Contact Angle					Sliding Angle				
Condensation Cycles	0	1	2	3	4	0	1	2	3	4
Surface 1	111.91	108.12	109.55	109.96	110.25	-	-	-	-	-
	110.55	111.06	111.05	111.25	111.36	-	-	-	-	-
Surface 2	110.40	110.38	107.99	110.92	109.65	-	-	-	-	-
	113.60	112.48	111.30	108.90	108.97	-	-	-	-	-
Surface 3	113.15	113.34	112.10	110.20	109.83	-	-	-	-	-
	110.14	108.63	108.12	109.15	108.84	-	-	-	-	-
Surface 4	112.47	109.90	109.61	111.29	112.56	-	-	-	-	-
	110.76	109.46	110.85	111.24	111.26	-	-	-	-	-
Surface 5	110.82	109.90	111.83	110.31	109.13	-	-	-	-	-
	110.12	111.98	107.55	108.23	110.35	-	-	-	-	-
Average	111.39	110.32	110.05	109.93	110.22	-	-	-	-	-
Standard Deviation	1.29	1.73	1.60	1.26	1.20	-	-	-	-	-

Table A.21: Contact angles and sliding angles on salt contaminated, Teflon® coated surfaces after being cleaned via condensation

	Contact Angle					Sliding Angle				
Condensation Cycles	0	1	2	3	4	0	1	2	3	4
Surface 1	110.83	117.09	121.24	119.47	120.79	45.15	37.85	33.35	35.35	34.95
	114.66	118.82	118.13	119.61	119.08	37.40	33.35	31.44	32.55	33.35
Surface 2	110.44	118.20	119.60	117.86	119.07	41.25	38.70	33.75	35.50	34.90
	112.53	119.76	118.22	118.98	120.26	38.90	35.35	34.70	32.40	31.65
Surface 3	109.87	119.13	120.43	118.59	120.56	37.45	32.65	33.40	34.20	34.60
	112.11	119.66	119.89	120.57	118.71	39.55	32.20	35.15	35.90	34.58
Surface 4	105.25	117.78	121.49	120.61	119.85	38.70	32.40	34.40	34.95	33.25
	111.67	120.84	119.07	120.76	118.98	38.70	32.85	35.80	34.75	33.70
Average	110.92	118.91	119.76	119.56	119.66	39.64	34.42	34.00	34.45	33.87
Standard Deviation	2.73	1.20	1.26	1.05	0.80	0.87	0.28	1.03	0.71	0.67

Table A.22: Contact angles and sliding angles on salt contamianted, proprietary coated surfaces after being cleaned via condensation. Note that water droplets did not roll off these surfaces at 90°and so no SA was measured

	Contact Angle					Sliding Angle				
Condensation Cycles	0	1	2	3	4	0	1	2	3	4
Surface 1	100.30	109.35	108.08	109.82	108.34	-	-	-	-	-
	98.61	106.11	109.60	107.18	107.01	-	-	-	-	-
Surface 2	101.49	107.98	110.18	109.55	110.58	-	-	-	-	-
	104.80	108.94	107.71	107.36	109.93	-	-	-	-	-
Surface 3	105.43	107.06	108.51	110.01	110.56	-	-	-	-	-
	104.44	109.43	108.33	108.59	108.37	-	-	-	-	-
Surface 4	100.65	108.01	108.79	109.49	110.01	-	-	-	-	-
	104.45	110.84	109.03	107.36	107.21	-	-	-	-	-
Average	102.52	108.47	108.78	108.67	109.00	-	-	-	-	-
Standard Deviation	2.56	1.49	0.81	1.21	1.46	-	-	-	-	-

Table A.23: Contact angles and sliding angles on tobacco contaminated, Teflon® coated surfaces after being cleaned via condensation

	Contact Angle					Sliding Angle				
Condensation Cycles	0	1	2	3	4	0	1	2	3	4
Surface 1	105.90	117.67	120.32	117.18	119.19	90.00	53.05	54.75	49.45	48.40
	107.23	120.03	120.74	119.54	119.05	71.25	50.40	53.55	49.95	49.70
Surface 2	114.95	119.35	119.28	120.54	119.53	66.25	55.30	51.65	51.90	49.80
	106.38	117.75	117.01	118.60	119.51	81.75	58.45	57.55	52.35	51.20
Surface 3	109.41	119.21	119.07	120.22	120.40	71.30	63.80	54.90	54.60	51.40
	104.77	118.12	118.91	117.93	120.57	77.35	53.95	54.75	51.75	50.75
Surface 4	107.35	119.74	119.36	119.83	117.59	66.80	55.80	49.00	51.70	49.60
	109.63	119.57	118.99	118.95	117.67	63.45	56.45	49.85	49.15	48.55
Average	94.97	104.22	104.17	104.45	104.29	70.35	54.23	53.99	51.61	51.05
Standard Deviation	3.52	1.88	1.11	1.16	0.99	8.82	4.35	2.88	1.85	2.36

Table A.24: Contact angles and sliding angles on tobacco contamianted, proprietary coated surfaces after being cleaned via condensation. Note that water droplets did not roll off these surfaces at 90° and so no SA was measured

	Contact Angle					Sliding Angle				
Condensation Cycles	0	1	2	3	4	0	1	2	3	4
Surface 1	100.30	109.35	108.08	109.82	108.34	-	-	-	-	-
	98.61	106.11	109.60	107.18	107.01	-	-	-	-	-
Surface 2	101.49	107.98	110.18	109.55	110.58	-	-	-	-	-
	104.80	108.94	107.71	107.36	109.93	-	-	-	-	-
Surface 3	105.43	107.06	108.51	110.01	110.56	-	-	-	-	-
	104.44	109.43	108.33	108.59	108.37	-	-	-	-	-
Surface 4	100.65	108.01	108.79	109.49	110.01	-	-	-	-	-
	104.45	110.84	109.03	107.36	107.21	-	-	-	-	-
Average	102.52	108.47	108.78	108.67	109.00	-	-	-	-	-
Standard Deviation	2.56	1.49	0.81	1.21	1.46	-	-	-	-	-